

MODEL TEST ON THE EFFECTS OF SOME ROOT
PROPERTIES ON PULLOUT CAPACITY

SITI SARA SEERA BINTI MUSTAPA KAMIL

FACULTY OF ENGINEERING
UNIVERSITY OF MALAYA
KUALA LUMPUR

2013

MODEL TEST ON THE EFFECTS OF SOME ROOT
PROPERTIES ON PULLOUT CAPACITY

SITI SARA SEERA BINTI MUSTAPA KAMIL

THESIS SUBMITTED IN FULFILMENT OF THE
REQUIREMENTS FOR THE DEGREE OF MASTER OF
ENGINEERING SCIENCE

FACULTY OF ENGINEERING
UNIVERSITY OF MALAYA
KUALA LUMPUR

2013

UNIVERSITI MALAYA

ORIGINAL LITERARY WORK DECLARATION

Name of Candidate: SITI SARA SEERA BINTI MUSTAPA KAMIL (I.C/Passport No:)

Registration/Matric No: KGA080074

Name of Degree: MASTER OF SCIENCE ENGINEERING

Title of Project Paper/Research Report/Dissertation/Thesis ("this Work"):

MODEL TEST ON THE EFFECTS OF SOME ROOT PROPERTIES ON PULLOUT CAPACITY

Field of Study:

I do solemnly and sincerely declare that:

- (1) I am the sole author/writer of this Work;
- (2) This Work is original;
- (3) Any use of any work in which copyright exists was done by way of fair dealing and for permitted purposes and any excerpt or extract from, or reference to or reproduction of any copyright work has been disclosed expressly and sufficiently and the title of the Work and its authorship have been acknowledged in this Work;
- (4) I do not have any actual knowledge nor do I ought reasonably to know that the making of this work constitutes an infringement of any copyright work;
- (5) I hereby assign all and every rights in the copyright to this Work to the University of Malaya ("UM"), who henceforth shall be owner of the copyright in this Work and that any reproduction or use in any form or by any means whatsoever is prohibited without the written consent of UM having been first had and obtained;
- (6) I am fully aware that if in the course of making this Work I have infringed any copyright whether intentionally or otherwise, I may be subject to legal action or any other action as may be determined by UM.

Candidate's Signature

Date

Subscribed and solemnly declared before,

Witness's Signature

Date

Name:

Designation

ABSTRACT

The study is aimed to investigate the morphology functional of plant root systems in relation to their roles in providing anchorage and stability to the plant. Since the adoption of bioengineering technique in solving numerous geotechnical failures has rapidly increased these days, this research can be beneficial in providing additional knowledge towards a greater insight of soil-root mechanical interactions. The anchorage of different types of root systems was investigated together with the influences of several mechanical factors on their development. The roles of root branching patterns and root tapering behaviour as well as root material stiffness to the anchorage and stability of plant have been selected as the mechanical factors to be studied. The research was conducted and completed by carrying out a series of laboratory pullout test using physical models. Throughout this study, pullout resistances of the artificial root models were measured by subjecting the various patterns of the physical root models to the vertical uprooting forces using a laboratory pullout machine. The laboratory tests were chosen to conduct quick experiments on the root pullout strength. By doing so, the identical soil samples could be prepared while various and common simple root patterns could be developed and studied in great details. Model experiments were successfully verified as well as confirming the theoretical predictions that demonstrate the importance of root branching pattern in the stability of plant through root anchorage controlled by the number of lateral root, angle and position of the lateral root to the taproot and the total length of taproot in a root system. A second model study on a series of tapered root models has also revealed the behaviour of root tapering in weakening the anchorage of soil-root composites due to the response of confining pressure by the soil medium that acted on the components of root model during pullout.

The confining pressure was higher at the root tip compared to the other points of the upper root length to the lateral branching point as a consequence of force concentration at a smaller area of root tip. This caused the point to bend easily and quickly that led into less resistance of the tapered root models to pullout. While investigating on the influences of root material stiffness as one of the major sources of soil-root anchorage to the stability of plants, the aluminum root models were identified to be more difficult to uproot in contrast to the flexible root material made out of high density polyethylene (HDPE) material. As the high density polyethylene (HDPE) material represents the flexible root models, the pullout resistances generated were less than those produced by the uniform aluminum root models which represent the harder and stiffer root models. In a conclusion, root morphologies and the highlighted mechanical factors studied have impressively proven in being such a significant influence on the root anchorage of plants and this knowledge can be considered beneficial if vegetation is to be practiced extensively.

ABSTRAK

Kajian bertujuan mengkaji akan kebolehfungsian morfologi fungsi sistem akar tumbuhan dalam memberikan ikatan dan kestabilan kepada tumbuhan. Sejalan dengan pertumbuhan mendadak pengaplikasian teknik biokejuruteraan ini dalam menyelesaikan pelbagai masalah kegagalan geoteknikal, kajian ini diharap dapat memberi manfaat dalam menyediakan pengetahuan tambahan ke arah tinjauan yang lebih luas berhubung dengan interaksi mekanikal tanah-akar. Jenis ikatan sistem akar yang berlainan telah dikaji beserta dengan pengaruh beberapa faktor mekanikal seiring dengan perkembangan tumbesaran tumbuhan. Peranan corak cabang akar, sifat tirus akar, serta kekakuan bahan akar untuk ikatan dan kestabilan tumbuhan telah dipilih sebagai faktor-faktor mekanikal untuk dikaji. Kajian itu dilaksanakan dengan menjalankan satu siri ujian makmal tarik keluar dengan menggunakan model fizikal. Sepanjang kajian ini, rintangan tarik keluar model akar tiruan telah diukur berdasarkan kepada daya tindakan angkatan tarik keluar menegak yang didedahkan ke atas pelbagai corak model akar fizikal dengan menggunakan mesin tarik keluar makmal. Ujian makmal telah dipilih bagi menjalankan eksperimen segera bagi mengkaji kesan kekuatan tarik keluar akar. Melalui teknik ini sampel tanah yang serupa boleh disediakan selain daripada kepelbagaian corak mudah biasa akar boleh dibangunkan dan dipelajari dalam butir-butir yang lebih terperinci. Eksperimen model telah berjaya membuktikan dan mengesahkan jangkaan teori yang menunjukkan akan kepentingan corak cabang akar dalam mempengaruhi kestabilan tumbuhan melalui tambatan akar yang dikawal oleh bilangan akar sisi, sudut dan kedudukan akar sisi kepada akar tunjang, serta panjang jumlah akar tunjang dalam sistem akar. Satu kajian model kedua pada siri model akar tirus juga telah membuktikan akan kepentingan kawasan permukaan akar dalam ikatan

tanah-akar di mana model akar didapati diikat lebih baik dengan peningkatan kawasan sentuhan tanah-akar. Ujian tarik keluar ke atas pelbagai corak model akar tirus telah mengurangkan luas permukaan sentuh dalam model akar kepada rangka tanah dan dengan itu telah memberi kurang kesan rintangan kepada tarik keluar. Sementara kajian mengenai pengaruh kekukuhan bahan akar sebagai salah satu sumber utama penambat tanah-akar bagi kestabilan tumbuh-tumbuhan, model akar aluminium telah dikenal pasti sebagai lebih sukar untuk ditarik keluar berbanding dengan bahan akar fleksibel yang diperbuat daripada polietilena berketumpatan tinggi (HDPE). Sebagai bahan polietilena berketumpatan tinggi (HDPE) yang mewakili model akar fleksibel, rintangan tarik keluar yang dijana adalah kurang daripada yang dihasilkan oleh model akar aluminium yang mewakili model akar yang lebih keras dan lebih kukuh. Kesimpulannya, kajian mengenai morfologi akar dan faktor-faktor mekanikal yang diketengahkan telah terbukti hebat dalam memberi pengaruh yang besar kepada ikatan akar tumbuh-tumbuhan dan pengetahuan yang diperolehi boleh dianggap bermanfaat jika teknik pengaplikasian tumbuh-tumbuhan ingin diamalkan secara meluas.

ACKNOWLEDGEMENT

In the name of Allah, the Most Gracious and the Most Merciful

First and foremost, I would like to head my deepest gratitude to the Almighty Allah S.W.T for his guidance and blessings. This thesis represents the dedicated efforts of numerous peoples, many of them whom deserve special mention: I would like to express my utmost appreciation and full respects to my supervisor and co-supervisor, Prof. Dr. Faisal Hj Ali, Dr. Normaniza Osman and Prof. Ir. Dr. Roslan Hashim for giving me the opportunity to conduct this project research. I would like to thank them for their dedicated guidance, supervision, willingness to share their expertise and very useful advice in respect to my thesis project from the beginning until the end of this thesis project, thus making my thesis successful.

My special thank is also expressed to the most important people in my life, my beloved parents and family, Encik Mustapa Kamil bin Zainal , Puan Samsiah Mohamad and to all of my sisters, Ivani, Ashikin and Sofhia, for all her helps, inspirations and endless supports. Thank you for always be there to support and guide me throughout my life.

There is no word to describe how thankful I am to them.

Siti Sara Seera binti Mustapa Kamil

January 2013

LIST OF CONTENTS

ORIGINAL LITERARY WORK DECLARATION.....	ii
ABSTRACT.....	iii
ABSTRAK.....	v
ACKNOWLEDGEMENT.....	vii
LIST OF CONTENTS.....	viii
LIST OF FIGURES.....	x
LIST OF TABLES.....	xiii
CHAPTER 1: INTRODUCTION.....	1
1.1 Background.....	1
1.2 Objectives of Research.....	5
1.3 Scope of Study.....	5
1.3.1 The Influences of Root Branching Patterns in Resisting Uprooting.....	5
Forces	
1.3.2 The Behaviour of Root Tapering when Subjected to Axial Forces.....	6
1.3.3 The Effect of Root Material Stiffness to Uprooting Resistances.....	6
1.4 Outline of Research.....	6
CHAPTER 2: LITERATURE REVIEW.....	8
2.1 Introduction.....	8
2.2 Soil Bioengineering.....	8
2.3 Mechanical Engineering Influences of Vegetation.....	13
2.3.1 Root Tensile Strength.....	13
2.3.2 Root Pullout Resistance.....	16
2.3.3 Shear Resistance.....	18
2.3.4 Root Cohesion.....	23
2.4 Root Morphology.....	24
2.4.1 Root System and the Pattern of Root Growth in Trees.....	24
2.5 Modes of Root Failure.....	28
2.6 Pullout of Analogue Roots.....	32

CHAPTER 3: RESEARCH MATERIALS AND METHODS.....	38
3.1 Introduction.....	38
3.2 Research design/ programme.....	38
3.2.1 The Artificial Root Models.....	38
3.2.2 Embedment for Root Models	48
3.3 Research Materials.....	48
3.3.1 Material for the Artificial Root Models.....	48
3.3.2 Material for Soil Medium.....	49
3.3.3 Material and design of pullout tank.....	50
3.4 Research Test.....	51
3.4.1 Soil Property Test	51
3.4.2 Mechanical Test.....	53
3.4.3 Pullout Test.....	54
3.4.3.1 Pullout Test Apparatus.....	54
3.4.3.2 Procedures of Pullout Test.....	58
 CHAPTER 4: RESULTS.....	 61
4.1 Introduction.....	61
4.2 Soil and Material Properties.....	61
4.3 The Influences of Root Branching Pattern in Resisting Pullout Forces.....	73
4.4 The Behaviour of Root Tapering when Subjected to Axial Forces.....	89
4.5 The Influences of Root Material Stiffness to Uprooting Resistances.....	104
CHAPTER 5: CONCLUSION AND RECOMMENDATIONS FOR FUTURE	
WORK.....	118
 REFERENCES.....	 122
APPENDICES.....	127

LIST OF FIGURES

Figure 2.1:	The factors that affecting both soil and root strength	9
Figure 2.2:	Examples of the simple and complex uprooting failure	17
Figure 2.3:	Deformation of analogue roots during shear in dry sand	20
Figure 2.4:	Root geometry of tree	24
Figure 2.5:	Patterns of root growth in trees	26
Figure 2.6:	Schematic of root reinforcement and the failure of a root during soil displacement	29
Figure 2.7:	Artificial root model with different topologies and branching angles	33
Figure 2.8:	Representative behaviour of rubber and wood models during pulled out	34
Figure 2.9:	Applied mechanical loadings to plant root systems	36
Figure 2.10:	Analysis of analogue and soil movement around the model	36
Figure 2.11:	Head load-displacement responses for root-analogue	37
Figure 3.1:	Diagram showing the distinction between (a) herringbone and (b) dichotomous branching pattern	41
Figure 3.2:	Various types of artificial root model pattern	42
Figure 3.3:	Uniform aluminum artificial root model with the diameter along the root length was uniformly	44
Figure 3.4:	Tapered aluminum artificial root model with the diameter along the root length was gradually tapering	46
Figure 3.5:	Sieving machine	52
Figure 3.6:	The automatic soil compactor	52
Figure 3.7:	Shear box test machine	53
Figure 3.8:	Universal Tensile Machine (INSTRON 5582)	54
Figure 3.9:	LVDT transducer	55
Figure 3.10:	Laboratory pullout machine with a specially designed wedge and barrel system	57
Figure 3.11:	Controller and vibrator	58
Figure 3.12:	Wedge and Barrel	58

Figure 3.13:	The opening	60
Figure 3.14:	Layout model of the artificial root model in tank	60
Figure 4.1:	Particle size distribution chart	63
Figure 4.2:	Graph of dry density against moisture content	65
Figure 4.3:	Shear stress against horizontal displacement graph	67
Figure 4.4:	Vertical displacement against horizontal displacement graph	67
Figure 4.5:	Shear stress against vertical stress graph	68
Figure 4.6:	Graph of tensile test for Aluminum material of different diameter 8 mm and 10 mm	72
Figure 4.7:	Graph of tensile test for High Density Polyethylene (HDPE) material of different diameter 8 mm and 10 mm	72
Figure 4.8:	Uprooting resistance of aluminum root models with different branching pattern	75
Figure 4.9:	The pullout force of different patterns of uniform aluminum root models	77
Figure 4.10:	The resistance of uniform aluminum root models to pullout in descending order	78
Figure 4.11:	Pullout resistances of type 1 root models D1, H1 and C1, which is greater than the type 2 root models, D2, H2 and C2, respectively	84
Figure 4.12:	The maximum pullout forces for herringbone root pattern, H1 and H2 is higher than that of in dichotomous root pattern, D1 and D2, respectively	88
Figure 4.13:	Uprooting resistance of tapered aluminum root models with different branching pattern	91
Figure 4.14:	The uprooting resistance of different branching pattern of tapered aluminum root models	92
Figure 4.15:	The resistance of tapered aluminum root models to pullout in descending order	93
Figure 4.16:	Pullout resistances of type 1 root models D1, H1 and C1 is greater than the type 2 root models, D2, H2 and C2, respectively	96
Figure 4.17:	The maximum pullout force for herringbone root models H1 And H2, is greater than the dichotomous root pattern, D1 and D2, respectively	98

Figure 4.18:	Comparison of pullout force generated by uniform and tapered aluminum root models according to the root pattern studied	102
Figure 4.19:	Comparison of pullout force generated by uniform and tapered aluminum root models according to the root pattern studied	103
Figure 4.20:	Uprooting resistance of flexible (HDPE) root models with different branching pattern	106
Figure 4.21:	The uprooting resistance of the flexible root models with different branching patterns	108
Figure 4.22:	The resistance of flexible root models to pullout in descending order	109
Figure 4.23:	Pullout resistances of type 1 root models D1, H1 and C1, is greater than that of in the type 2 root models, D2, H2 and C2, respectively	112
Figure 4.24:	The maximum pullout force for herringbone root pattern H1 and H2, is greater than dichotomous root pattern, D1 and D2, respectively	113
Figure 4.25:	Comparison of pullout force generated by aluminum and HDPE root models based on the individual pattern	114
Figure 4.26:	Comparison of pullout force generated by aluminum with uniform shape and flexible (HDPE) root pattern according to the root patterns	116

LIST OF TABLES

Table 2.1:	Various types of bioengineering method	11
Table 2.2:	List of advantages and disadvantages of various bioengineering methods	12
Table 2.3:	Tensile strength and Young's modulus of trees and shrubs species	15
Table 2.4:	Area and shear strength of roots	22
Table 2.5:	Description of root growth pattern in trees	27
Table 2.6:	Examples of root failure curves and associated root morphologies	30
Table 2.7:	Maximum pullout resistance of the model roots	35
Table 3.1:	Description of artificial root model pattern	41
Table 3.2:	Uniform aluminum artificial root model	43
Table 3.3:	Tapered aluminum artificial root model	45
Table 3.4:	Flexible artificial root model	47
Table 4.1:	Dry sieving result	62
Table 4.2:	Bulk density result	64
Table 4.3:	Compaction test results	64
Table 4.4:	Vertical stress of each loading	65
Table 4.5:	Particle density of sand	69
Table 4.6:	Ranges of angle of friction (ϕ) for sands	70
Table 4.7:	Results of the material tensile properties	71
Table 4.8:	Results of the maximum pullout resistances of uniform aluminum root models from the overall tests	75
Table 4.9:	Selected results of the maximum pullout resistance of uniform aluminum root models	76
Table 4.10:	Uniform aluminum artificial root model after the pullout test	79
Table 4.11:	Total vertical and horizontal stresses acting on root models with different branching angle	81
Table 4.12:	Results of the maximum pullout resistance of tapered aluminum root models from the overall tests	90

Table 4.13:	Selected result of the maximum pullout resistance of tapered aluminum root models	91
Table 4.14:	Tapered aluminum artificial root model after the pullout test	94
Table 4.15:	Maximum uprooting resistance of the uniform and tapered aluminum and root models	99
Table 4.16:	Reduction of the root surface area in tapered aluminum root models	102
Table 4.17:	Results of the maximum uprooting resistances of flexible root models from the overall tests	106
Table 4.18:	Selected result of the maximum pullout resistance of flexible root models	107
Table 4.19:	Flexible artificial root model after the pullout test	110
Table 4.20:	Maximum uprooting resistance of the uniform aluminum and flexible (HDPE) root models	114

CHAPTER ONE

INTRODUCTION

1.1 Background

Vegetation practice for the treatment and protection of unstable soil has been recently applied vigorously throughout the world. The proficiency of this technique in minimising the occurrence of soil failures had been globally recognized and the potential of this method to be adopted in the critical and prestigious civil structures in the future is sensible to be considered due to the successful history of this method in earlier trials (Gray and Leiser, 1982, Clark and Hellin, 1996, Lawrance, 1994).

In this technique, live plants play a principal role as a main structural element in maintaining the equilibrium forces of soil skeleton between the destructive forces of soil instability and constructive or regenerative forces of soil stability (Morgan and Rickson, 1995). Through the reinforcement generated by root linkages which spread out from trees, vegetation serves as a vital component in transmitting shear stresses within the soil to tensile resistance of the roots. Vegetation root basically interacts with the soil in which it is grown through the formation of a new structural composite composed of soil and root materials over the existence of roots with high tensile strength that penetrated into the soil matrix with lower tensile strength (Mattheck et al., 1997). In this context,

the roots need to have sufficient embedment and adhesion with the surrounding soil to make use of their available tensile strength (Norris and Greenwood, 2006).

Beyond the commercialization of this technique, the understanding of the mechanical interactions of the soil-root matrix however needs to be well understood where concern should be taken especially in the selection of the most suitable species to be used on unstable soil. This is due to the variability and complexity of the root systems that will most possibly source into the dissimilarity of the reinforcing and strengthening effect. Although numerous advances have been made in the times of yore, it is still not yet known on which shape of the root system that is best to increase the tree mechanical stability (Fourcaud et al., 2008). This is a consequence of the detailed mechanism of soil root composites combined with unseen processes below the ground hence greatly complicates the quantification of the root-soil interaction (Mickovski et al., 2007).

Vegetation generally may improve soil stability in two main ways: mechanically as well as hydrologically (Coppin and Richards, 1990, Gray and Sotir, 1996, and Greenwood et al., 2004). In a direct mechanical way, the soil-root composites stability has been recognized to be influenced and controlled by four primary components; pullout resistance, shear resistance, tensile resistance, and root cohesion. Each of these components has been identified as being interrelated to each other in promising strength to the soil-root anchorage as studied and verified by previous researchers.

In regards to the importance of these components, there were a number of studies with the focus primarily based on the responses and influences of those components into the soil-root anchorage. Unfortunately, study on the pullout resistance had received regrettably little attention (Mickovski et al., 2007) although most of the failures that

frequently occurred in trees were through the uprooting (Nicoll et al., 1995, Cucchi and Bert, 2003) before it finally ends up with various types of damages. Hence, the root pullout resistance could be considered as an additional component of the soil shear strength.

Root pullout resistance generally refers to the ability of plant root in resisting trees from being pulled out of the soil. It is one of the most important factors that need to be considered in the analysis of rooted soil matrix because to the engineers, not only the ultimate capacity is important, the load – displacement response of the root during the pullout action that could be achieved throughout this pullout study for the proper analysis of the behaviour is also significant. For plants with both lateral and tap roots which are more suitable for residual soil, the knowledge on mobilization of resistance and load sharing between them is important as well. This reflects how pullout resistance of even very simple idealized root analogues is a complex process affected by a number of root and soil mechanical phenomena. Values of the resistance are normally measured under controlled experimental conditions which basically provide indirect information on the below ground biomass development and density of the root system.

In this study, it greatly simplified the complex anchorage of rooted soil matrix to improve the understanding of the soil-root interactions through the utilization of analogue roots to be subjected to vertical external loading, controlled by several root and soil properties. Real roots were substituted with model or analogue roots since plant roots have a wide range of stiffness and rigidity along with the span of more than three orders of magnitude in root diameter depending on the species and root type that complicate the detailed investigation on them. Hence, consideration on the implications of the pullout capacity of root branching pattern, tapering effects and relative flexibility

of the roots due to progressive failure when undergoing axial displacement using analogue root models should be extensively practiced.

Though the idea of using these artificial root models is often criticized of its artificiality, the workability of this method was verified in providing such a numerous benefits into a detailed study of soil rooted matrix interactions (Stokes et al., 1996, and Mickovski et al., 2007). This alternative is also vital as it offers another option to study the interaction of soil-root composites instead of using real roots which are usually damaged during the pullout tests, thus lack of information could be obtained and studied.

Throughout this study, the vertical axial displacement was measured by subjecting the root models to vertical uprooting forces instead of the measurement of the lateral displacement attributable to an earlier research on soil nail that denotes little effects on reinforcement while subjected to lateral pressure, with the predominant reinforcement occurring through the mobilization of axial forces through interface shear (Schlosser et al. 1992). This report was then strengthened by Mickovski et al., 2007 in his study that identified the behaviour of flexible root models reinforcement in his physical simulation study that bent across the shear plane until they are oriented to be pulled out axially. The basis of those findings clearly verified the significances of the vertical axial forces in manipulating the anchorage and stability of plants in the surrounding soil in which they are grown.

1.2 Objectives of research

The primary focus of this research is therefore to determine the anchorage efficiency of typical root system architectures representing selected properties of root characteristics. In detail, it is to investigate the influence of root branching patterns in resisting uprooting forces and the behaviour of root tapering when subjected to axial forces as well as the effect of root material stiffness to uprooting resistance using analogue root models in a comprehensive study of soil rooted matrix interactions. This method is a good alternative to difficult and time-consuming field experiments which aid in identifying the parameters which needing greatest study since the mechanical properties of the materials used were known. The analogue roots were developed based on simple root patterns with the purpose to conduct quick experiments on root pull-out strength by carrying out a series of laboratory pullout tests using physical models which are subjected to vertical uprooting forces using a laboratory pullout machine.

1.3 Scope of study

1.3.1 The Influence of Root Branching Patterns in Resisting Uprooting Forces

The root branching pattern is frequently revealed as an important factor in influencing root pull out resistances (Stokes et al., 1996, Mickovski et al., 2007). This study was conducted with the aim to study on the response of simple root systems with different branching angles undergoing axial lift or uprooting forces. Since the existence of real root systems are various and complex, therefore it is essential to understand the behaviour of simpler systems (dichotomous, herringbone and combination of root

patterns) before attempting to comprehend the behaviour of more complex real root systems.

1.3.2 The Behaviour of Root Tapering in Resisting Uprooting Forces

A series of studies have been conducted in conjunction with studying the behaviour of root tapering while subjected to the uprooting forces construed through the idea of using artificial root models designed in tapered. Root models were developed similarly to the patterns of previous cases (Section 1.3.1) but the diameter along the root length was gradually tapered (decreased) as to present the reduction of the root area surface.

1.3.3 The Effect of Root Material Stiffness to Uprooting Resistances

Two different model materials with dissimilar tensile strength were selected to embrace a wide range of root stiffness. There are aluminum rods representing the harder and stiffer root models while the High Density Polyethylene (HDPE) rods were employed to represent more flexible root models. Although both materials used were not exactly simulating the strength of the real roots, it is assumed that the strength of the real roots is located between the strength of these two extreme points.

1.4 Outline of research

This thesis is divided into five chapters. The first chapter presents the introduction and objectives as well as the lines of investigation throughout this thesis. Chapter two expresses the literature review from the previous researches where it looks deeper into the concept of soil bioengineering in slope design, basic theories of root modelling and

root modelling using finite element analysis by past researchers. This literature is important to verify the theory as well as the methods adopted in this study. The method of pull-out test is included in chapter three where it describes the methods and stages applied during the pullout tests. The complete full results and discussion from the laboratory tests are then elaborated in chapter four, followed by chapter five which concludes the findings of this study as well as highlighting on the recommendations for future related works.

CHAPTER TWO

LITERATURE REVIEW

2.1 Introduction

This chapter begins with the introduction and explanation on the practice of soil bioengineering technique in this recent world. It is then followed by an elaboration on the mechanical engineering influences of vegetation towards soil stability. Details on root morphology concerned on the root system and pattern of root growth are then explained in the next subtopic and continued with the description on modes of root failure. The previous pull-out studies using analogue root models conducted by former researchers have also been reviewed and briefly elaborated. Finally, the description on the practice of finite element in root modelling which was previously studied in conjunction with studying the behaviours and responses of these root models during the uprooting mechanisms.

2.2 Soil bioengineering

Soil bioengineering is a practical alternative technique which offering more traditional and sustainable method of soil stabilization. Throughout this green solution, living

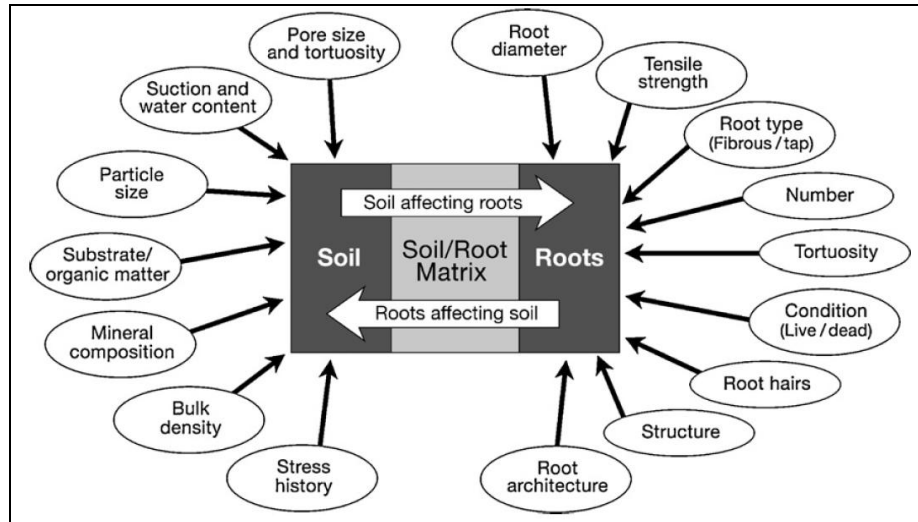


Figure 2.1: The factors that affecting both of soil and root strength (Loades et al., 2009)

materials were used as a main structural element by employing them in near-natural constructions. Besides of protecting nature, this technique also was found in providing a safe, structurally sound and aesthetically pleasing environment of a place. Nevertheless, in some situations of critical cases, the applications of these bioengineering solutions independently are inadequate like on a very steeply sloping site where in this context, contributions of the conventional methods are required for the additional safety of public and the built structure.

In promoting this new technique, a few attentions however need to be alert especially in the selection of the vegetation itself. As this technique combines biological elements with the engineering design principles, including plan and design, thus, requirements of those elements therefore need to be satisfied. The selected vegetation must be ensured to be more sustainable over time as it is self-regenerating. It must be also be able to respond dynamically and naturally to the changing site conditions and ideally without compromising or losing its engineering properties.

In this case therefore, eco-engineers, planners and decision makers need to understand of these complex interactions especially in terms of the mechanical reinforcement of soil by the roots as well as the effects of changes in the management strategies if these techniques are considerably to be used (Figure 2.1). Various bioengineering methods and the major advantages and disadvantages of each soil bioengineering technique are listed (Table 2.1 and Table 2.2).

Table 2.1: Various types of bioengineering method (Donat, 1995)

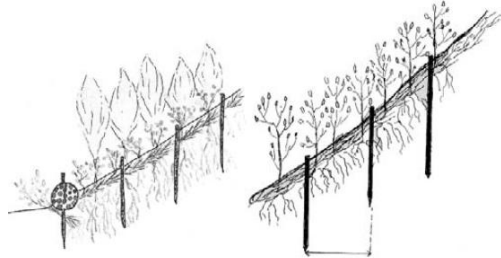
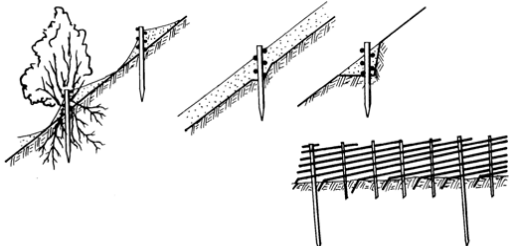
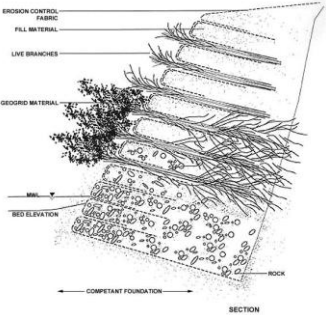
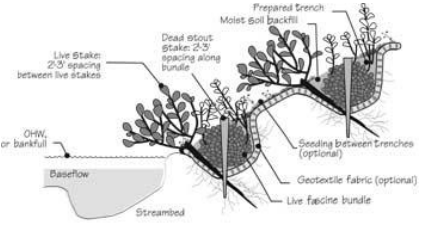
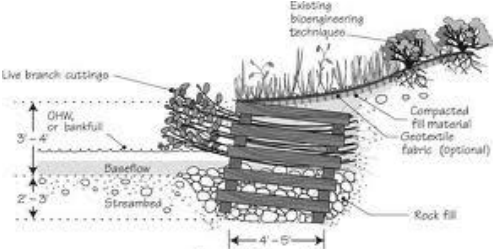
Method	Figure	Application
<p>Bush- mattress construction with wood pegs</p>		<ul style="list-style-type: none"> erosion of banks and slopes improvement of riprap, bank repair
<p>Wattle fences</p>		<ul style="list-style-type: none"> stabilization of top soil and slopes of fine material
<p>Vegetated geogrids</p>		<ul style="list-style-type: none"> for rebuilding very steep eroded streambanks particularly useful where land has been previously lost and needs to be restored
<p>Fascines (bush wattles)</p>		<ul style="list-style-type: none"> stabilization of top soil layers, slopes of fine material or bank toes, drainage of wet zones
<p>Live cribwall</p>		<ul style="list-style-type: none"> areas where a catastrophe (soil instability) has already occurred for stabilization of parts of slopes, water channels, and toes of slopes

Table 2.2: List of advantages and disadvantages of various bioengineering methods (Donat, 1995)

Methods	Material/plant species	Advantages	Disadvantages
Bush-mattress construction with wood pegs	Salix, Eleagnus, Platanus	<ul style="list-style-type: none"> • immediately effective • flexibility in protection • material easily available 	<ul style="list-style-type: none"> • high demand on labour • occasionally thinning of thicket necessary
Wattle fences	Salix, Platanus	<ul style="list-style-type: none"> • rooted fences retain and stop moving soil • easily combined with other method • flexibility in protection 	<ul style="list-style-type: none"> • high labour and material costs • securing effect is small • potential lack of local material • easily damaged
Vegetated geogrids	Dormant branches that enough to reach the back of the trench to be filled and to extend slightly beyond the surface slope	<ul style="list-style-type: none"> • Efficient minimization of bank erosion • Higher initial tolerance of velocity than traditional brush layering techniques 	<ul style="list-style-type: none"> • requires both heavy equipment and intensive manual labour to install
Fascines (bush wattles)	Salix Vitex, chestnut peggs	<ul style="list-style-type: none"> • fast and simple • little soil movement • useful for wet slopes and zones • promotes development towards climax 	<ul style="list-style-type: none"> • flexible branches necessary • susceptible to rockfall and shearing • labour intensive
Live cribwall	Round or square in diameter, at timber (0.10-0.25 m, 1.0-1.5 m spacing)	<ul style="list-style-type: none"> • fast stabilization • can be constructed in a horizontal line • provide active drainage and the increase of the root systems' armouring effects 	<ul style="list-style-type: none"> • the lumber can lack durability

2.3 Mechanical Engineering Influences of Vegetation

Soil-root composites stability has been revealed to be influenced and controlled by four main mechanical components known as pullout resistance, shear resistance, tensile resistance, as well as root cohesion. These four main components have been recognized in having such a unique relationship between each other in enhancing and promising strength into soil-root composites.

2.3.1 Tensile Root Strength

The significance of root tensile strength in governing soil stabilisation has been well recognized and investigated in great detail over the years (Burroughs and Thomas, 1977, Schiechlt, 1980, Tosi, 2007). The measurement of root tensile strength could be estimated either by carrying field pull-out test or by performing standard laboratory tests using a Universal Tensile Testing machine. Root tensile strengths generally show high strengths values with small root diameters and vice versa (Norris and Greenwood, 2006). Based on the previous studies, the tensile strength was revealed to decrease with the increasing root diameter following a power law curve, while the tensile force was revealed to increase with the increasing of root diameter following a second-order polynomial regression curve (Tosi, 2007). This phenomenon occurred as correlated to the cellulose content of the roots, where the numbers of these complex microfibrils are identified to be higher in smaller roots compared to the older one.

Cellulose is particularly resistant in tension due to its microfibrillar structure that has been found to be optimal for resisting failure in tension (Sjostrom, 1992). Cellulose is made up of polymer chains consisting of glucose units which are linked together by

highly resistant hydrogen bonds (Delmer and Amor, 1995). These cellulose chains are then grouped together in a hemicellulose matrix and the entire structure is termed as microfibril. Each layer of the wood cell wall which made up of many microfibrils then arranged in a helical structure. When these microfibrils are aligned at an angle almost parallel to the cell axis, as in young wood, the combined effect of these cellulose chains give a high resistance in tension, but a low bending strength (Archer and Tieszen, 1986). Table 2.3 summarized the tensile strengths for the selected shrubs and trees which have been measured by different investigators.

Table 2.3: Tensile strength and Young's modulus of trees and shrubs species (Mafian, Huat & Ghiasi, 2009)

Species	Common Name	Tensile Str. (MPa)	Young's Mod. (MPa)	Reference
Tree Species				
<i>Abies concolor</i>	Colorado white	11		Schiechtl (Wu 2007)
<i>Acacia confuse</i>	Acacia	11		Schiechtl (Wu 2007)
<i>Acacia mangium</i>	Acacia	54		Normaniza <i>et al.</i> (2008)
<i>Acer sacharinum</i>	Silver maple	15–30	600	Beal (Wu 2007)
<i>Alnus</i>	Alders	32-52		Schiechtl (Wu 2007)
<i>Betula pendula</i>	European white birch	38		Schiechtl (Wu 2007)
<i>Dillenia suffruticosa</i>	Simpoh Air	16-26		Mafian (2009)
<i>Hibiscus tiliaceus</i>	Hibiscus	15-27		Mafian (2009)
<i>Leucaena leucocephala</i>	Leucaena	105		Normaniza <i>et al.</i> (2008)
<i>Nothofagus fusca</i>	Red beech	32		Schiechtl (Wu 2007)
<i>Picea</i>	Spruces	16-28		Schiechtl (Wu 2007)
<i>Pinus</i>	Pines	10-33		Schiechtl (Wu 2007)
<i>Populus</i>	Poplars	5-38	200-300	Wu (2007)
<i>Pseudotsuga</i>	Firs	19-55		Schiechtl (Wu 2007)
<i>Quercus robur</i>	Oak	20		Schiechtl (Wu 2007)
<i>Sambucus callicarpa</i>	Pacific red elder	19		Schiechtl (Wu 2007)
<i>Salix</i>	Willows	18–37	200–300	Hathaway and Penny (Wu 2007)
<i>Tilia cordata</i>	Linden	26		Schiechtl (Wu 2007)
<i>Tsuga heterophylla</i>	Western hemlock	20		Schiechtl (Wu 2007)
Shrub Species				
<i>Castanopsis chrysophylla</i>	Golden chinkapin	18		Schiechtl (Wu 2007)
<i>Ceanothus velutinus</i>	Ceanothus	21		Schiechtl (Wu 2007)
<i>Cytisus scoparius</i>	Scotch broom	33		Schiechtl (Wu 2007)
<i>Melastoma malabathricum</i>	Melastoma	30		Normaniza <i>et al.</i> (2008)
<i>Lespedeza bicolour</i>	Scrub lespedeza	71		Schiechtl (Wu 2007)
<i>Tsuga heterophylla</i>	Western hemlock	16		Schiechtl (Wu 2007)

2.3.2 Root Pullout Resistance

Root pullout resistance generally is roots ability in resisting trees from being pullout out of the soil. According to Schaetzl et al. (1988), they implied the term of the tree uprooting itself as a tree that fallen with most of its larger roots intact and tearing up soil in the process (Figure 2.2). Uprooting occurs when lateral or vertical forces which applied to the tree overcome the root anchorage (Putz, 1983). When stem strength is strong, then soil to root adhesion becomes the weak link in the system and finally leads to the uprooting to occur (Schaetzl et al., 1988).

This pullout resistance is likely to be only a little less than the resistance which measured in root tensile strength. In the case of no pull out data available, the tensile strength data may be used as a rough guide to the maximum pull out resistance available (Greenwood et al., 2004). Though the concepts for both of these tensile and pullout resistances sound identical, but they are basically and practically different. In pullout test, the forces which applied on the plants during the mechanism acting across a larger root area where it involves multiple branches and longer root lengths. Contrarily in tensile test, root samples commonly cut into a standard length, clamped into the machine and tested individually accordance to standard to the point of failure.

Studies by Norris (2005) have reported several factors that influenced the resistances of root pullout. From the study it was revealed that pull out resistance of hawthorn and oak roots were generally affected by the intra species differences, inter-species variations as well as the root size diameter, where the roots with smaller diameter was revealed in generating lower pull out resistance or breaking force than the roots with larger diameter.

Gregory (2006) derived a formula to calculate the force required to pull a root out of the soil which was strongly dependent on the area of contact between the root and the soil, and the shear strength of the soil:

$$F = \pi D L \sigma \quad (\text{eqn 2.1})$$

where D is the root diameter, L is the root length, and σ is the shear strength of the soil.

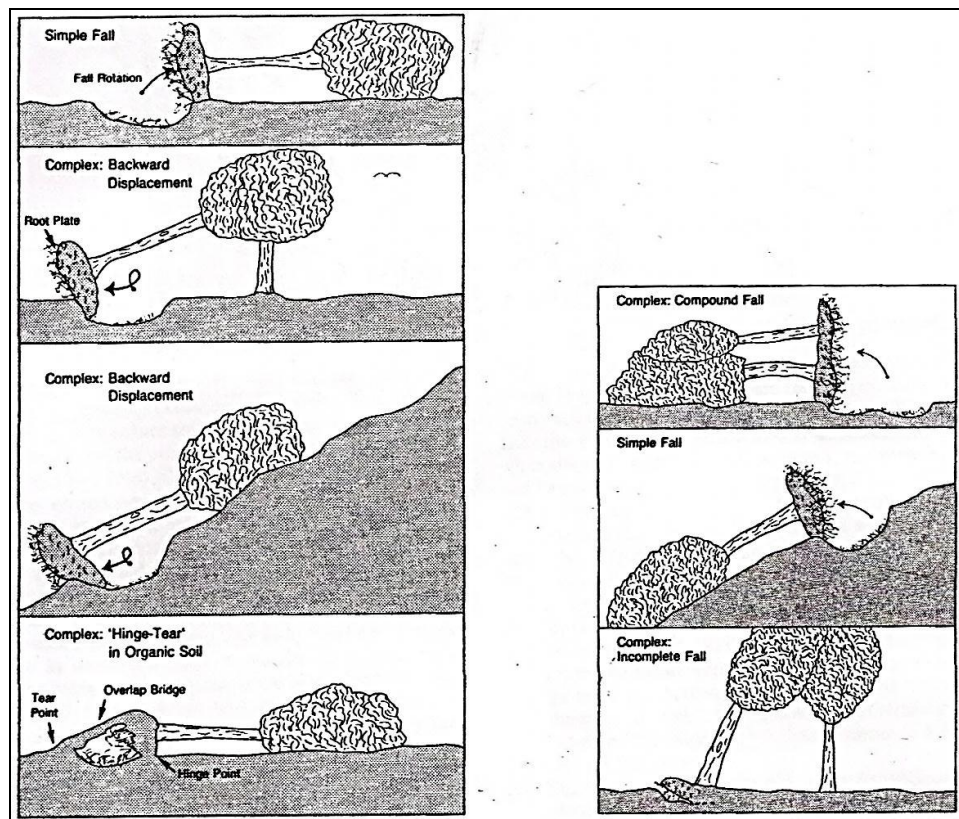


Figure 2.2: Examples of a simple and complex uprooting failure (Schaetzl et al., 1988)

2.3.3 Shear resistance

The shear strength of soil is its resistance to shearing stresses. It is a measure of soil resistance to deformation by continuous displacement of its individual soil particles. Shear strength in soils primarily depends on the interactions between the soil particles and shear failure occurs when the stresses between the particles are slide or roll passing each other.

In soil-root composites, the shear strength however is different as the available soil shear strength is strengthened by the additional strength provided by the root networks. With the ability of the tree roots in resisting tension, therefore increased shear strength of the soil-root composites (O'Loughlin, 1974, Shewbridge and Sitar, 1989).

As for in non-rooted soil, shear strength is generally calculated by the Mohr-Coulomb equation:

$$s = c' + \sigma' \tan \phi \quad (\text{eqn 2.2})$$

where s is the soil shear strength, c' is the soil cohesion, σ' is the effective normal stress on the shear plane and ϕ is the soil friction angle. In a different way, when the soil is permeated by fibres (synthetic or natural as in the case of roots), the displacement of soil, as a consequence of shear tension, generates friction between the soil particles and fibre surfaces, causing the fibres to deform and mobilized their tensile strengths. In such way, some of the shear tension can be transferred from soil to fibres, producing a reinforcement of the soil matrix itself.

If the soil is rooted, then the increased shear strength can be expressed as an additional cohesion:

$$s_r = s + c_r \quad (\text{eqn 2.3})$$

where s_r is the shear strength of soil reinforced by roots and c_r is the increase of shear strength due to presence of roots (or root cohesion). Assuming that roots are flexible, elastic and oriented perpendicularly to the slipping plane, when the soil layer moves and the roots within the shear zone bend, the tangential component of tensile strength directly counterbalances the shear force and the normal component increases the confining pressure. By further assuming that the soil friction angle is not affected, the additional root cohesion can then be defined as:

$$c_r = tR (\sin \delta + \cos \delta \tan \phi) \quad (\text{eqn 2.4})$$

where tR is the average mobilized tensile strength of roots per unit area of soil and δ is the angle of root deformation in the shear zone. Based on field observations and laboratory experiments, Wu et al. (1979) observed that for common values of δ and ϕ , the term $(\sin \delta + \cos \delta \tan \phi)$ varies between 1.0 and 1.3 and proposed a simplified form of equation 2.5:

$$c_r = 1.2 tR \quad (\text{eqn 2.5})$$

Even if all the above assumptions have not always been completely verified, field and laboratory direct shear tests confirmed the validity of the model (Waldron and Dakessian, 1981), which is commonly used to evaluate the contribution of roots to soil stabilisation (Abernethy and Rutherford, 2001, Roering et al., 2003, Schmidt et al., 2001, Wu and Sidle, 1995). The mobilised roots tensile strength per unit area of soil

(t_R) can be determined as the product of the average tensile strength of roots (TR) and the fraction of the soil cross-section occupied by roots (AR/A):

$$t_R = TR(AR/A) \quad (\text{eqn 2.6})$$

where the term AR/A is called root area ratio (RAR) and it can be determined by counting roots, divided into size classes within a given soil, and by measuring their cross-section.

Study conducted by Mickovski et al. (2007) on root behaviour during direct shear tests on root analogues in soil had confirmed that these mechanisms were closely related to the pullout tests. Figure 2.3 shows an example of root displacement which observed during this study for an array of three single analogue taproots with different inclination from the vertical crossing a shear plane. When the top of the shear box is displaced to the left, the analogue roots intersecting the shear plane mobilise tensile stress providing reinforcement of the shear plane.

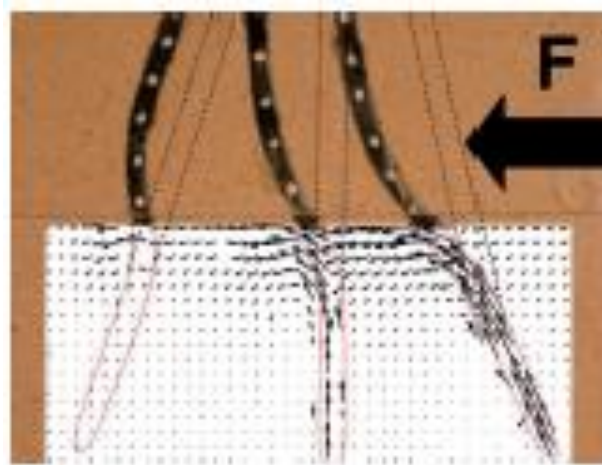


Figure 2.3: Deformation of analogue roots during shear in dry sand (Mickovski et al., 2007)

Depending on their orientation, the authors had concluded that the different amounts of tensile force were mobilised in the roots where roots with ‘favourable’ orientation (the root to the right on Figure 2.3) quickly mobilise their tensile resistance and started to pull out from the soil. However, the roots with less favourable orientation (the root to the left on Figure 2.3) needed larger displacement as they bent before experiencing significant tensile strains. This phenomenon shows that soil containing roots with a range of orientations can slowly mobilise reinforcement from roots even at large shear displacements. Table 2.4 summarized the root shear strengths for the selected shrubs and trees which have been measured by different investigators.

Table 2.4: Area and shear strength of roots (Wu, 2007)

No.	Site	Soil	Species	Depth (m)	Dia. (mm)	a_r	S_r (kPa)	θ (°)	S_r/a_r	Reference
(a) S_r estimated from A_r										
1	Cincinnati, OH.	Colluviums, Eden silty loam	Surar maple	0.50	<2.5	1.4×10^{-4}	5.7 ^a 4.3 ^b	90	4×10^{-4} 3.1×10^{-4}	Riestenberg & Sovonick Dunford
2	Maybes Valley, AK	Till and colluviums,	Sitka spruce, w. hemlock, Alaska cedar	0.10 to 1.00	<1.3	$3.7 - 10 \times 10^{-4}$ ^a	4.3-12.6 ^a	90	1.1-1.3	Wu
3						3.7×10^{-4}	5.0 ^b	90	1.30	Wu <i>et al.</i>
4	Whitehall Forest, GA	Residual, CL	White oak	1.30	15.0	30×10^{-4}		90		Barker
5	Hong Kong	Decomposed granite	Acacia candlenut, Chinese banyan	0-1.5	<1.0	$0.5 - 15 \times 10^{-4}$	0.5-30.0 ^d		1×10^4	Greenway
6	New Zealand		Willow & poplar cutting, 1 year old		<1.0	$A_c = 5.2 \text{cm}^2$				Hathaway
7	Netherlands		Marram grass	0.15	<0.3	$1.5 - 15 \times 10^{-4}$	1.5-5.0 ^d	0-180		Wu
8	Alps		Grass	0.25 to 0.75	<1	$2.0 - 8.0 \times 10^{-4}$ ^c	2.80	0-180		Schiechl
9					<2	6.0×10^{-4} ^c	6.00			Schiechl
10					<4	2.0×10^{-4} ^c				Schiechl
(b) S_r from in-situ shear tests										
11	Oregon	Slick rock-Preacher loam	Hemlock	0.30 to 6.00	<3	$10 - 80 \times 10^{-4}$	1.0-8.0		0.1×10^4	Wu <i>et al.</i>
12	California		Pinus contorta						0.1×10^4	Zieme
13	Japan	Loam	Alder			$0-2.0 \times 10^{-4}$	0-1.0		0.05×10^4	Endo & Tsuruta
14		Loam	Cryptomeria japonica 6 years old	0.50	<1	2.5×10^{-4}	4.00	60-120	0.6×10^4	Abe & Iwamoto
15	Thailand	Residual, SC-SM	Hopea odorata, Dipterocarpus alatus	0.50 to 1.00	<0.5	$1.0 - 2.2 \times 10^{-4}$	0.9-1.9	90	0.7-1.1 $\times 10^4$	Nilaweera
16	New Zealand	SM	Pinus radiata		<1.5	8.0×10^{-4}	1.90	27-127	0.2×10^4	Wu & Watson
17	Thailand		Vetiver grass	1.00	<0.2	1×10^{-4}	2.50		2.5×10^4	Hengchaovenich
(c) S_r from laboratory shear tests										
18	California		Barley ^e	0.30	<0.05	$0.2 - 0.8 \times 10^{-4}$	0.6-2.6		3×10^4	Waldron
19	Tamascal Ranch, CA	Castaic silty-clay loam	Chapattal ^e Grassland	0.20 to 0.45			0.6-3.0 0.9-2.4			Terwilliger
20	Israel	Chalk, clay	Alfaalfa	0.20 to 0.75	<0.3	3×10^{-3}	8		2.7×10	Operstein & Frydman

a: Calculated from measured σ_{ru}

b: Back-calculated from slope fail

c: Estimated from drawings of photographs of excavated roots

d: Calculated with $\sigma_{ru} = 10 \text{MPa}$

e: See Terwilliger, 1988 for species inventory

2.3.4 Root Cohesion

Cohesion is the shear strength or the force that binds together like particles in the structure of a soil. This force exists without any compressive stress. It is a component of shear strength of soil that is independent of interparticle friction.

In contrast, with the natural soil, soil-root composites however is different where the c' value is enhanced by c'_R therefore increase the strength properties of the soil. This would be appropriate for grass and shrub areas where fine root distribution with depth is consistent and easily defined. This is how the fine root network acts in a similar way to geosynthetic mesh elements. But for the larger tap and lateral roots of trees, the tensile reinforcement force elements within the analysis will be provided (Norris & Greenwood, 2006).

Some researchers (Wu et al., 1979, Waldron and Dakessian, 1981, Greenwood et al., 2004) have suggested that the reinforcing effect of vegetation can be considered in conventional slope design by adding an additional root 'cohesion' term, c_R , to the Mohr-Coulomb strength envelope for soil:

$$\tau_f = c' + c_R + \sigma' \tan \phi' \quad (\text{eqn 2.7})$$

Wu et al. (1979) recommended that the root cohesion term,

$$c_R = 1.2 \sigma_t A_r \quad (\text{eqn 2.8})$$

where σ_r is the tensile strength of the roots and A_r is the root area ratio defined as the area of the root crossing the shear plane divided by the total cross-sectional area of the shear plane.

2.4 Root Morphology

2.4.1 Root System and Pattern of Root Growth in Trees

Root is the organ of a plant body that typically lies below the surface of soil. The major parts of root system as could be observed in Figure 2.4 and there are basically two categories of root systems recognized as tap root and fibrous root. The function of root generally is to absorb water and dissolved mineral salts from the soil, to anchor the plant, as well as to store extra food made during the process of photosynthesis.

Tap root system is the primary root which is prominent and has a single, dominant axis, with the numeral lateral roots extending outward and grows vertically downward. It is most common in dicots and a persistent taproot system forms when the radical keeps growing while the smaller lateral roots form along the taproot.

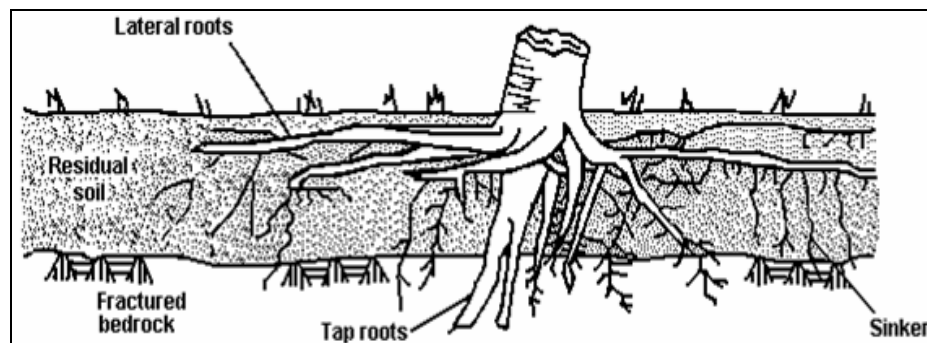


Figure 2.4: Root geometry of tree (Mafian, Huat & Ghiasi, 2009)

The architecture of taproots was identified to be strongly influenced by the characteristics of soil in which it is grown. For example, deep rich soils favour the development of vertical taproots in many oak species while clayey soils promote the growth of multiple taproots. Differently with fibrous root system, it is the primary root which is not dominant and the whole root system is fibrous and branches in all directions. It is most common in monocots and the main function of this fibrous root is to anchor the plant.

The differences morphology in root systems usually closely connected to the physiological functions of the particular components of the roots. They may be characterized base on the number, length, diameter of the particular root components, direction of extension of seminal, seminal adventitious and nodal roots and also the branching (rooting angle between plant axis and root) as explained by Gregory et al. (1987), and Kono et al. (1987).

Therefore the strengthening effect provided by different types of root systems of plants to soil stability are dissimilar via the fiber reinforcement near the soil surface in where they were grown plus the competency in binding soil structure through root anchorage. Figure 2.5 shows the common patterns of root growth in trees (after Yen, 1972) as provided with the description of those root growth pattern as shown in Table 2.5.

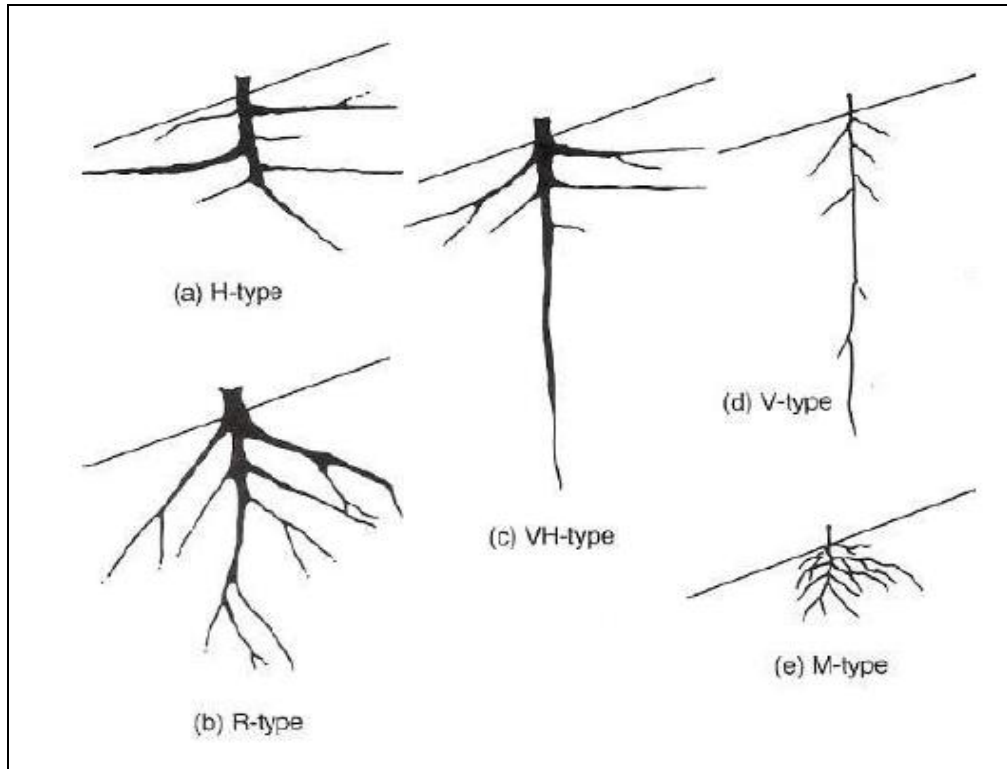


Figure 2.5: Patterns of root growth in trees (Yen, 1972)

Table 2.5: Description of root growth pattern in trees (Yen, 1972)

Pattern of root growth	Maximum depth of root	Extension direction	Root matrix beneath soil	Remarks
H-type	Moderate	Horizontally Lateral roots extend in wide	60% found in the top 60 cm	Beneficial in soil reinforcement, soil stabilization and wind resistance
R-type	Deep	Obliquely or perpendicular to the slope	20% found in the top 60 cm	
VH-type	Moderate to deep	Vertically and Horizontally Strong tap root with widely extended lateral roots	80% found in the top 60 cm	Beneficial in soil stabilization and wind resistance
V-type	Moderate to deep	Vertically Strong tap root with lateral roots		Wind resistance
M-type	Deep	Vertically Profuse and massive main roots with narrow lateral extend	80% found in the top 60 cm	

2.5 Modes of Root Failure

Based on the study conducted by Norris (2005), there were three different modes of failure which related to the soil-root relationship responded in the shape of roots and the curve of root failure as observed in hawthorn roots. Root length and the type of root branching had identified in giving such a major influence to the way of root failure (Greenwood et al., 2004, Norris, 2005). From the study it has been pointed out that roots which have no branches has observed to tend to fail in tension and pulling straight out of the ground with minimal resistance (Figure 2.6). For this type of root pattern, failures occur rapidly at a weak point right after the root reaches its maximum pullout resistance. The root easily slips out of the soil due to the gradual tapering (progressive decrease in root diameter along its length) which means that as the root is pulled out, it is moving through a space that is larger than its diameter and finally results in no further bonds or interaction with the surrounding soil.

However it is different for roots with multiple branches, where the roots generally tend to fail in stages as each branch breaks inside the soil. These roots can be separated into two different groups. First are those that initially reach their maximum peak force, maintain a high force and progressively decrease as the root branches fail after a significant strain. In this case, forked roots require a greater force to be pulled out as the cavity above the fork is thinner than the root which is trying to move through the cavity. This result in deformation of the soil as the root moves through the soil.

Another failure that could be observed in multiple branches is those that break with increasingly applied force. Roots that have multiple branches or forked branches also can undergo tensile failure but predominantly fail in stages as each branch breaks within

the soil. These roots break with increasingly applied force in stages in the form of stepped peaks corresponding to the progressive breaking of roots of greater diameters. The root progressively releases its bonds with the soil until final tensile failure. Table 2.6 shows the examples of root failure curves and associated root morphologies obtained from the study conducted by Norris, (2005).

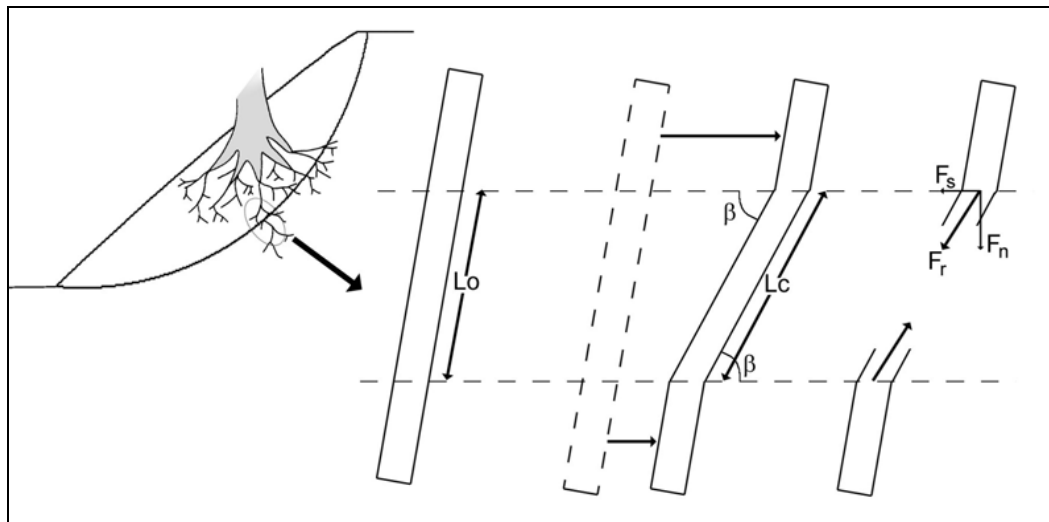


Figure 2.6: Schematisation of root reinforcement and the failure of a root during soil displacement. A root passing a shear zone—indicated by the dashed horizontal lines—is extended from its original length L_0 — L_c . This generates the root force $F_r = \sigma_r \cdot A_r$ can be resolved by the angle of root inclination β into components normal and parallel to the shear plane, respectively, F_n and F_s (Norris, 2005)

Table 2.6 Examples of root failure curves and associated root morphologies
(Norris, 2005)

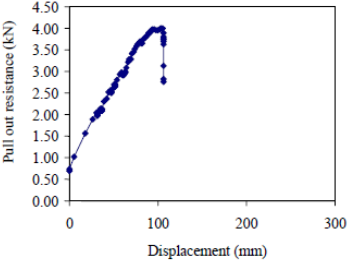
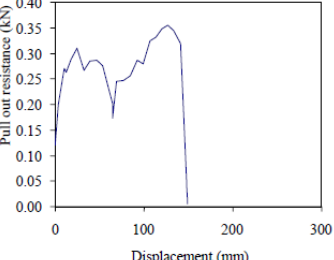
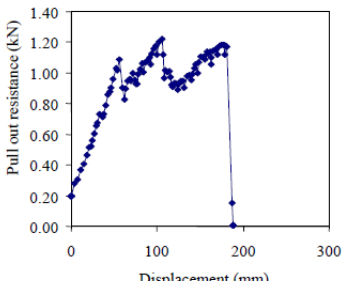
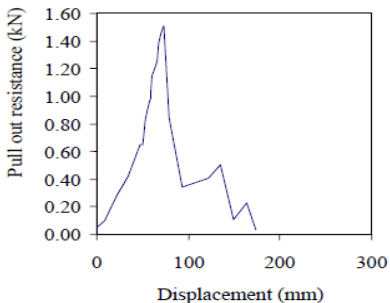
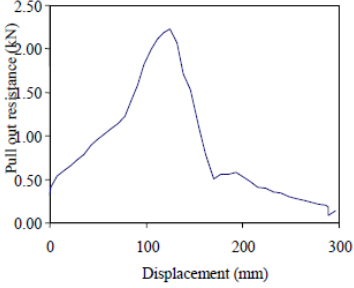
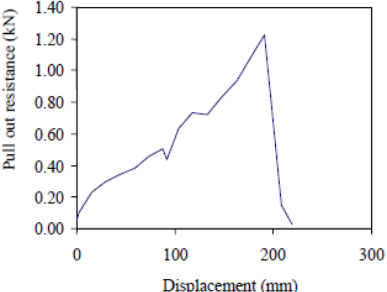
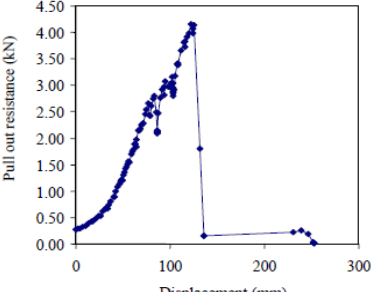
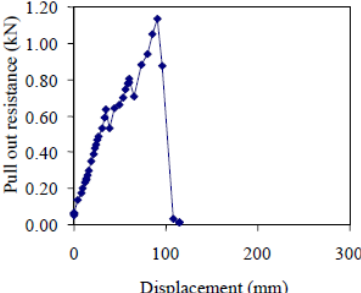
Failure curve	Root morphology	Suggested failure type
	 <p data-bbox="901 705 997 739">d = 26.7 mm $\ell_T = 1610$ mm</p>	<p data-bbox="1141 593 1404 694">Type A failure. Root is long and with no or few branches.</p>
	 <p data-bbox="901 1041 997 1075">d = 7.4 mm $\ell_T = 745$ mm</p>	<p data-bbox="1125 840 1428 996">Type B failure. A rapid rise in resistance with a maintained resistance before an abrupt failure. Root is branched.</p>
	 <p data-bbox="901 1400 997 1433">d = 26.8 mm $\ell_T = 762$ mm</p>	<p data-bbox="1125 1265 1428 1377">Type B failure. A maintained high resistance before failure. Root is branched.</p>
	 <p data-bbox="885 1724 997 1769">d = 15 mm $\ell_T = 362$ mm</p>	<p data-bbox="1141 1624 1412 1713">Type B failure. Peaked failure curve as forked roots break.</p>

Table 2.6, continued

Failure curve	Root morphology	Suggested failure type
	 <p data-bbox="906 622 1018 667">d = 21.3 mm $\ell_T = 2010$ mm</p>	<p data-bbox="1150 517 1406 607">Type B failure. Peaked failure curve as forked roots break.</p>
	 <p data-bbox="906 949 1018 994">d = 11.2 mm $\ell_T = 885$ mm</p>	<p data-bbox="1150 792 1406 882">Type C failure. Stepped failure. Root is multibranched.</p>
	 <p data-bbox="906 1328 1018 1373">d = 28.2 mm $\ell_T = 1167$ mm</p>	<p data-bbox="1150 1211 1406 1301">Type C failure. Stepped failure. Root is multibranched.</p>
	 <p data-bbox="906 1727 1018 1771">d = 19.6 mm $\ell_T = 245$ mm</p>	<p data-bbox="1150 1592 1406 1682">Type C failure. Stepped failure. Root is multibranched.</p>

2.6 Pullout of Analogue Roots

The use of analogue roots as a new practice for the quantification of root reinforcement has gained a greater acceptance in these recent years especially in the measurement of root pullout resistance. These artificial root models are used as to replace and simulate real roots of whole plants like grasses, bulbs, crop plants and trees (Ennos, 1989, 1990, Easson et al., 1995, Stokes et al., 1996, Yoshioka et al., 1998, Bailey et al., 2002, Mickovski and Ennos, 2003, Mickovski et al., 2005, Mickovski et al., 2007). The use of this physically-based modeling has its own advantages especially in providing a solution into the detailed mechanisms of soil root composites that arose due to the variation of the natural biology as well as various unseen processes below the ground. Although the application of this method does not perfectly simulate the physical characteristics and behaviours of the real roots, but throughout this way, researchers could be able to save a lot of their time instead of waiting for a certain period for the trees and plants to grow up.

Stokes et al. (1996) conducted a simulation study towards the investigation on the influences of architectural and anchorage efficiency of root systems using artificial root models subjected to axial force. Artificial models of root systems with different topologies and branching angles made out of copper coated steel wire were developed throughout this study. The material chosen however was criticized for their artificiality since steel wire is very unlike woody material. In this study, results had verified that uprooting resistance increased with the increment of sand depth (Waldron and Dakessian, 1981). As deeper the root models were embedded below the soil layer, therefore more resistance the root systems to pullout due to the increase in friction and hence cohesion between the sand particles (Mattheck, 1993). Furthermore, the root

systems with branched structures also were identified as more difficult to uproot at greater depths than those without branches. The influences of lateral length also could be observed throughout this study where the longer the laterals side, the more resistance the root systems to pullout. But, out of all findings, the authors had concluded that root depth in soil as the most influenced factor in determining soil-root anchorage.

By similar principal and several additional variations, Mickovski et al. (2007) conducted a study on the influences of material stiffness, branching pattern and soil matric potential to resist pullout force. Different materials were used as to embrace a wide range of root stiffness as well as the architecture of root analogues (Figure 2.7). Viton O–ring rubber was used for modelling the more flexible herbaceous roots while linden wood dowels were used to model the harder, lignified roots of shrubs and trees.

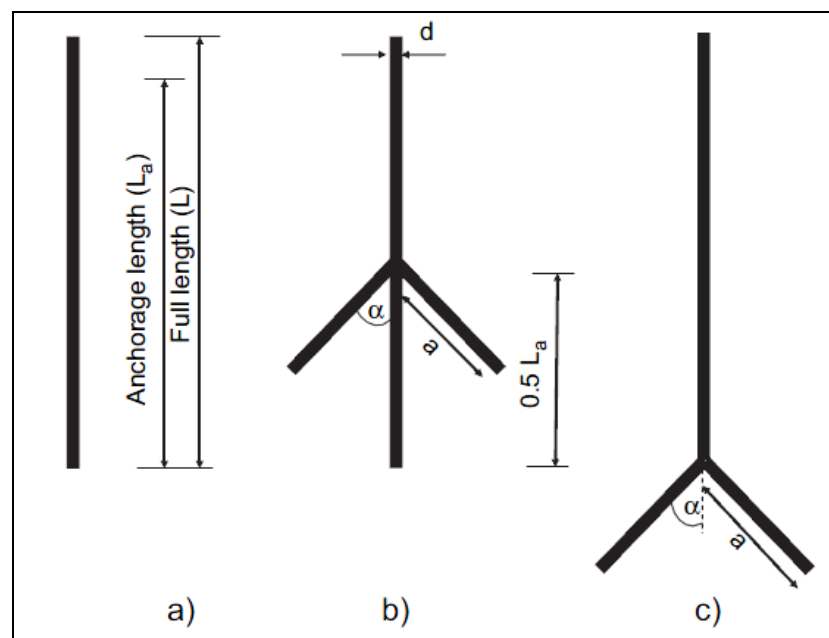


Figure 2.7: Artificial root model with different branching patterns and angles (Mickovski et al., 2007)

According to the study, it was revealed that the maximum pullout resistance of roots in sand was highly depended on the material stiffness, root architecture and the pore water suction of the sand. In terms of root architecture, it was observed that the maximum pullout resistance increased in the order of tap, herringbone and dichotomous root pattern where dichotomous root pattern was shown to have the highest pullout resistance compared to other root patterns for all root and soil conditions (Table 2.7). It occurred due to the influences of the existence and position of the lateral roots which fitted out to each of these root models where deeper these lateral roots were located beneath the soil layer, so the harder the root models to be uprooted.

Study also had recognized the influence of the material stiffness towards the pullout resistance. More rigid model roots were shown to have a greater pullout resistance than more flexible root models. Through the Particle Image Velocimetry, (PIV) technique which used throughout this study, wooden model roots had observed to mobilize their interface shear strength simultaneously over the whole root even at very small displacements therefore offering more resistance to pullout.

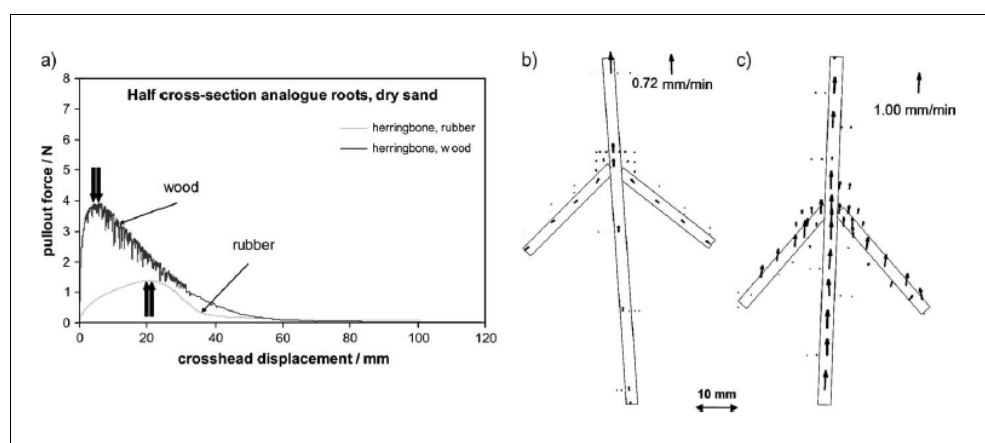


Figure 2.8: Representative behaviour of rubber and wood root models during pulled out (Mickovski et al., 2007)

Table 2.7: Maximum pullout resistance of the model roots (Mickovski et al., 2007).

Root pattern	Peak pullout force (N)	Extension at peak (mm)	Peak pullout force (N)	Extension at peak (mm)
Rubber	Dry sand		Wet sand	
Tap	1.03	7.36	2.96	59.18
Herringbone	1.79	10.67	6.43	70.95
Dichotomous	2.57	44.76	7.35	161.00
Wood	Dry sand		Wet sand	
Tap	1.08	1.25	7.18	3.36
Herringbone	3.66	3.27	17.81	5.76
Dichotomous	7.76	8.27	31.47	7.55

In a different way, the rubber root models mobilized their interface shear strength progressively with depth with the flexible laterals bending to follow the path of least resistance (Figure 2.8).

The same study was also conducted by Hamza et al. (2007) however with a slightly different methodology used. Two single non-branched root systems were investigated which was for a simple straight and bent root models, (root analogue 1a and 1b) with an additional two or four lateral branches, (root analogue 3 and 4) (Figure 2.9). Figure 2.10 shows photographs taken during the pullout of root analogues with single pair of laterals. It can be seen that the first pair of laterals is pulling out of the soil and a surface soil plug is lifting above the laterals.

During the axial displacement, there is a clear difference between the axial forces required to pull the branched root analogues from the ground compared to the non-branched root analogue. Taproot systems with no laterals had shown in generating the lowest pull-out capacity which is achieved at the smallest displacement, whereas the

system with two pairs of laterals required the largest force to be pulled out of the ground as the second pair of laterals contributes to the root analogue capacity (Figure 2.11).

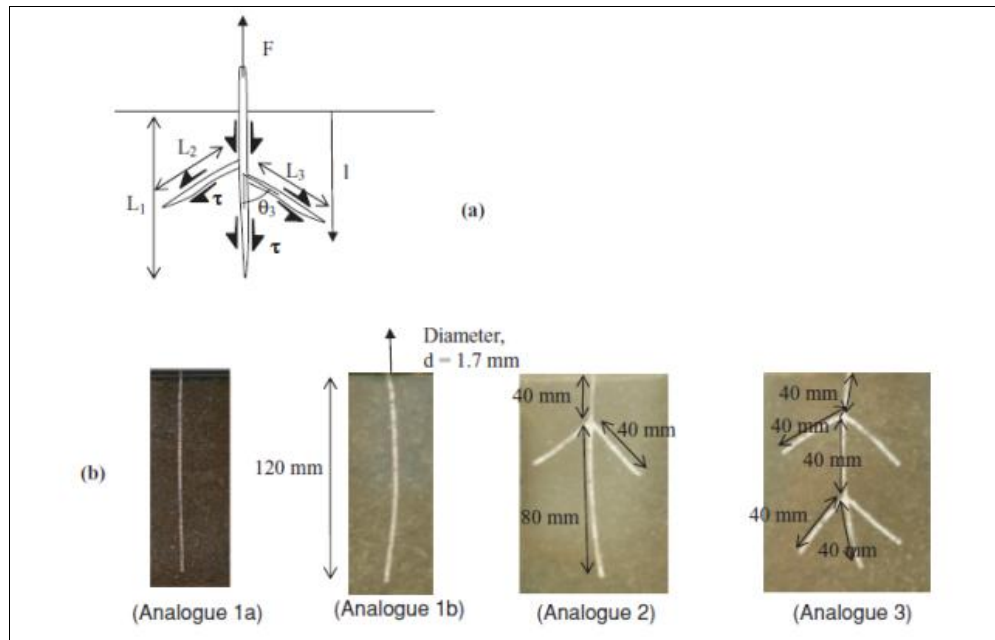


Figure 2.9: Applied mechanical loadings to plant root systems (Hamza et al., 2007)

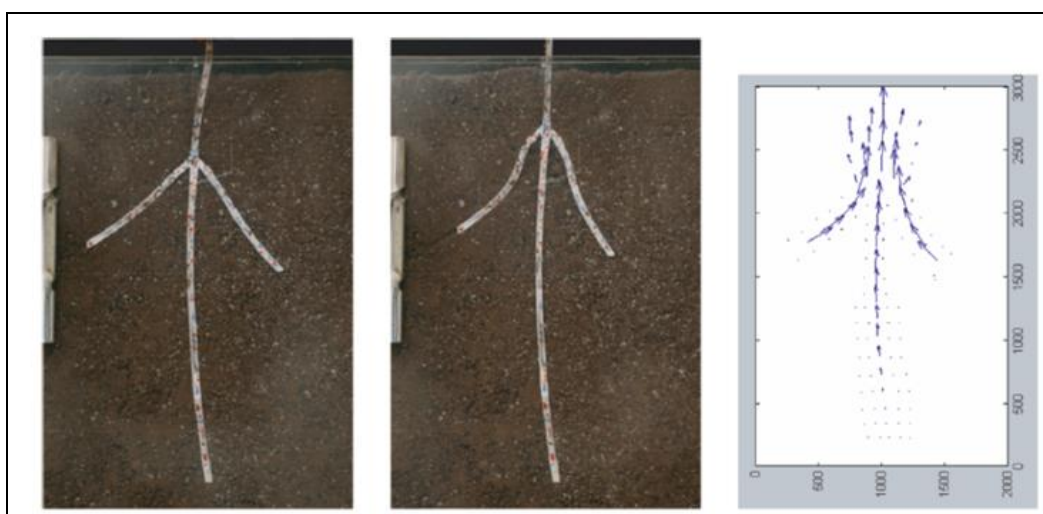


Figure 2.10: Analysis of root analogue and soil movement around the model (Hamza et al., 2007)

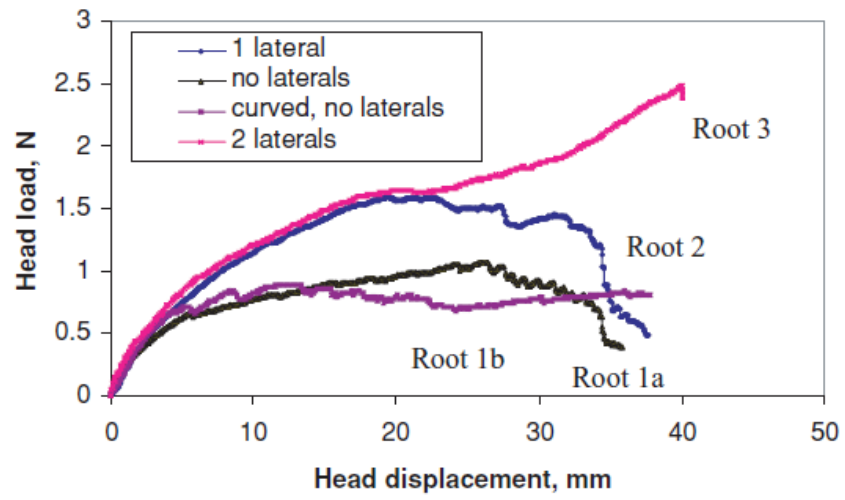


Figure 2.11: Head load-displacement responses for root-analogue (Hamza et al., 2007)

CHAPTER THREE

RESEARCH MATERIALS AND METHODS

3.1 Introduction

This chapter begins with the research design and programmes to explain the relevance of the concepts applied as well as the methods utilized throughout this pulling out study predominantly in the fabrication of pulling out machine and the development of physical root models. It is then continued by the research materials part that structurally explained on the recommended ideas in the decision-making process of research materials selection that differentiated this study from previous similar investigations. Finally, this chapter pursued with the explanation of the research test, elaborating in details the steps of pulling out procedures for the readers' better comprehension.

3.2 Research design/ programme

3.2.1 The Artificial Root Models

Many root simulation models have been developed for plants embracing a wide range of approaches. A basic difference in approach exists between those models that use architectural information to simulate the growth of individual roots within the root system and those that do not. In this study, root architecture has become the primary

focus of the study where the analogue root models were subjected to external pullout forces controlled by several other root properties.

Simplifications of the root form were conducted to provide axially symmetrical root systems for the representation of root behaviour to make the root models less vulnerable to other external factors. As based on the actual pattern of real roots, there are two kinds of branching that can be distinguished: either the apex continues to grow straight and produces second-order lateral branches (Lloret & Casero, 2002) resulting in herringbone-like systems as described by Fitter (1987), or two terminal apices appear and replace the former single apex at the tip of the root as found in dichotomous-like structures (Figure 3.1). The actual forms observed in reality however, do not result from these development strategies only as growth is also punctuated by other biological phenomena but from a purely geometric point of view, most of the root morphologies observed in nature can be seen as a combination of these basic characteristics.

Therefore based on the findings, artificial root models in this study have been developed as based on the explained theoretical concept as similarly proposed and developed to physical root models by Mickovski et al. 2007. It is necessary to understand the behaviour of the simpler system before attempting to understand the behaviour of more complex real root systems. Understanding the mechanics of simpler root systems will lead to an increased insight into the real root systems in terms of both their load capacity and biological design. This knowledge can be incorporated into a breeding technique in order to produce a good quality of clones towards the selection of suitable and high potential soil-bioengineering plants which will be a great economic value on exposed sites with poor soils (Stokes et al., 1996).

In terms of the basis of tap and lateral root lengths applied in this study, the specifications were basically related to the dimension of the tank parameters due to the variation of size and dimension of real roots. The tank was designed to simulate a small portion of soil area so that more specific studies can be carried out in detail.

The artificial root models studied are divided into three major root pattern categories comprised of dichotomous structure, herringbone structure and the combination structure. Each of these root patterns consist of one individual tap root with the diameter of approximately 10 mm and two or more lateral roots with the diameter of approximately 8 mm. These lateral components were welded to the vertical elements using identical welding material of the root models to increase the rigidity of the joint. This is similar to the bifurcating points in real root systems that are usually more rigid than the rest of the root (Stokes & Mattheck, 1996).

Although root models developed were supposed to perform as one continuous body in this simulation work, unfortunately the cost to fabricate mould for the root models to be cast is costly, especially for tapered aluminum root models. Therefore, welding joint method was thought as the best approach presently where more specific studies are needed to overcome this limitation and scarcities in future studies.

The differences between these root models varied from the length and angle of the lateral roots joined to the tap roots (Figure 3.2). The descriptions for each root pattern studied are narrated in Table 3.1. While dichotomous and herringbone root patterns were developed with a pair of lateral roots, the combination of root patterns however was developed with 2 pairs of lateral roots which are placed at 45 ° and 90 ° to the taproot respectively.

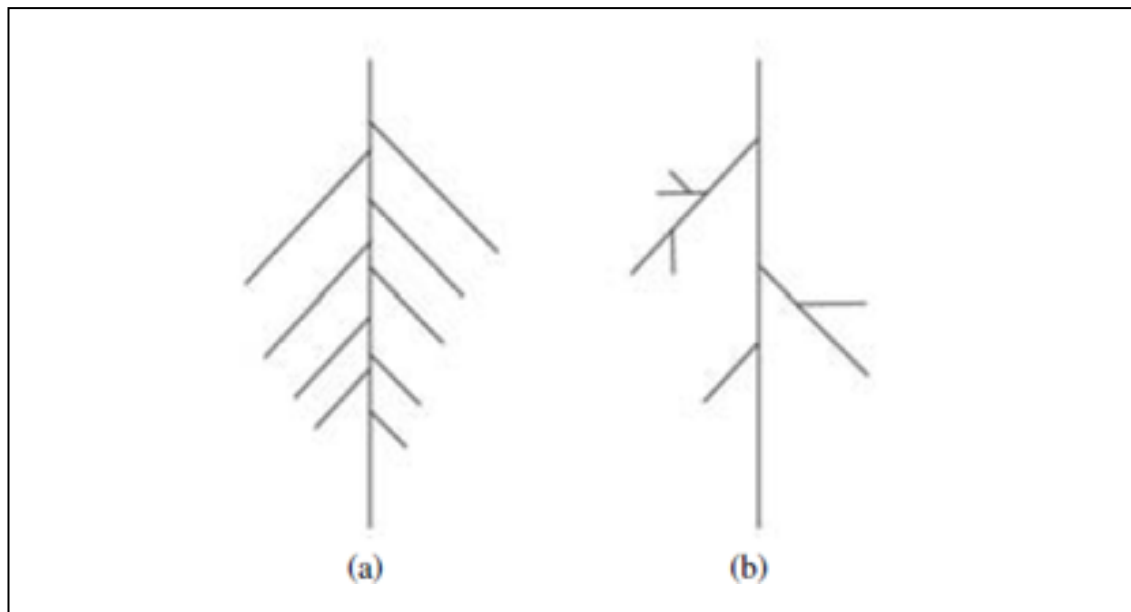


Figure 3.1: Diagram showing the distinction between (a) herringbone, and dichotomous branching pattern. (Modified and reproduced with permission from Fitter et al., New Phytologist; New Phytologist Trust, 1991)

Table 3.1: Description of artificial root model pattern

Structure Type	Root model name	*Angle of lateral roots (°)	Length of taproot (cm)	Length of lateral roots (cm)
Taproot	T1	0	60	15
Dichotomous I	D1	45	30	15
Dichotomous II	D2	90	30	15
Herringbone I	H1	45	60	15
Herringbone II	H2	90	60	15
Combination I	C1	45 & 90	60	15
Combination II	C2	90	60	15

For a better insight to the development of the physical root models studied throughout this thesis, Tables 3.2, 3.3 and 3.4 denote the diagram of the artificial root models for each different case studied. Table 3.2 demonstrates the rigid artificial root model made out of aluminum rods with different branching patterns. The results obtained throughout this study will be compared with the results obtained from other cases studied.

Table 3.3 indicates the artificial root models designed in tapered. The pattern and material for these tapered root models were similar for the development of the aluminium artificial root models in previous studies. However, the diameter along the root length was gradually made in tapered (Figure 3.4) contradictory with the aluminium root models in which the diameter along the root length was uniformly developed (Figure 3.3) to represent the reduction in the root surface area.

Finally, table 3.4 reflects the flexible artificial root models made out of the High Density Polyethylene (HDPE) rod. The branching patterns of the artificial root models for this case study were developed similarly to the aluminium root models. However, the material stiffness was different.

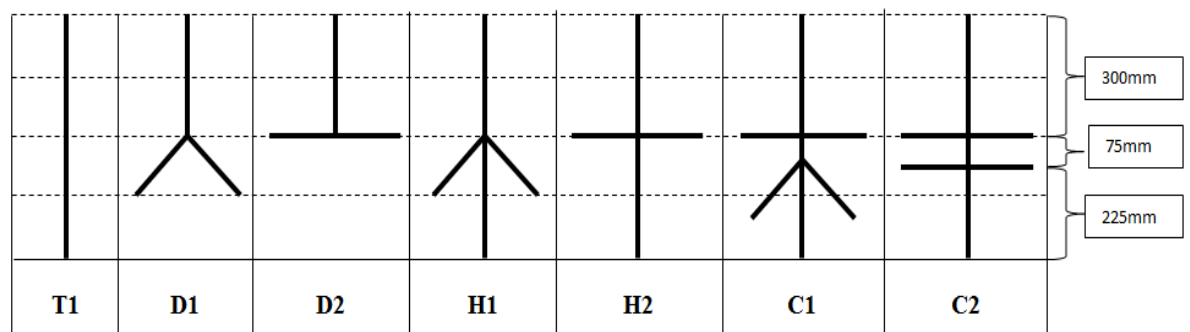
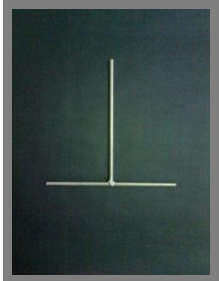


Figure 3.2: Various types of artificial root model pattern

Table 3.2: Uniform aluminum artificial root model

Structure Type	Diagram	Structure Type	Diagram
Dichotomous I (D1)		Dichotomous II (D2)	
Herringbone I (H1)		Herringbone II (H2)	
Combination I (C1)		Combination II (C2)	
Taproot (T1)			

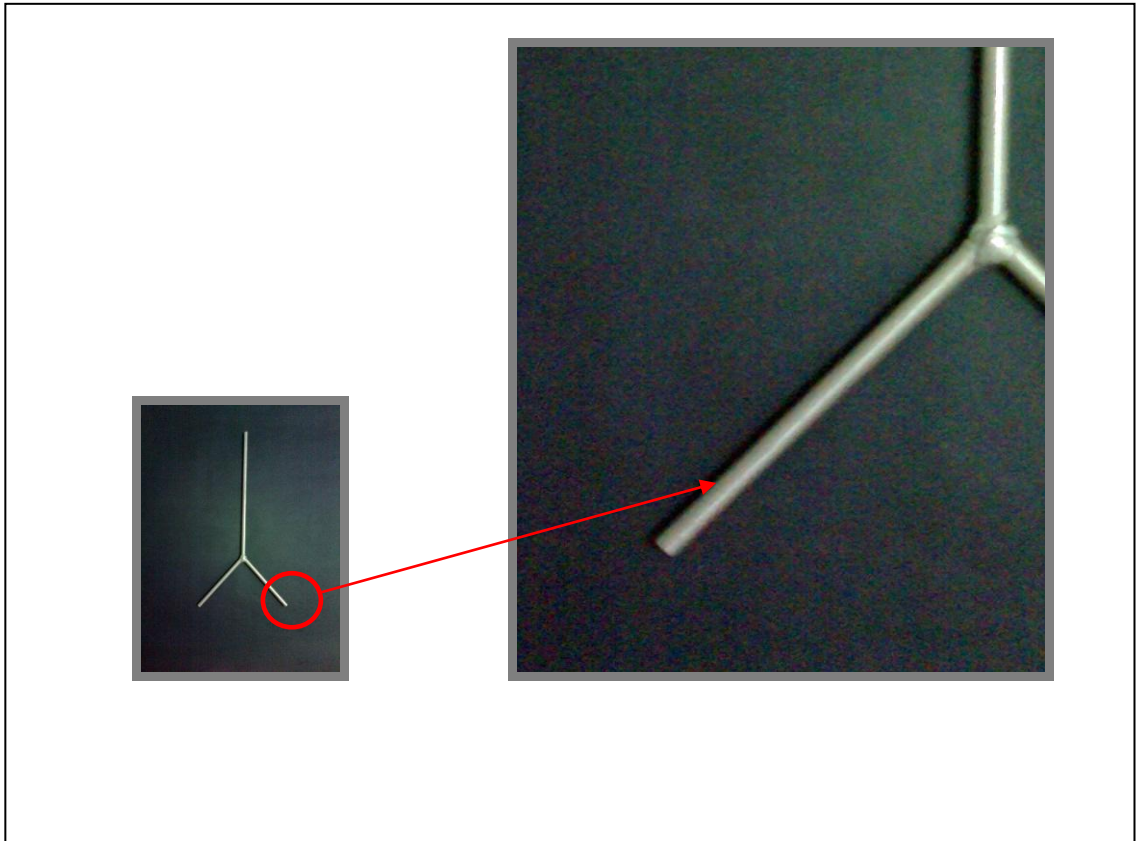
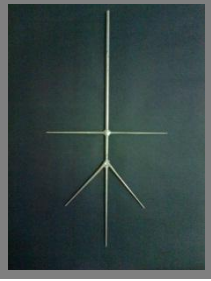
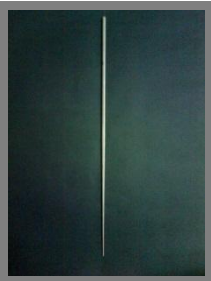


Figure 3.3: Uniform aluminum artificial root model with the diameter along the root length was uniformly developed

Table 3.3: Tapered aluminum artificial root model

Structure Type	Diagram	Structure Type	Diagram
Dichotomous I (D1)		Dichotomous II (D2)	
Herringbone I (H1)		Herringbone II (H2)	
Combination I (C1)		Combination II (C2)	
Taproot (T1)			

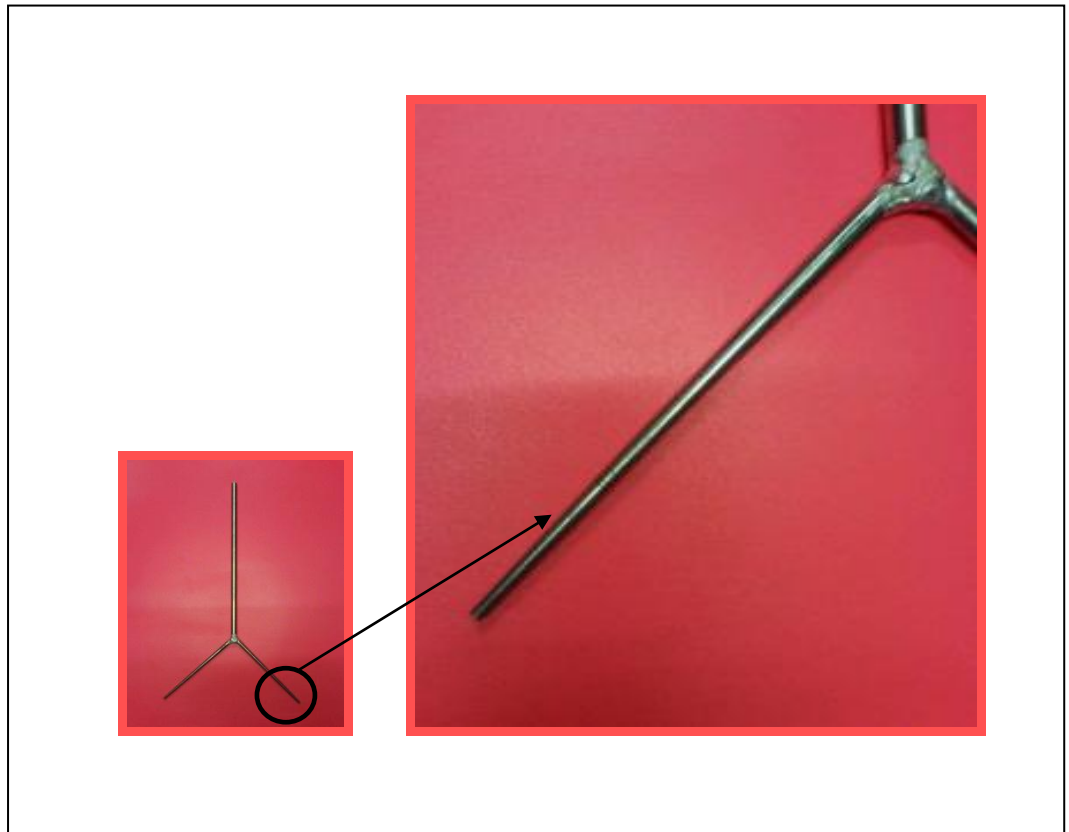
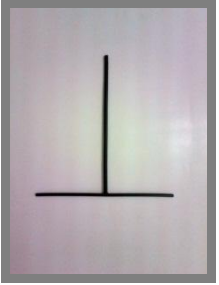
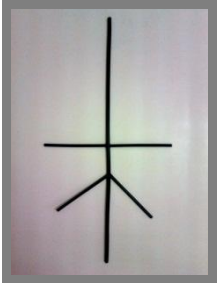
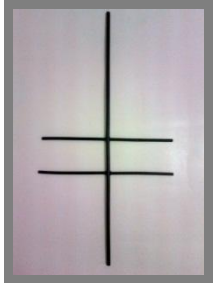


Figure 3.4: Tapered aluminum artificial root model with the diameter along the root length was gradually tapering

Table 3.4: Flexible artificial root model

Structure Type	Diagram	Structure Type	Diagram
Dichotomous I (D1)		Dichotomous II (D2)	
Herringbone I (H1)		Herringbone II (H2)	
Combination I (C1)		Combination II (C2)	
Taproot (T1)			

3.2.2 Embedment for Root Models

The root model was set up on frame hanger where the centre point of the upper laterals of root model was located at 0.5 m of a tank depth of 1 metre (centre of the tank). The tank was then filled up with sand approximately 60% of the tank capacity based on the research needs. The depth of sand embedment therefore ranged from 0.1 m up to 0.4m from the root tips to the sand surface depending on the physical root pattern which is commonly found in grasses with shallow rooting depth.

Grasses have been purposely studied due to their fast growth to offer dense protective ground cover. Due to the meristem being at ground level, moderate damage to the plant does not cause lasting damage and fast regrowth can occur. From this point of view, we therefore concerted in giving additional focus in minimizing soil erosions through the application of grasses on geotechnical structures and unstable slopes to look into an advanced prevention from such critical failures to occur.

3.3 Research Materials

3.3.1 Material for the Artificial Root Models

Studies in the past have publicized on the various materials used in the development of artificial root model like rubber, woods, plasticine and steel as well as plastic materials in regards to pullout testing. Therefore by a similar principal, two contrasting materials have been chosen to embrace a wide range of root stiffness throughout this laboratory investigation. There are aluminium rods representing the harder and stiffer root models while the High Density Polyethylene (HDPE) rods were used to represent more flexible

root models. Although both materials employed were not exactly simulating the strength of real roots, it was assumed that the strengths of real roots are located between the strength of these two extreme points.

a) Aluminum

Aluminium is basically a soft, durable, lightweight, malleable metal. The strength yielded by pure aluminium is about 7–11 MPa, while aluminium alloys may yield strengths ranging from 200 MPa to 600 MPa. Aluminium has about one-third of the density and stiffness of steel. It is ductile and easily machined, cast, drawn and extruded, making it one of the most suitable materials to simulate stiff roots.

b) High Density Polyethylene (HDPE)

High Density Polyethylene (HDPE) is the high density version of polyethylene plastic. The HDPE has little branching, giving it stronger intermolecular forces and tensile strength than lower-density polyethylene. It is also harder, more opaque and able to withstand somewhat higher temperatures (120 °C for short periods, 110 °C continuously). The tensile strength of the HDPE is about 37 N/mm², a good modeling material which is close to the tensile strength of real roots.

3.3.2 Material for Soil Medium

Soil specimens were used to embed the artificial root model to cause the root specimen or model to resist uprooting forces when subjected to external vertical forces. Different types of soil will give different maximum pullout resistances of the root model due to

the different properties of soil medium. For example, the sand which is commonly used in nearly all related studies whether fine or coarse graded, or in other cases, wet or dry cases for testing (Mickovski et al., 2007). Throughout this study, sand medium has been decided to be used due to the sand natural particles distribution that makes it easier to be compacted and removed for another root model to be pulled out compared to other types of soils.

3.3.3 Material and design of pullout tank

Throughout this study, the circular tank was chosen as the best shape selected for the development of pullout container due to the greater rigidity of their walls under internal lateral pressure instead of using rectangular tank which provided when only small capacity tank is required. Due to the proposed artificial root models also, the circular tank was observed to be large enough to avoid boundary effect on the test results since root models were developed axial symmetrically (Walker, 1964) as equivalent to the behaviour of the symmetrical circular tank.

Boundary effects are theoretically most significant in regions where the soils behavior is most changed due to excessive pore-pressures, whether this is an attenuation of accelerations due to the loss of strength of loose soils, or acceleration spikes transmitted by the dilation of dense soils. It should be taken into consideration since it will influence the root-soil frictional resistance, soil plastic flow around the root-soil plate and temporal changes in soil properties. In nature, the boundary condition which influence uprooting includes the obstacle in the soil e.g. stones or bedrock, changes in soil density and waterlogging, resulting to the death of root tips (Gucchi et al, 2004). However, the equipment is provided with drainage valve that allows future similar

testing to be done on saturated sandy soils while the effects of boundary condition need to be taken into account.

3.4 Research tests

3.4.1 Soil Property Test

Sand was used as a soil medium in this investigation. In order to investigate the properties of the sand used, a range of test was carried out as follows:

(a) Dry Sieving test

Dry sieving test (Figure 3.5) was carried out in accordance with **BS 1377: Part 2 1990: Clause 9.2**. The main objective of this test is to determine the classification of the sand used using particle size analysis. Before sieving, the sample is oven dried for 24 hours to ensure the dryness of the particles.

(b) Particle density

The objective of this test is to determine the density of non-cohesive soil containing particles finer than 20 mm. It is carried out in accordance to the **BS 1377: Part 2: 1990: Clause 8.3**.



Figure 3.5: Sieving machine

(c) Compaction test

Compaction test was carried out in accordance to the **BS 1377: Part 2: 1990: Clause 3.3**. The objective of this test is to determine the relationship between dry density and moisture content. Compaction with vibration hammer and British standard compaction mould is used in performing this test (Figure 3.6).



Figure 3.6: The automatic soil compactor



Figure 3.7: Shear box test machine

(d) Direct shear test

The objective of this direct shear test is to determine the shear strength, friction angle and cohesion of sands which used as a soil medium in this study when optimum moisture content is added. The apparatus used for this test is the laboratory shear box (Figure 3.7).

3.4.2 Mechanical Test

(a) Tensile test

Tensile test is used to determine the mechanical properties of the materials chosen. In this test, a piece of material is pulled until it fractures. During the test, the specimen elongation and applied load is measured. Strain and stress are calculated from these values, and are used to construct a stress-strain curve. From this curve, the elastic modulus and yield strength are determined. The highest load in the tensile test gives the



Figure 3.8: Universal Tensile Machine (INSTRON 5582)

tensile or ultimate strength. These quantities indicate the ductility of the material. Figure 3.8 shows the Universal Tensile Machine (INSTRON 5582).

3.4.3 Pullout Test

3.4.3.1 Pullout Test Apparatus

(a) LVDT transducer

LVDT transducer (Figure 3.9) was used to measure the displacement during the pullout test in unit of mm. Before the tests get started, the calibration step has to be carried out in order to ensure the accuracy of the LVDT transducer. Calibration on the equipment to is necessary to reduce the errors and increase the accuracy of the test.



Figure 3.9: LVDT transducer

(b) Data Logger

Data logger was used as to record the data needed throughout the experiments. The data logger consists of 9 channels, where it can record 9 different readings simultaneously. However, only two channels were needed to measure the vertical pullout forces and the axial displacement of the root models during the pullout tests. Data logger consists of floppy slot for us to insert diskette for data recording. Other than that, the reading can be printed out straight away for checking purpose. Most importantly, the interval of each time a data is recorded can be set as 10 or 15 seconds and the data logger will keep on functioning until we stopped it. This way, it saves us a lot of time and conveniences during the running of a test that required more than an hour to be completed.

(c) S- Beam Load Cell

S-Beam load cell with capacity 5kN was used in this study to measure the pullout force which applied during the test. Before this load cell is connected to the data logger for force measurement, it has to be calibrated first (Appendix A).

(d) Pullout Machine

Figure 3.10 demonstrates the pullout machine which was firmly fixed with various components such as the vibrator, controller, motor, cylinder tank, frame hanger, grip and the opening. The dimension of the cylinder tank is 0.8 m in diameter and 1 m in height. The controller (Figure 3.11) which is fixed to the machine functions in controlling the frame hanger to move upward or downward with a maximum rate of 1.5 mm/min. The rate of motion can be reduced by pressing the “downward” button. To begin the pullout process, the “FWD/REV” button has to be pressed to indicate which direction of frame hanger it has to move to. For “FWD”, it indicates the downward direction while “REV” denotes the upward direction.

As for the vibrator (Figure 3.10), the number displayed on the screen indicates the ongoing applied vibration rate. As the number increases, the vibration rate will be stronger and this means that the sand will be denser. However, in this test, vibration could affect the pullout results as it will cause the soil medium to be densely packed and hence compacted. For this test, the vibration duration is set to 15 minutes with a vibration rate of 60 Hz shown on the screen.

The motor is located on top of the tank and connected to the S-Beam load cell and frame hanger. While the frame hanger serves as a holder, the barrel was set up and the wedge was installed where both components were connected to the load cell system by two steel rods (Figure 3.12). Just before fastening the nuts, the barrel and wedges must be positioned around the crown of the root models. Appropriate wedges were chosen depending on the size of the crown. This is vital to prevent a slippage between the wedges and root models surface.



Figure 3.10: Laboratory pullout machine with specially designed wedge and barrel system

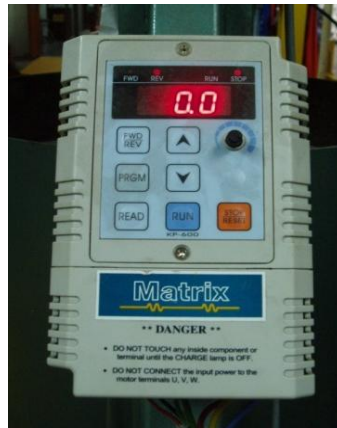


Figure 3.11: Controller and vibrator



Figure 3.12: Wedge and barrel

3.4.3.2 Procedures of Pullout Test

Before the test was carried out, the root model was set up on the frame hanger where the centre point of the root model was located at 0.5 m of the tank (centre of the tank) and after that, the tank was filled with sand at around 60% of the tank capacity based on the research needs. The vibrator was then switched on for 15 minutes with a constant rate, 60 Hz. Every time a new session of pullout test need to be conducted, the compacted

sand should be removed through the opening (Figure 3.13) and the same sand mixing procedure is repeated on another root model which needs to be pulled out. The tests for each of the root models studied were repeated three times with three similar model replicates in order to ensure the accuracy of pullout results obtained since the results varied because the experimental techniques differed from an author to another and the shape of the root systems and their topology were not usually taken into consideration. Figure 3.14 demonstrates the model layout of root model in tank for clearer understanding of the setup.

Right after the soil preparation was done, the transducer was set on the top of the tank with the tip in contact with the frame hanger while the load cell and transducer are connected to the data. The interval of the time taken by each set of data is set to be 15 seconds. By pressing the “RUN” button on the controller and the “start” button on the data logger simultaneously, the pullout test begins. The test can be stopped until the displacement reaches 100 mm. The graph of the pullout load against displacement is plotted.



Figure 3.13: The opening

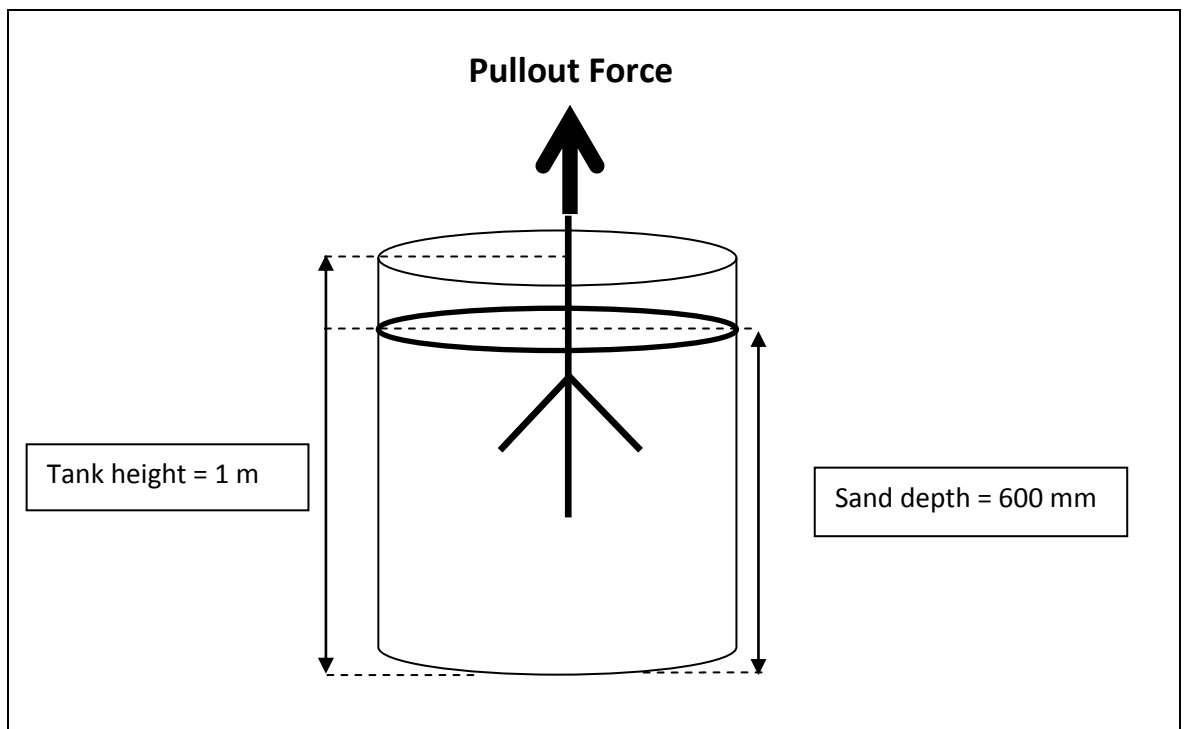


Figure 3.14: Layout model of the artificial root model in tank

CHAPTER FOUR

RESULTS AND DISCUSSIONS

4.1 Introduction

Chapter four exhibits the results and discussions through the completion of study, consisting of five sub chapters and begin with a description of soil and material properties involved. This is then followed by a section which presents the results obtained from the case studied on the investigation on the influences of root branching pattern of physical root models in resisting pullout forces. The results afterwards were used as control to be compared with the results obtained from the other two case studies which looked into the behaviour of root tapering in resisting uprooting forces and the influences of root material stiffness to uprooting resistances. Also attached in this chapter are the tables and figures to provide a better explanation on the results presented.

4.2 Soil and material properties

4.2.1 Soil medium

Poor-graded uniform sand was used as a soil medium throughout this study. The sand had the maximum dry bulk density, $\rho_{\max} = 1777 \text{ kg/m}^3$ with 6% of the optimum moisture content and the specific gravity of 2.65. To obtain the shear strength parameters of the

sand, a series of direct shear tests were carried out. This method showed that this type of soil has cohesion, c of 8.33 kN/m^2 and angle of friction, $\phi = 39.5^\circ$. Sand instead of other type of soil was chosen throughout this study since it is easier to be compacted besides could be easily removed out of the tank for repetition of tests.

4.2.1.1 Physical Test Results

a) Dry Sieving Test

- Soil Description : Mining Sand
- Initial dry mass: 1500.0 g

Table 4.1: Dry Sieving Result

BS Sieve Size (mm)	Mass of sieve (g)	Mass of sieve + sand (g)	Mass of sand retained (g)	Percentage Retained (%)	Cumulative Percentage Passing (%)
3.35	482.4	611.8	129.4	8.63	91.37
2	411	570.7	159.7	10.65	80.72
1.18	390.4	607.6	217.2	14.49	66.23
0.6	421.5	750.8	329.3	21.97	44.26
0.425	330.4	518	187.6	12.51	31.75
0.3	321.3	499	177.7	11.85	19.9
0.212	308.7	442.9	134.2	8.95	10.95
0.15	305.7	403.4	97.7	6.52	4.43
0.063	290	351.5	61.5	4.1	0.33
Pan	273.7	278.5	4.8	0.32	0.01
Total			1499.1	100	

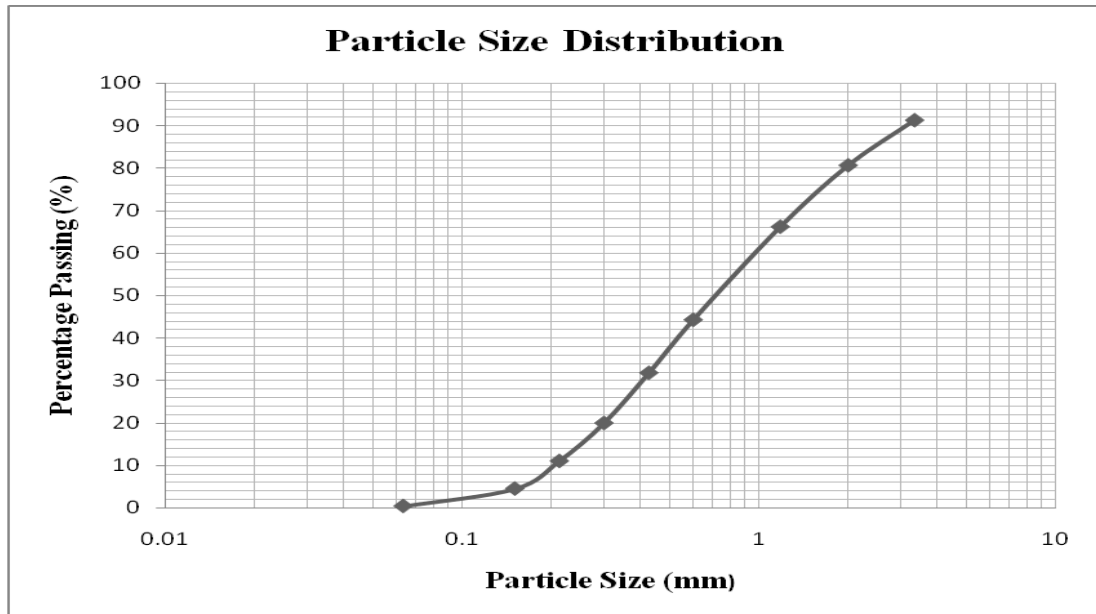


Figure 4.1: Particle Size Distribution Chart

Based on the dry sieving results, a particle size distribution chart (Percentage passing versus particle size) is plotted. Refer Figure 4.1.

- Discussion and Calculation:

From figure 4.1, $D_{10} = 0.21$; $D_{30} = 0.41$; $D_{60} = 0.98$;

$$Cu = D_{60}/D_{10} = 0.98/0.21 = 4.67$$

$$Cc = D_{30}^2 / D_{60} * D_{10} = 0.81$$

- **If well-graded sand, $1 < Cc < 3$ and $Cu > 6$;**
- In this case, the mining sand sample is **poor-graded uniform sand.**

b) Compaction test

Determination of bulk density

Table 4.2: Bulk density result

Sample no.	1	2	3	4	5
Wt of cylinder (g)	7952	8042	8123	8131	8110
Wt of cylinder + wet soil (g)	6282	6282	6282	6282	6282
Wt of wet soil (g)	1670	1760	1841	1849	1828
Volume of cylinder (m ³)	977.35	977.35	977.35	977.35	977.35
Bulk density (Mg/m ³)	1.709	1.801	1.884	1.892	1.870

Determination of dry density and water content

Table 4.3: Compaction Test result

Container no.	P1	P2	P3	P4	P5
Wt of can (g)	6.97	7.61	7.03	7.01	7.02
Wt of can + wet soil (g)	99.25	109.74	143.24	129.17	113.04
Wt of can + dry soil (g)	97.81	106.47	135.53	120.26	103.47
Wt of water (g)	1.44	3.27	7.71	8.91	9.57
Wt of dry soil (g)	90.84	98.86	128.50	113.25	96.45
Water content (%)	1.59	3.31	6.00	7.87	9.92
Dry density (Mg/m ³)	1.68	1.74	1.78	1.75	1.70

The Dry density and moisture content relationship

- Graph of dry density against moisture content is plotted (Figure 4.2).
- **The optimum moisture content = 6.00 %**
- **The maximum dry density = 1.78 Mg/m³**

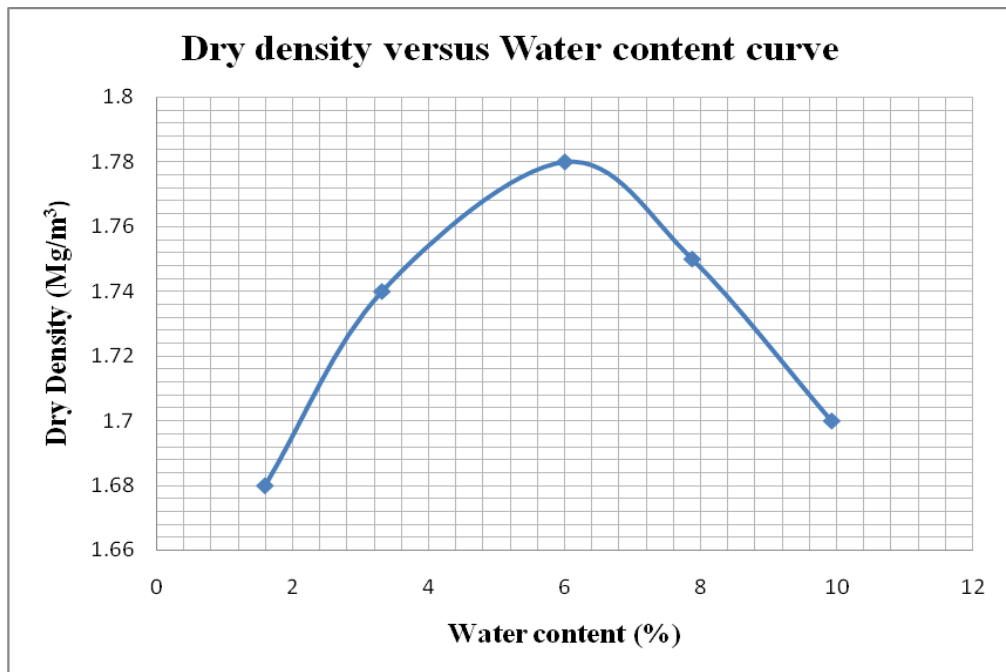


Figure 4.2: Graph of dry density against moisture content

c) Direct shear test

Determination of Vertical Stress

Table 4.4: Vertical Stress of each loading

Loading at Hanger (kg)	1	2	3
Vertical Stress, σ_n (kPa)	28.716	55.966	83.216
Moisture content before test (%)	6.12	5.93	5.13
Moisture content after test (%)	5.88	5.31	5.09
Bulk density (Mg/m ³)	0.901	1.009	1.027

Graph Plotting (Appendix A)

- Graph of Shear Stress against Vertical Displacement is plotted. (Figure 4.3)
- Graph of Vertical Displacement against Horizontal Displacement is plotted. (Figure 4.4)
- Graph of Shear Stress against Vertical Stress is plotted. (Figure 4.5)

Result from graph

- Based on Figure 4.5, the equation of the line plotted is $y = 0.825 x + 8.3282$.
This equation also can be written as $\tau = 0.825 \sigma + 8.3282$.
- By compare to the Mohr-Coulumb theory, which is $\tau = \sigma \tan \varphi + C$.
- $C = 8.3282$ and $\tan \varphi = 0.825$
- Thus, the friction angle, $\varphi = \tan^{-1}(0.825) = 39.5^\circ$.
- The cohesion, $C = 8.3282$

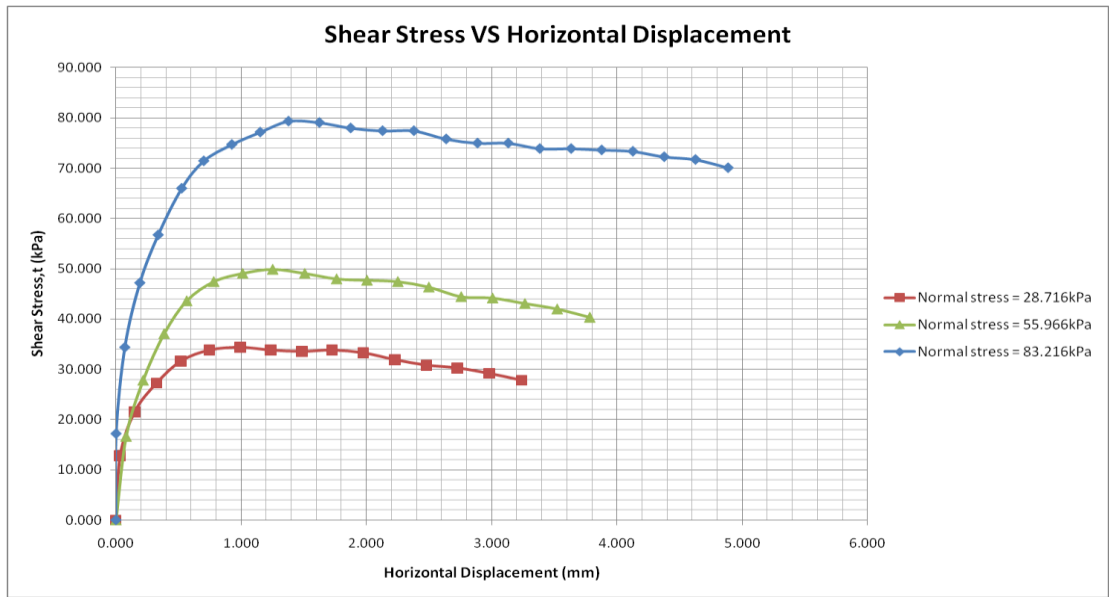


Figure 4.3: Shear Stress against Horizontal Displacement graph.

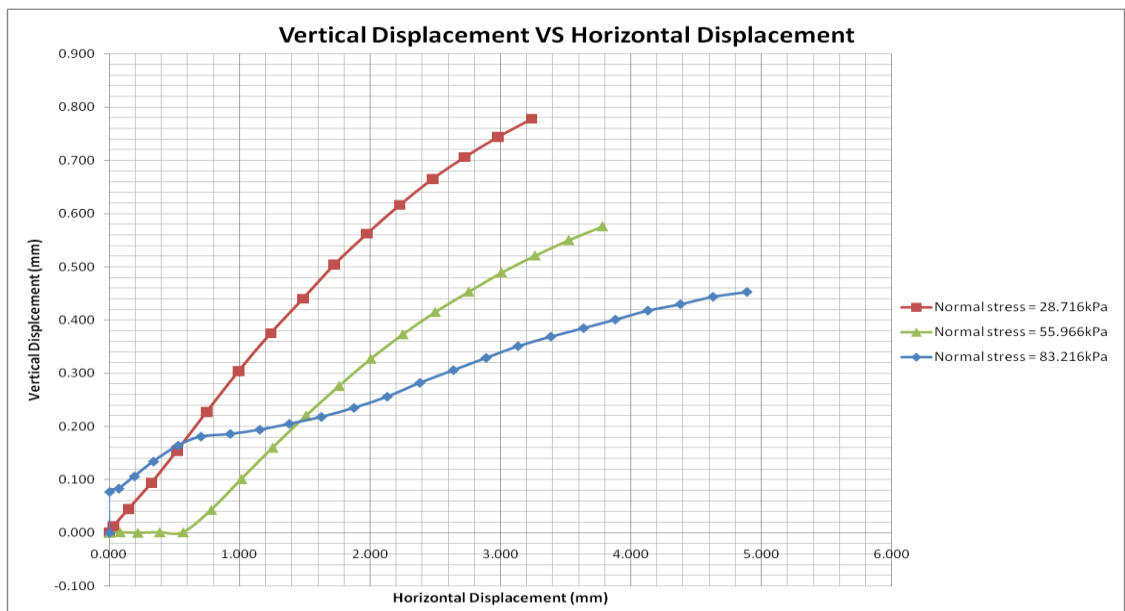


Figure 4.4: Vertical Displacement against Horizontal Displacement graph.

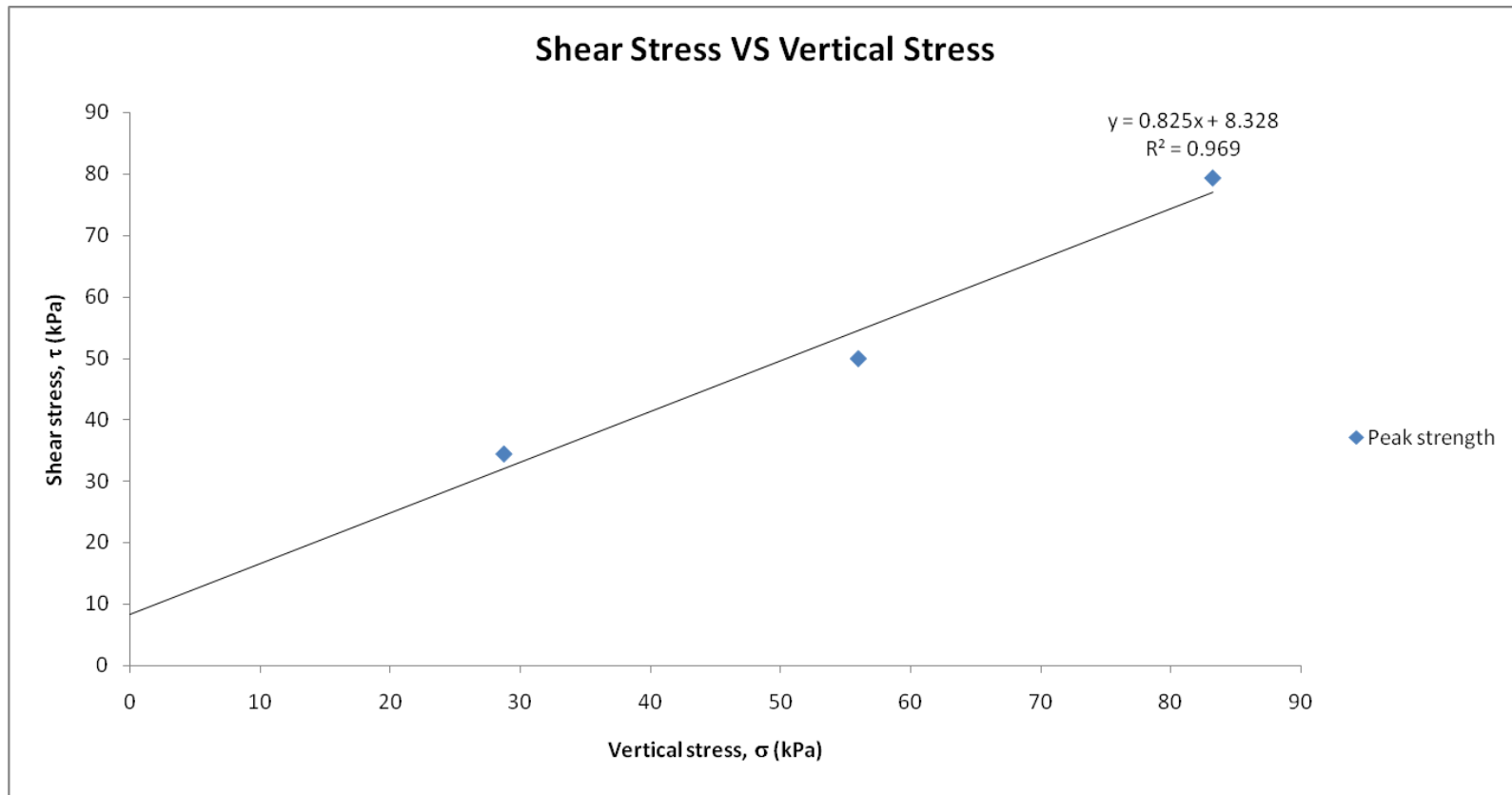


Figure 4.5: Shear Stress against Vertical Stress graph.

d) Particle Density

Table 4.5: Particle density of sand

	Mass (g)
Density Bottle (m_1)	22.78
Density Bottle + Dry soil (m_2)	32.80
Density Bottle + soil + water (m_3)	81.19
Density Bottle + full water (m_4)	74.95

$$\text{Particle Density, } \rho_s = \frac{(m_2 - m_1)}{(m_4 - m_1) - (m_3 - m_2)} = 2.65$$

4.2.1.2 Discussion on Soil properties test

The type of soil medium used in this pullout test is the mining sand. After conducting a few soil tests to justify the characteristics of the soil, it can be concluded that:

- The mining sand with grey colour is poorly graded uniform sand.
- The optimum moisture content is 6.00 % and the maximum dry density is 1.78 Mg/m³.
- The friction angle is, $\phi = \tan^{-1}(0.825) = 39.5^\circ$.
- The cohesion, $c = 8.3282$.

This result can be explained by the existence of various types of soil particles in the mining sand sample. The percentage of fine sand particles is 10.1 %, medium sand particles is 33.9 %, the percentage of coarse sand is 36 % while fine gravel particles is 11 % and the remaining 9% is silt particles. Conducting compaction test onto the sand could be tricky and hard. This is due to the small cohesion which is worsened by its incapability to absorb water. With the increment of water content added to the sand sample, sand particles were found to be more difficult to trap the water particles and

Table 4.6: Ranges of angle of friction (ϕ) for sands

Various type of sand	Loose (ϕ)	Dense (ϕ)
Uniform sand, rounded particles	27°	35°
Well graded sand, angular particles	33°	45°
Sandy gravel	35°	50°
Silty sand	(27°- 30°)	(30°- 34°)

sustain them, causing the sand sample to “bleed” when too much water content is added. The low availability of percentage of finer soil particle like the silt and clay was also found to be affecting the compaction results. In order to gain a better result, the sand sample will have to be sieved before the test starts to eliminate the coarse sand and gravel particles.

The direct shear test is tested with saturated sand sample after adding the optimum moisture content of 6 % into the dry sand sample. This caused the sand sample to be densely packed together. Due to this existing moisture content, the sand sample’s cohesion is 8.3282. The moisture content has been absorbed by the clay mineral particle that exists in the sand sample. Although the amount of clay may be small in the sand sample, the cohesion of the sample could be affected. Basically, the purpose of this test is to determine the shear strength of the sand sample. Based on Table 4.6, the sand specimen used falls in the category of dense uniform sand. In some cases, the dense sand will show the peak value of angle of friction (ϕ) in plane strain which can be 4° or 5° higher than the corresponding value, which is also satisfactory to our results of angle of friction that equals to 39.5°. This phenomenon can be explained by the existence of degree of interlocking between sand particles in the dense sand sample. Before shear failure can take place, this interlocking must be overcome in addition to the frictional resistance at the points of contact. The effect of interlocking will be the greatest in the case of very dense, well-graded consisting of angular particles.

4.2.2 Material properties

The aluminium and High Density Polyethylene (HDPE) rods used to develop artificial root models simulated several typical patterns of real roots. Aluminium was chosen to present harder and stiff root models while the HDPE rods were used to represent flexible root models. Although both materials used are not exactly simulating the real strength of the real roots, it has been assumed that the strengths of the real roots are located between the strength of these two extreme points.

Table 4.1 demonstrates the tensile properties of both materials which were used in this study. It is clearly shown that the aluminium rod with a bigger diameter had a greater strength than the smaller diameter (Figure 4.1), therefore it had been chosen to represent the taproot while the smaller diameter represented the lateral roots. Similarly to the aluminium, the High Density Polyethylene (HDPE) rod with a bigger diameter also gave higher strength compared to the smaller ones (Figure 4.2).

Table 4.7: Results of the material tensile properties

Specimen Name	Aluminum		HDPE	
	S1	S2	S1	S2
Diameter (mm)	10	8	10	8
Max Load (kN)	21.990	12.422	0.794	0.511
Maximum Stress(MPa)	312.209	253.430	12.482	11.565
Break Load(kN)	14.223	10.793	0.653	0.436
Extension at Break(mm)	25.054	30.262	151.566	150.067
Modulus (MPa)	25,435.830	15,260.556	461.449	367.809
Stress at 0.2% Yield(MPa)	292.262		7.930	

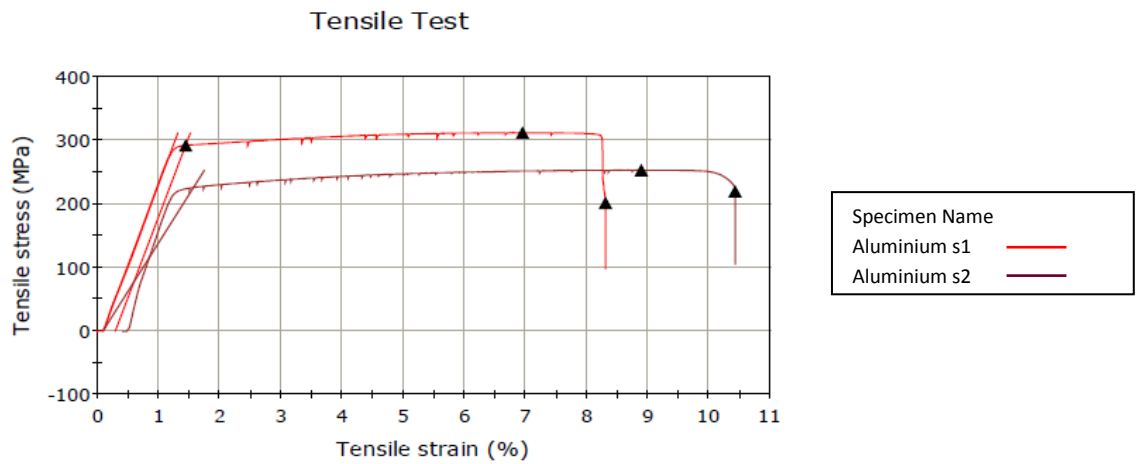


Figure 4.6: Graph of tensile test for aluminium material of different diameter, 8 mm and 10 mm

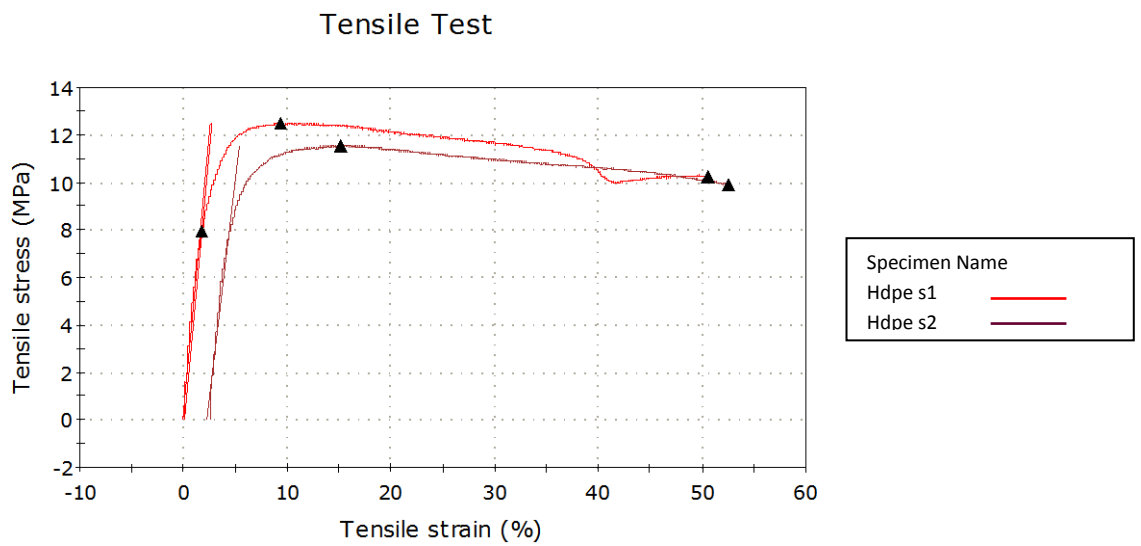


Figure 4.7: Graph of tensile test for High Density Polyethylene (HDPE) material of different diameter 8 mm and 10 mm

4.3 The Influences of Root Branching Pattern in Resisting Pullout Forces

The results through a series of pullout tests on aluminum uniform root models revealed that there was a strong relationship between the influences of root branching pattern and root pullout resistance as presented in Table 4.8. The tests for each of root models studied were repeated for three times with three similar model replicates to ensure the accuracy of the pullout results. Results were observed as relatively close to each other due to the root pattern respectively (Figure 4.8). Data from the preliminary test for each of the root models was selected to be studied in detail as it was highlighted in Table 4.9 which also denotes data of the vertical displacement at the maximum resistances during the pullout tests.

From the results, it is clearly shown that the maximum uprooting resistance increased in the order of $D2 < D1 < T1 < H2 < H1 < C2 < C1$ (Figure 4.10). The C1 root pattern was demonstrated to have the maximum pullout resistance which is approximately 5.5 times greater than the lowest resistance exhibited by the D2 root pattern (Figure 4.9). The graph clearly reflected the increase of pullout resistances with the increase of the vertical displacement at the early stage of the pullout test for each of the root models studied (Figure 4.9). Each root model was revealed to give almost identical trend of the pullout force-displacement curves which is characteristically jagged oscillations.

By referring to the similar graph also, there was a single peak curve and value that could be identified at each of the pullout force-displacement curve, with the initial pullout force rapidly rising with a relatively small displacement to a maximum peak failure. The resistances however, started to gradually decrease as the root models were further vertically displaced right after reaching the maximum peak. This is perhaps due

to the gradually releases of the soil-root bonds as the root model was further extracted out of the soil and finally resulted into the reduction of the soil-root interfaces area (Mickovski et al., 2010).

Table 4.10 presents the aluminum uniform root models after subjected to the pullout test. The T1 root model was observed to be the most unaffected model after experiencing the pullout force. However, the response was different to root models with lateral structures as they were not rigid enough to counteract the resistance of the sand. The D1 root pattern displayed the biggest deflection with the laterals downwardly bent at the angle of 8° from the original laterals position (45° to the taproot) similarly to the H1 root pattern. The D2 root pattern showed a deflection of laterals which bent at the angle of 3° from its original position (90° to the taproot) similarly to the H2 root pattern.

For the C1 and C2 root patterns, both showed similar angles of deflection for their upper laterals which downwardly bent at the angle of 1° from their original axes (90° to the taproot) which are less affected compared to the lateral roots that buried deeper in the sand layer which are more affected. The couple of the lower laterals of the C1 root pattern (position at 45° to the taproot) deflected at the angle of 4° from its original laterals position while for the C2 root pattern, the couple of the lower laterals deflected at the angle of 10° from its original lateral axes (90° to the taproot). It was first expected that the angle for the couple of the lower lateral for the C1 root pattern to bend at larger angle compared to the lower laterals for the C2 root pattern as similarly resulted in type 1 of the dichotomous (D1) and herringbone (H1) root pattern but the results generated for the C1 root pattern was against the hypothesis.

Table 4.8: Results of the maximum pullout resistances of uniform aluminium root models from the overall tests

Root pattern	Max. pullout force (N)			Mean
	1	2	3	
T1	231	231	222	228.0±3.0
D1	204	201	218	207.7±5.2
D2	93	95	90	92.7±1.5
H1	307	328	326	320.3±6.7
H2	245	245	263	251.0±6.0
C1	510	494	527	510.3±9.5
C2	376	360	352	362.7±7.1

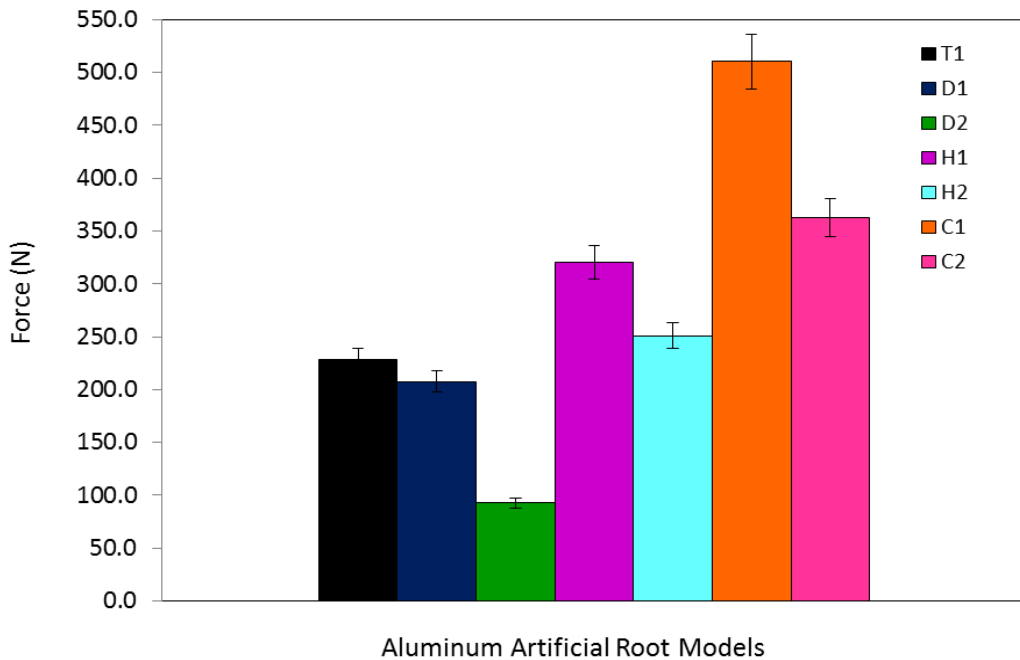


Figure 4.8: Uprooting resistance of uniform aluminium root models with different branching pattern. Error bars indicate \pm SE.

Table 4.9: Selected results of the maximum pullout resistance of uniform aluminum root models

Root pattern	Maximum pullout force (N)	Displacement (mm)
C1	510	4.29
C2	376	5.07
H1	307	10.92
H2	245	22.96
T1	231	15.08
D1	204	6.79
D2	93	2.6

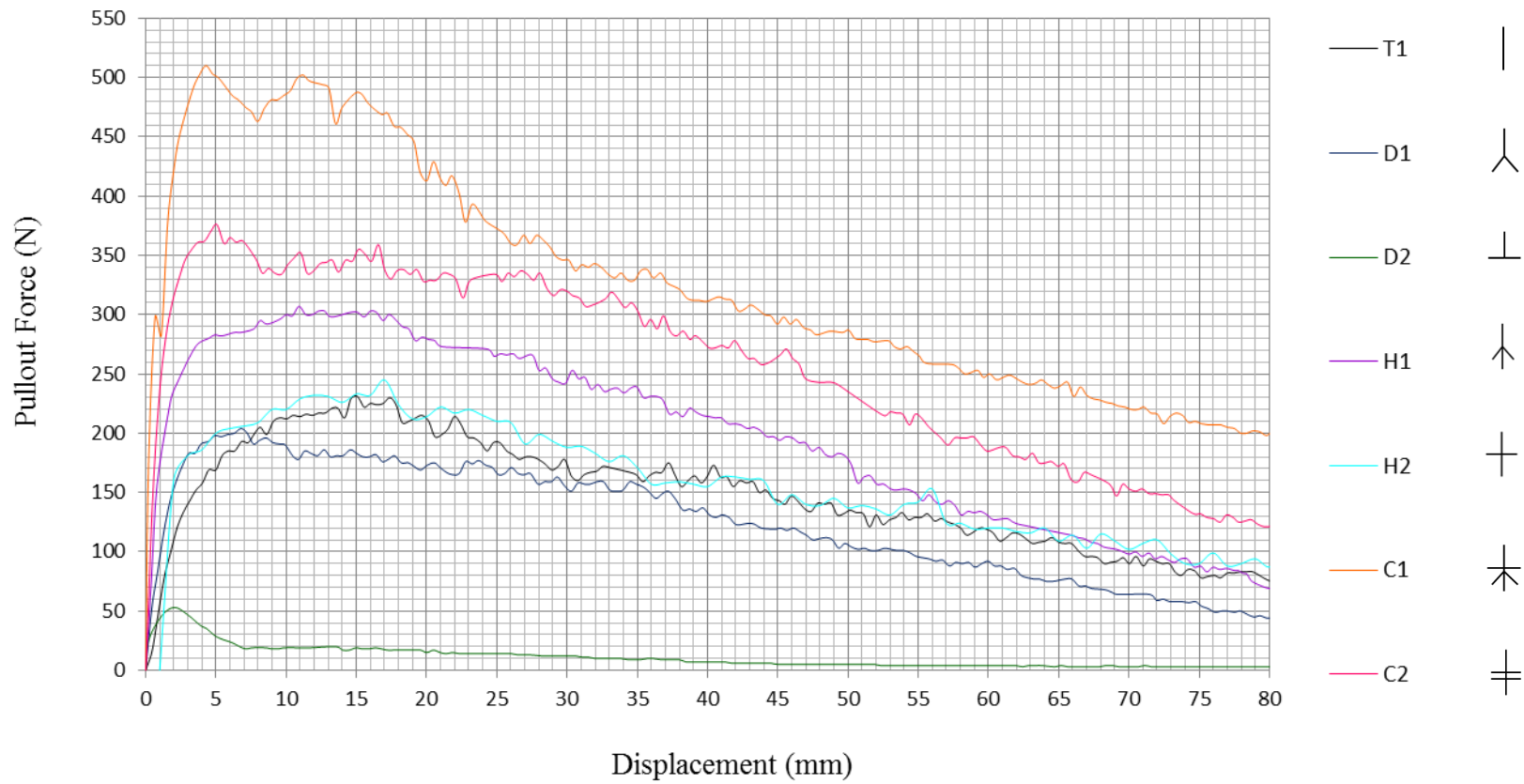


Figure 4.9: The pullout force of different patterns of uniform aluminum root models

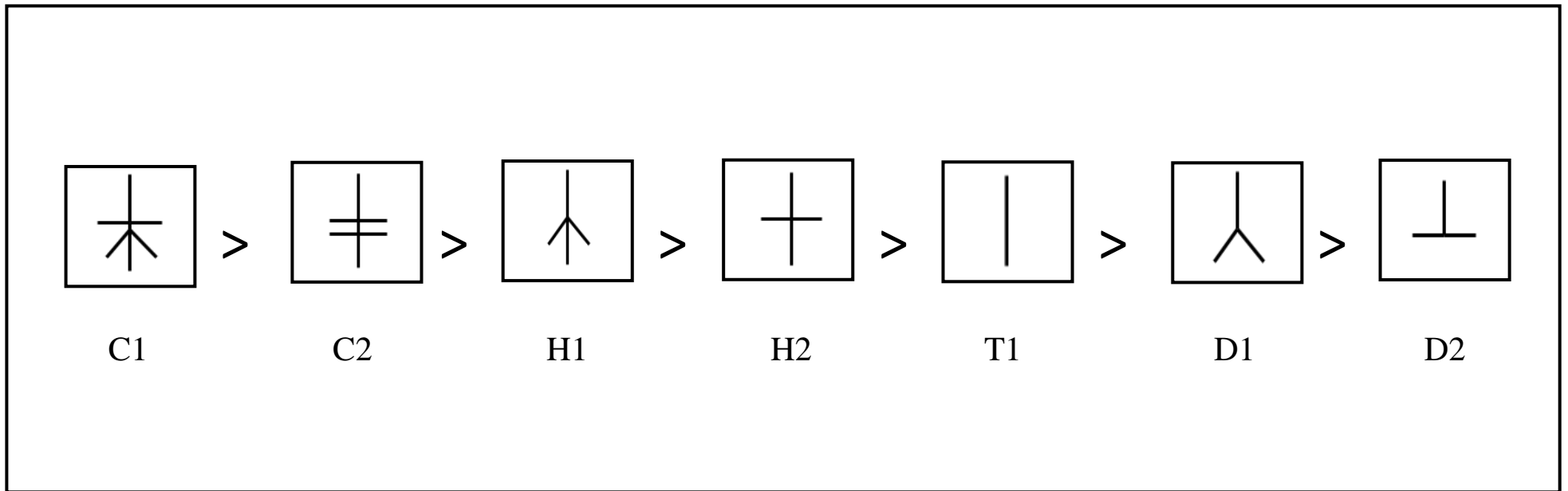
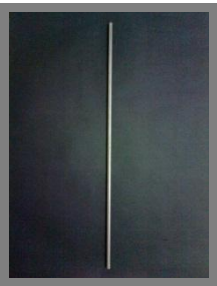


Figure 4.10: The resistance of uniform aluminum root models to pullout in descending order

Table 4.10: Uniform aluminum artificial root model after the pullout test

Structure Type	Diagram	Structure Type	Diagram
Dichotomous I (D1)		Dichotomous II (D2)	
Herringbone I (H1)		Herringbone II (H2)	
Combination I (C1)		Combination II (C2)	
Taproot (T1)			

4.3.1 The Influences of Angle and Position of Lateral Roots to Uprooting Resistance

The significance of the lateral structure in root systems reveals a major influence to the resistance of pullout. The pullout resistance of all type 1 root models, the D1, H1, and C1, in which the lateral roots are positioned at 45 degree to the taproot were greater than the type 2 root models, the D2, H2, and C2 in which the lateral roots are positioned at 90 degree to the taproot (Figure 4.11).

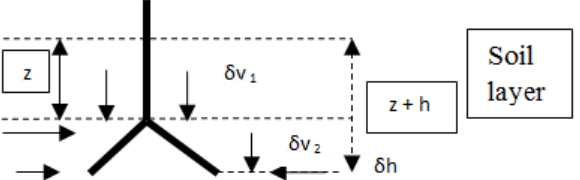
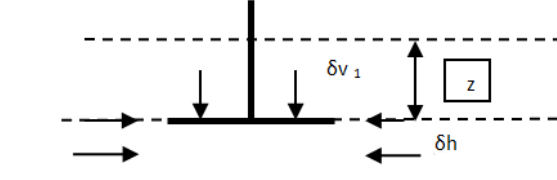
The pullout resistance generated by the D1 root pattern showed approximately 2.2 times more than the D2 root pattern in which the resistance increased about 54.4%. Meanwhile, for the H1 root pattern, the pullout resistance was about 1.3 times greater than the H2 root pattern in which the increment is about 20.2%. Lastly, the pullout resistance generated by the C1 root pattern was about 1.4 times greater than the C2 root pattern in which the increment is about 26.3%.

Mickovski et al. (2007) in a study have clarified the influences of these lateral structures on the soil-root anchorage. This is consequently due to the upward movements of the lateral structures that were said to be marginally smaller than the vertical movement of the axis during the pullout mechanism. When root models with lateral sides were subjected to the axial load, these lateral roots were identified to bend (Table 4.10) as the root-soil interface instantaneously mobilizes along the whole root, causing the soil above the joint to uplift and subsequently push the laterals upwards (Mickovski et al., 2007).

In regards to those findings (Mickovski et al., 2007), it was evidently understood on the reasons why in both types of combined root models, C1 and C2, the optimum pullout resistances were amongst the best. It was due to the influences of the maximum number of lateral roots embedded beneath the soil layer. As a result, it increased the surface contact area within the roots and surrounding soil which finally leads to the rapid transformation of tension to the soil skeleton as a consequence of the larger soil-root contact area during the pullout mechanism (Stokes et al., 1996).

The angle of the lateral structure in root systems has also been revealed in giving such a major influence to the resistance of pullout. Lateral roots were determined in resisting the pullout forces at the optimum angle of 45 degree to the taproot. This statement was proven by the results as obtained throughout this study in which for all type 1 root models for each root pattern, the D1, H1, and C1, in which the lateral roots are positioned at 45 degree to the taproot, the pullout resistances generated were greater than type 2 root models of the same root categories, D2, H2, and C2, in which the lateral roots are positioned at 90 degree to the taproot (Figure 4.11).

Table 4.11: Total vertical and horizontal stresses acting on root models with different branching angles

Case 1	Case 2
 <div data-bbox="295 1803 790 1937" style="border: 1px solid black; padding: 5px;"> <p>Calculation of total stress:</p> $\sum \delta_v = \delta_{v_1} + \delta_{v_2} = \gamma (z + h)$ </div>	 <div data-bbox="941 1803 1436 1937" style="border: 1px solid black; padding: 5px;"> <p>Calculation of total stress:</p> $\sum \delta_v = \delta_{v_1} = \gamma z$ </div>

These above circumstances are in accordance with an engineering theory of Mohr-Coulomb criteria of normal effective stress on the interface of roots which stated that soil stresses increased linearly with depth by deeper soil layers being more resistance to shear. Since the total vertical stress of soil increases with depth, hence for root models with the lateral roots positioned at 45 degree to the taproot, the resistances to pullout were observed to be higher as the lateral sides were further down embedded beneath the soil layer thus more forces are required to mobilize and overcome the amount and weight of the sand from the upper layer. In a different way, for type 2 root models in which the lateral roots are positioned at 90 degree to the taproot, the reduced amount and weight of the sand at the upper layer clearly explained the reason why this type of lateral roots are not able to sustain higher pullout resistance as illustrated in Table 4.11.

The results obtained throughout this study were fundamentally similar as discovered by Stokes et al. (1996), where they stated that the insertion angle of lateral roots on the tap root is important with an optimal angle at around 60° . Lateral roots with larger branching angles to the taproot (i.e. $> 45^\circ$) were revealed to be placed in torsion and therefore offering less resistance to uprooting when subjected to uplift movements. For that reason, the optimum radial branching angle for the lateral roots angle had been estimated to be positioned at at least 5 degree or less (i.e. $\leq 45^\circ$) to the taproot in order to ensure the maximum resistance to pullout. Roots held in tension were said to play a major role in resisting the uprooting of trees (Coutts, 1983, 1986).

The results of this study also showed agreement with the ones predicted in previous theoretical models of root anchorage studies (Dupuy et al, 2005); it was observed that the resistance of tap root was not mobilized during the simulations as these roots have no secondary branches and therefore was oriented mainly in the longitudinal direction.

The stresses never reached the yield value in roots, whereas the pulling resistance was limited mainly by the friction of the faces in contact and by the shearing of the soil around the root.

However, for root patterns with secondary segment, it increased the proportion of lateral axes resisting longitudinal displacement, thus verifying the significant impact of topology on resistance to uprooting (Wu et al., 1988; Fitter & Ennos, 1989; Riestenberg, 1994; Stokes et al., 1996). This root system was extracted with a block of soil during experimental pullout whereas a single isolated axis would have simply sheared out of the soil. Moreover, when axes are more vertical, neither the lateral roots held in tension nor the soil participate much in the uprooting mechanism. However, for root systems with horizontal roots, the soil contributions are maximal and the lateral roots are submitted to bending and therefore, there must be an optimal branching angle that maximizes resistance to pullout.

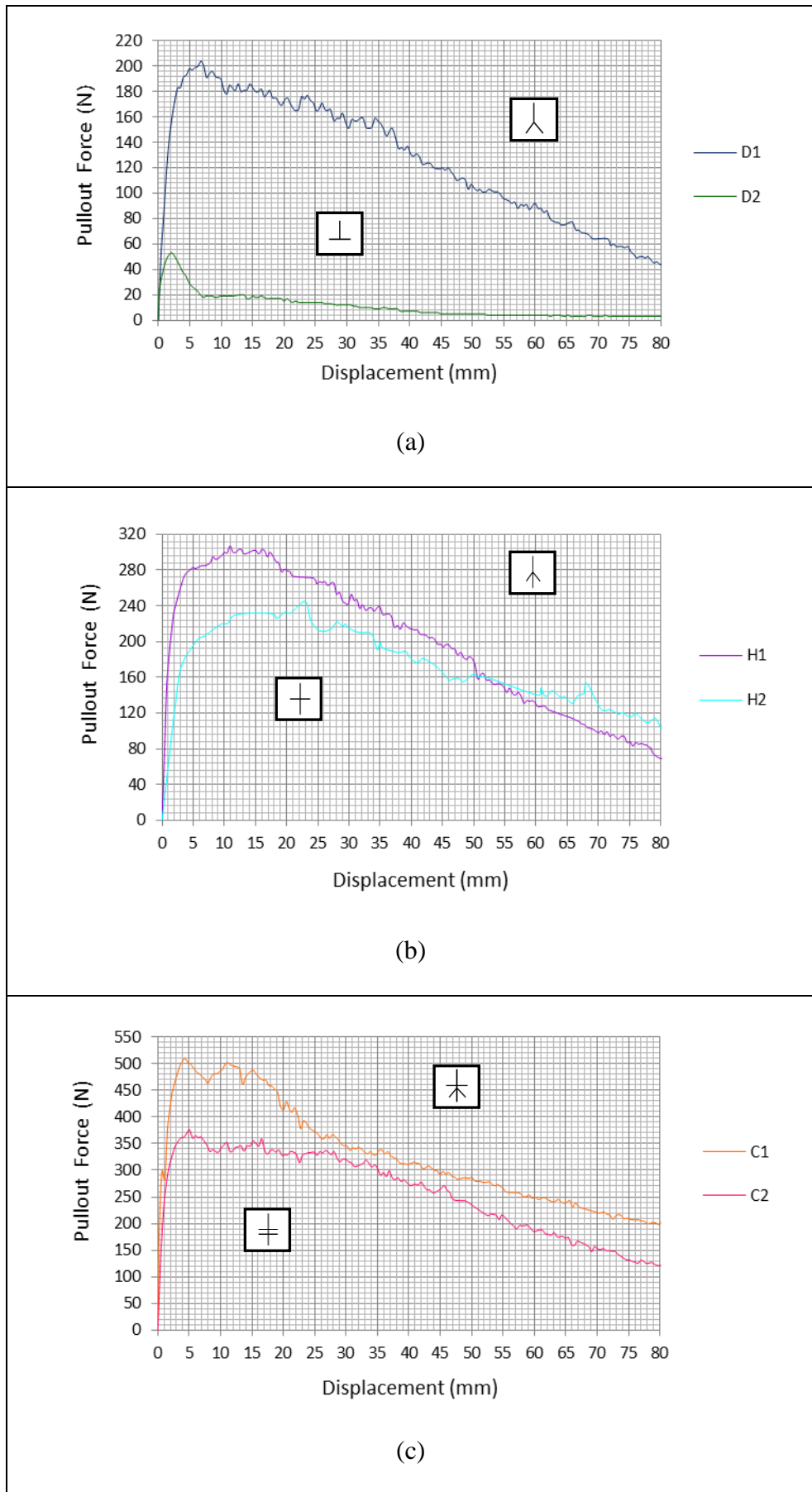


Figure 4.11: Pullout resistances of type 1 root models, D1, H1, and C1 which is greater than the type 2 root models, D2, H2 and C2, respectively.

4.3.2 The Influences of Taproot on the Uprooting Resistance

The length of taproot embedded beneath the soil layer had also been recognized in giving such a great influence to the capacity of pullout. As demonstrated in Figure 4.12, the pullout resistance for the H1 root model is observed to be greater than the D1 root model. In a similar result, the H2 root model has a greater pullout resistance than the D2 root model due to the influences of the additional length of taproot as designed for the H1 and H2 root models.

Through the additional length of taproot in the H1 root pattern, the pullout resistance generated denoted about 1.5 times greater than the D1 root pattern in which the increment of pullout resistance is about 33.6%. The H2 root pattern also exhibited a higher pullout resistance than the H1 root pattern in which the resistance is about 2.6 times greater or about 62% increment of the pullout resistance.

The previous studies (Stokes et al., 1996, Waldron and Dakessian, 1981) have confirmed that as the taproot grows longer, it penetrates deeper into the soil in which it is grown, where the shear resistance was known to be greater as the sand goes deeper. Under those circumstances, the root models therefore became more difficult to uproot not only due to the increment in friction and cohesion between the sand particles (Mattheck, 1993) but also with the decrease of soil-root interface area.

4.3.3 Summary

Branching and the development of lateral roots would normally increase the overall stability of the plant as well as changing the mechanism of root failure under uprooting

in which the laterals act as guy ropes under tension. This adaptation is also common in engineering practice (Broms 1981, Tomlinson, 1977). Laterally branching tap root systems resemble vertical piles which adds lateral wing or beam structures to increase their lateral stability. Throughout this study, pullout resistances were concluded to have a strong relationship with the architecture of root systems influenced by the number and angle of lateral roots in root systems combined with the total length of tap root that improved the anchorage of rooted soil matrix.

Compared to the models behaviour in this study and the behaviour of other physical root models studies (Mickovski et al. 2007), the greatest pullout resistance was recorded for the dichotomous pattern roots that have their lateral at the lowest point. This is followed by the herringbone pattern roots with the laterals at half of the length of its taproot, while the tap root consisting of only one vertical root showed the smallest resistance to pullout. This experiment revealed that root branching and morphology can greatly affect the pullout resistance of the root: branched roots such as the herringbone and dichotomous roots have 2 and 3 times greater pullout resistance than a non-branched tap root respectively. The results also demonstrated that the deeper the laterals are placed, the higher the pullout resistance because the normal effective on the interface for the deeper roots is larger.

This finding however, contradicts to the observation conducted throughout this study where the pullout resistance of herringbone root pattern was obtained to be higher than the pullout resistance generated by the dichotomous root pattern. This difference may be due to the different arrangement of the root models for herringbone root pattern where the lateral roots were placed at half of the length of the taproot while the dichotomous root pattern had their lateral at the lowest point of taproot. The laterals of

dichotomous were placed deeper in the sand layer thus the pullout resistance generated is higher because of the normal effective stress on the interface for deeper roots is larger. To compare the results in this study with the results obtained from previous related studies, the results varied because of the different experimental techniques from one author to another, together with the variation of root systems morphology and topology that were not usually taken into consideration. However, the results from these related studies were found as marginally linked to each other in complementary with the real concept of soil rooted matrix.

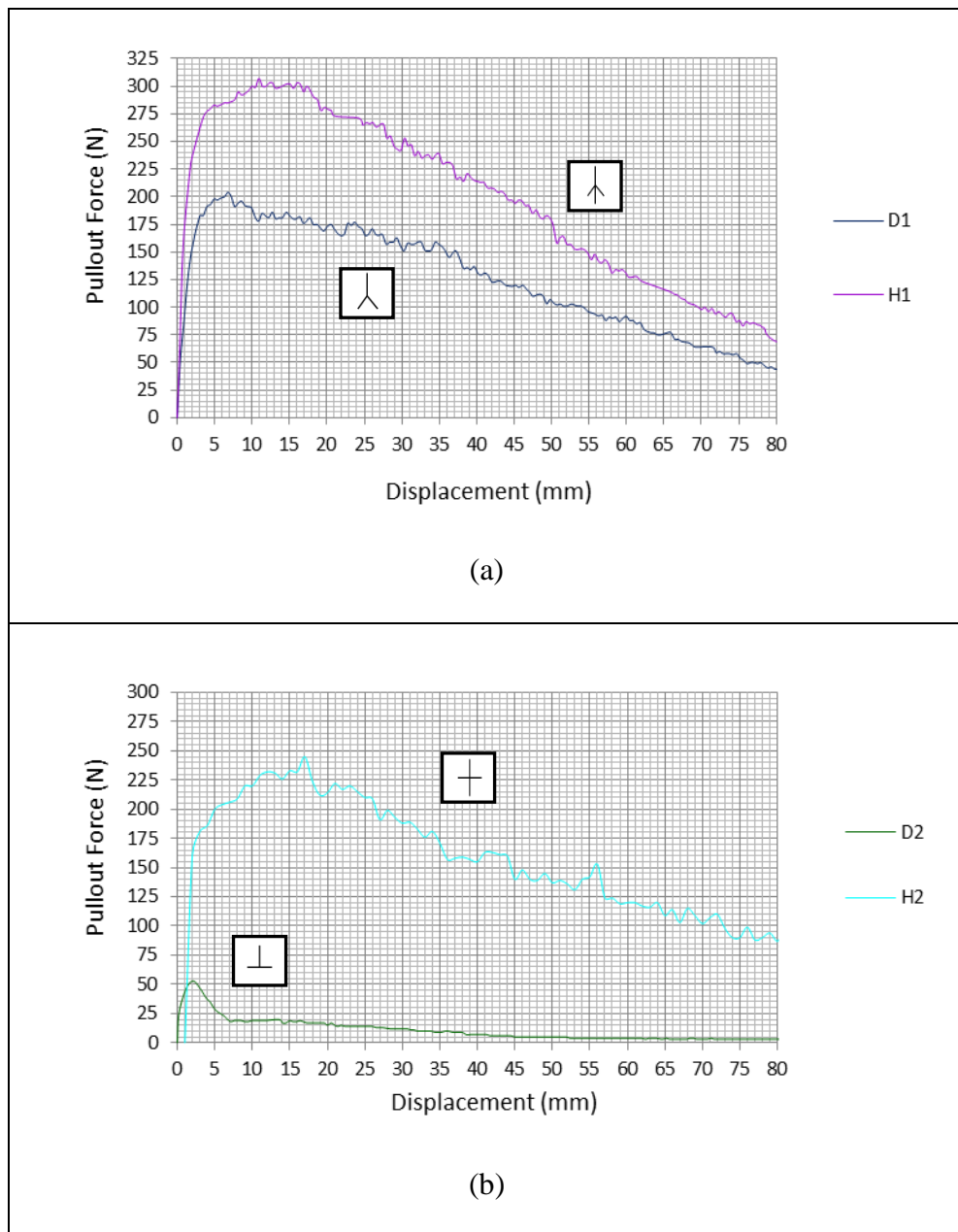


Figure 4.12: The maximum pullout forces for herringbone root pattern, H1 and H2 is higher than that of in dichotomous root pattern, D1 and D2, respectively.

4.4 The Behaviour of Root Tapering in Resisting Uprooting Forces

Results through the pullout test series on tapered root models are presented in Table 4.12. From the table, the results observed were relatively closer to each other due to the root pattern respectively (Figure 4.13) and results from the preliminary data were selected to be studied in detail as presented in Table 4.13. Data on the vertical movement of the root models during the maximum resistance were also recorded (Table 4.13).

From the table, it is characteristically shown that the maximum uprooting resistance increased in the order of $T1 < D2 < H2 < D1 < H1 < C2 < C1$ (Figure 4.15). The C1 root pattern was depicted to have the maximum pullout resistance, approximately 6.6 times greater than the T1 root pattern in which the resistance was shown to be the lowest. Figure 4.14 displays the uprooting resistance of seven different patterns of tapered root models against displacement. It is clearly demonstrated that the pullout resistance increased with the increase of upward movements at almost the same rate for each of the root model studied. Unfortunately, after the curves reached the maximum peak point, the forces immediately began to decrease gradually as the whole root was further displaced.

Table 4.12 denotes tapered root models after subjected to the pullout test. The T1 root model was observed to be the most unaffected model after experiencing the pullout force. However, the response was different with root models with lateral structures with the D1 root pattern showing the biggest deflection with the laterals downwardly bent at the angle of 14° from the original laterals position (45° to the taproot) following the H1 root pattern in which the laterals are deflected and bent at the angle of 6° from its

original position (45° to the taproot). The D2 root pattern however indicated the smallest angle of deflection in which the laterals downwardly bent at the angle of 1° from the original laterals axes (90° to the taproot) similarly to the H2 root pattern. For the C1 and C2 root patterns, both projected a similar angle of deflection for the couple of their upper laterals which downwardly bent at the angle of 1° from the laterals original axes (90° to the taproot) with the lateral root that was buried deeper in the sand layer being affected the most. The couple of the lower laterals of the C1 root pattern (position at 45° to the taproot) deflected at the angle of 11° from its original laterals position while for the C2 root pattern, the lower lateral structures deflected at the angle of 3° from its lateral original axes (90° to the taproot). Results obtained therefore, clearly verified the importance of laterals structures with the angle of 45° to the taproot to resist uprooting forces especially for root systems with tapering structure since the workability of the vertical taproots were found no longer effective enough to resist the uprooting due to the tapering behaviour that decreases the anchorage of those vertical elements with the surrounding soils.

Table 4.12: Results of the maximum pullout resistance of tapered aluminium root models from the overall tests

Root pattern	Max. pull out force			Mean
	(N)			
	1	2	3	
T1	62	85	72	73.0 ± 6.7
D1	182	182	184	182.7 ± 0.7
D2	78	82	75	78.3 ± 2.0
H1	267	260	254	260.3 ± 3.8
H2	164	172	143	159.7 ± 8.6
C1	410	395	381	395.3 ± 8.4
C2	332	347	325	334.7 ± 6.5

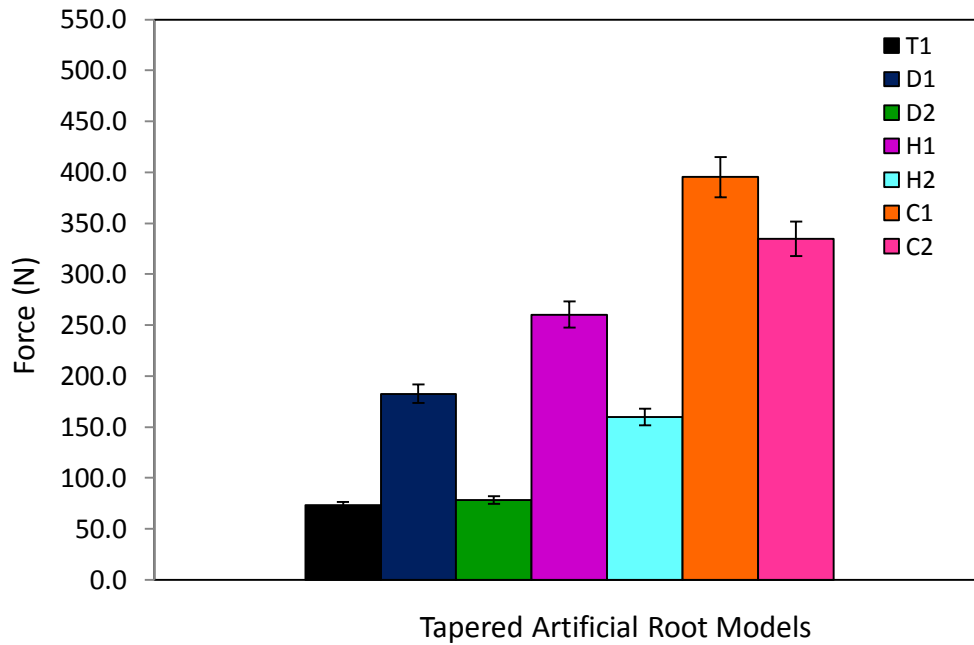


Figure 4.13: Uprooting resistance of tapered aluminium root models with different branching pattern. Error bars indicate \pm SE.

Table 4.13: Selected result of the maximum pullout resistance of tapered aluminium root models

Root pattern	Maximum pullout force (N)	Displacement (mm)
C1	410	5.41
C2	332	5.61
H1	267	4.56
D1	182	4.59
H2	164	2.63
D2	78	2.77
T1	62	2.9

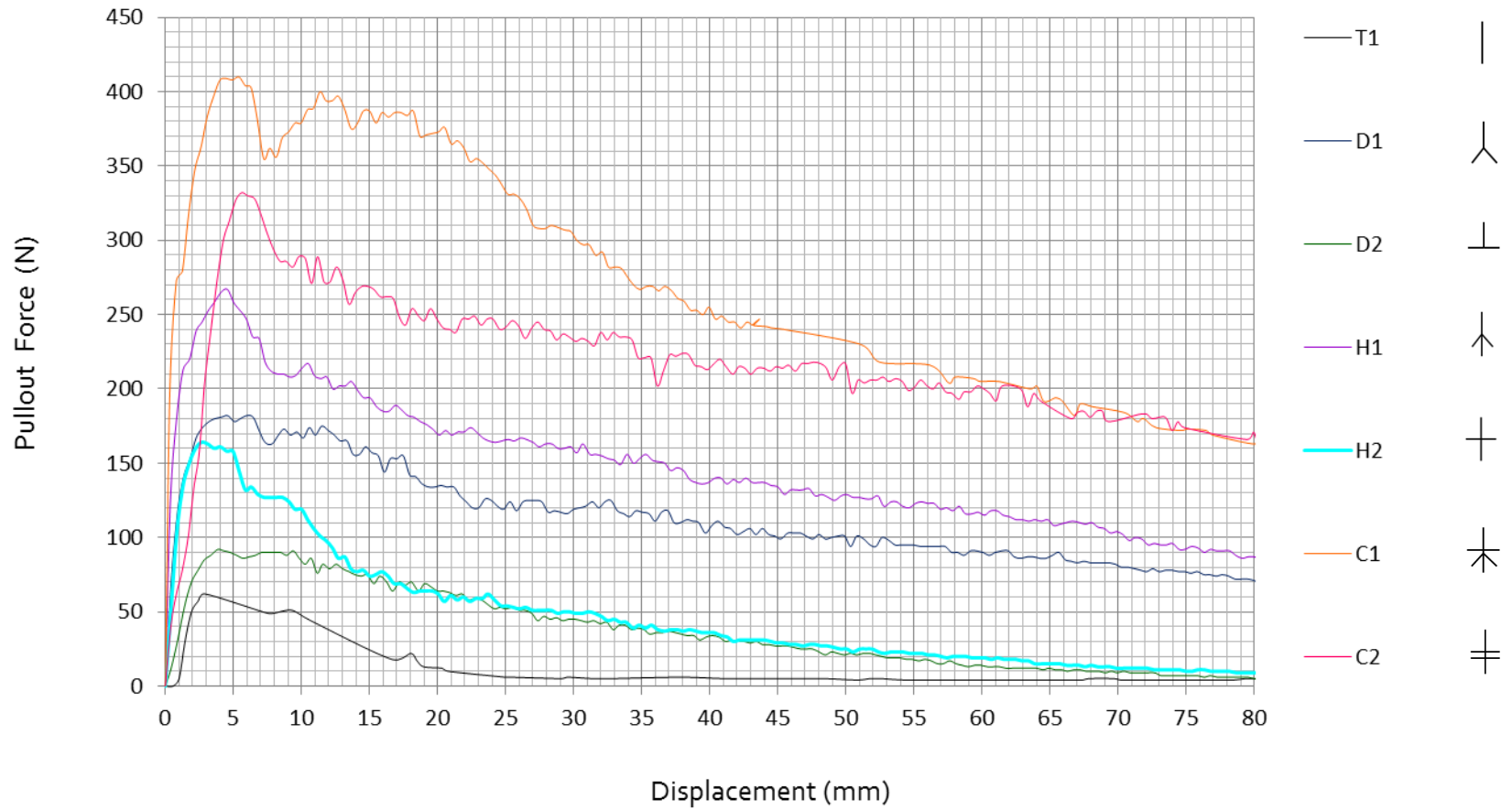


Figure 4.14: The uprooting resistance of different root branching pattern of tapered aluminium root models

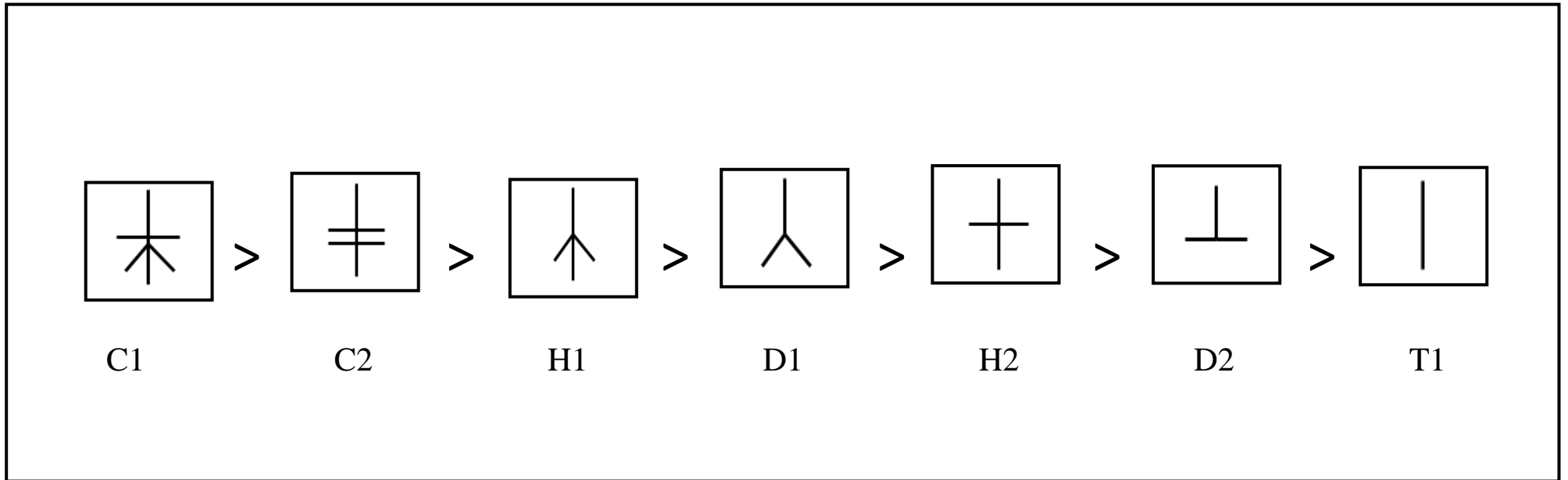
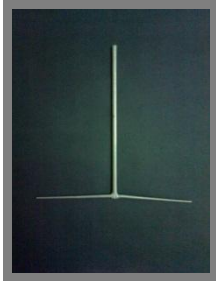
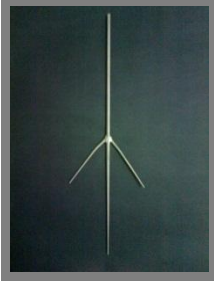
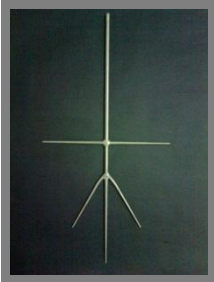
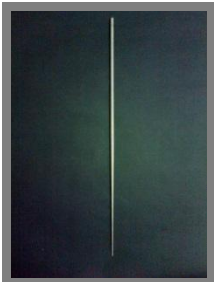


Figure 4.15: The resistance of tapered aluminum root models to pullout in descending order

Table 4.14: Tapered aluminum artificial root model after the pullout test

Structure Type	Diagram	Structure Type	Diagram
Dichotomous I (D1)		Dichotomous II (D2)	
Herringbone I (H1)		Herringbone II (H2)	
Combination I (C1)		Combination II (C2)	
Taproot (T1)			

4.4.1 The Influences of Angle and Position of Lateral Roots on Uprooting

Resistance of Tapered Aluminum Root Models

Results of tapered root model revealed many similarities and differences with those in the uniform aluminum root models. The similarities between both models were found depending on their respective mechanisms of anchorage. The significance of the number, angles and positions of the lateral roots were found to greatly influence the resistance of these tapered root models to pullout. Lateral roots were determined to resist pullout forces at best at the optimum angle of 45 degree to the taproot. This statement was proven by the pullout resistance in all type 1 root models, (D1, H1 and C1 with the lateral roots positioned at 45 degree to the taproot) which was greater than the type 2 root models of the same root categories, (D2, H2, and C2 with the lateral roots positioned at 90 degree to the taproot) (Figure 4.16). Although using these tapered root models had reduced the soil-root surface contact area, the influences of the angle and position of the lateral roots had again been discovered to be dominating the rules of the soil-root anchorage.

The pullout resistance generated by the D1 root pattern was proven to be about 2.3 times more resistance than the D2 root pattern in which the resistance increased by 57.1% while for the H1 root pattern, the pullout resistances generated about 1.6 times higher than the H2 root pattern in which the increment was about 38.6%. Lastly, for the C1 root pattern, the pullout resistance generated about 1.2 times greater than the C2 root pattern in which the increment was approximately 19%.

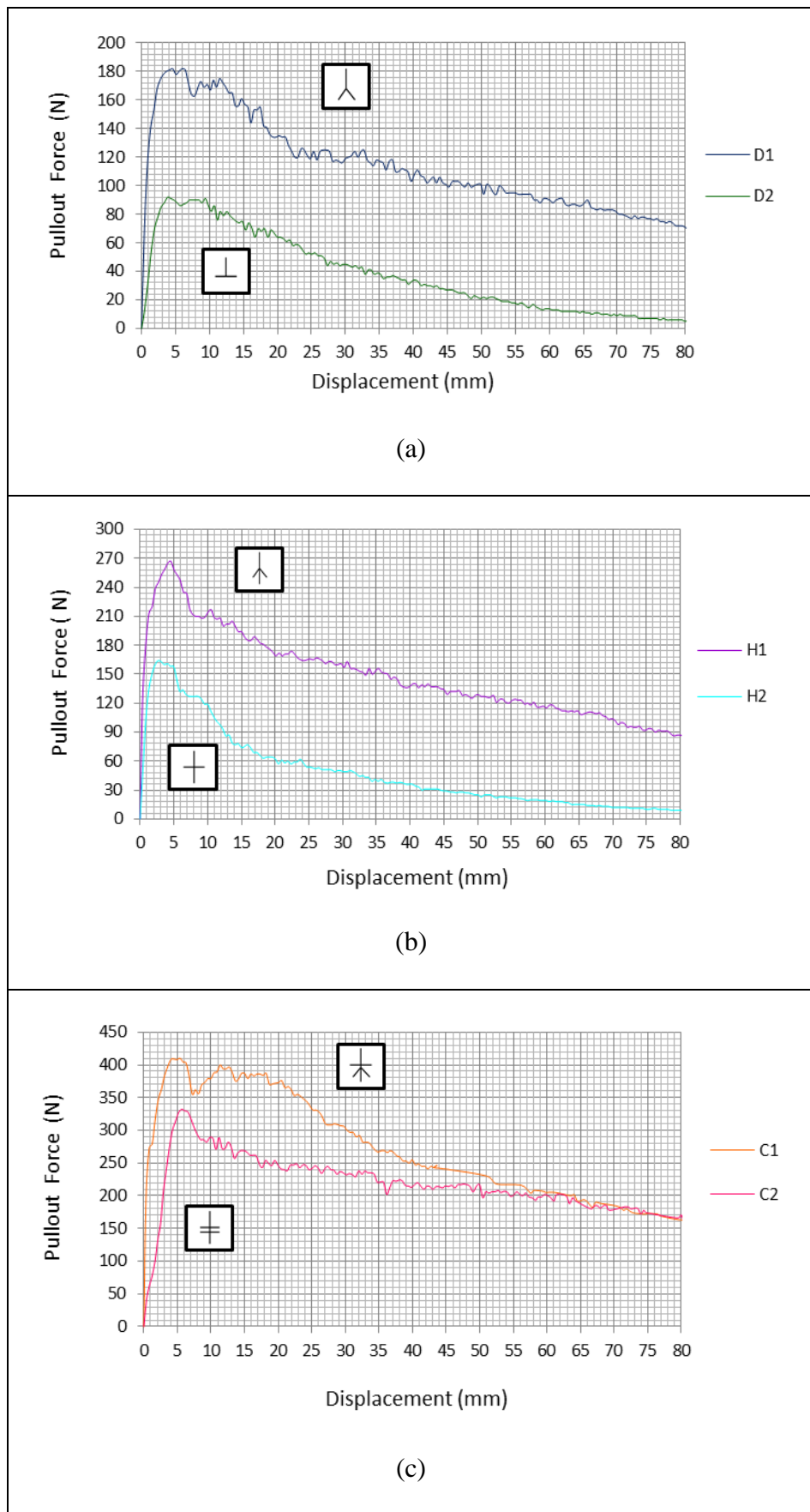


Figure 4.16: Pullout resistances of type 1 root models, D1, H1, and C1 is greater than the type 2 root models, D2, H2 and C2, respectively.

4.4.2 The Influence of Total Length of Taproot in Resisting Uprooting Force

The same observation was also observed throughout the study on tapered root models where the uprooting resistance was signified to be greater as the taproot grows longer (Figure 4.17). The Herringbone root models, H1 and H2 were demonstrated to have more resistance to pullout compared to the dichotomous root models, D1 and D2 where the resistance to pullout was lower due to the shorter taproot.

Through the additional length of taproot as observed in the H1 root pattern, the pullout resistance generated about 1.5 times greater than the D1 root pattern in which the increment of pullout resistance was 31.8%. Similarly, the H2 root pattern has a higher pullout resistance about 2.1 times, an increase by 52.4% than the D2 root pattern.

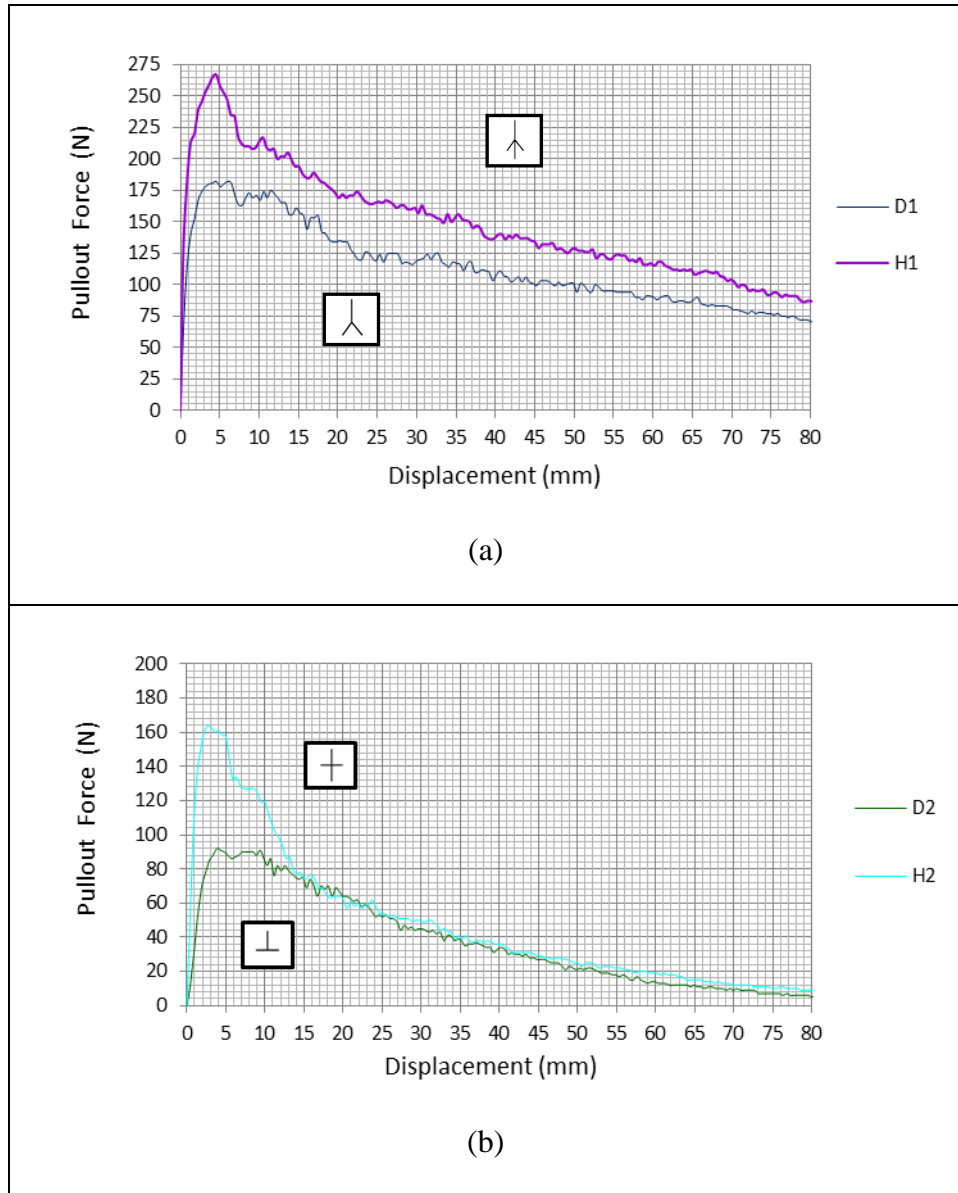


Figure 4.17: The maximum pullout force for herringbone root models, H1 and H2, is greater than the dichotomous root models, D1 and D2 respectively.

4.4.3 Comparison of the Maximum Uprooting Resistance of the Uniform and Tapered Aluminum Root Models

Table 4.15: Maximum uprooting resistances of the uniform and tapered aluminum root models

Type of roots	Max. pull out resistance (N)		Change (%)
	Uniform aluminum root model	Tapered aluminum root model	
T1	231	62	-73.16
D1	204	182	- 10.78
D2	93	78	-16.12
H1	307	267	-13.02
H2	245	164	-33.06
C1	510	410	-19.61
C2	376	332	-11.70

From the table (Table 4.15), it is clearly observed that for each of the uniform aluminum root model with the diameter along the whole root length which are uniform, the resistances generated were found to be slightly higher (Figure 4.17) than the tapered root model with the diameter along the whole root length which gradually decreased to the root tip based on the root pattern respectively. The T1 root pattern was shown as giving the highest changes of root surface area which is about 73.2% whilst the D1 root pattern was shown to have a lower change, 10.8%. This result may be due to the influences of root tapering behaviors that led into atypical response of soil particles on the surfaces of tapered root models via the influence of confining pressures to cause the anchorage of soil rooted with these tapered roots to reduce mechanically.

The confining pressure that acted on a root model is dependent upon the depth and specific weight of the surrounding soil. For cohesive soils, it is also dependent on the shear strength of the soil and for granular materials they are dependent on the angle of

friction. During pullout, force acts equally in all directions of the root models to cause pressure to be transmitted normally to the boundaries of the root models. Although the force applied to the root surface is similar at every point, the soil particles however applied higher pressure at the root tip compared to the other points of the upper root length to the lateral branching point as the point concentrates the force into a smaller area. This is due to the gradually decrease of root diameter along the whole root length to the root tip as it satisfies the engineering principles of soil pressure. Therefore, it bends the tip easily and quickly and finally leads to the less resistance of the tapered root models to pullout. In a different way, for the aluminium root models, the pullout resistance however, is greater due to the constant contact pressure along the whole root length due to the constant diameter.

This mechanism can also be attributed to the decreased contact surface area available to each subsequent diameter decrement which proceeds to the tendency of the less distribution level of the tensile resistance of the tapered root models to the soil skeleton during uprooting. The uniformity of the root models results in larger contact surface areas which help to spread as well as to transfer the tension level to the soil skeleton rapidly. The significance of the contact surface area in the soil-root anchorage could also be evidently verified through a simple theoretical formula (Equation 2.8) to predict the increase in shear strength due to the additional root 'cohesion' term, c_R , to the Mohr-Coulomb strength envelope for soil (Wu et al., 1979, Waldron and Dakessian, 1981, Greenwood et al., 2004), where A_r , represents the root area ratio defined as the area of the root crossing the shear plane divided by the total cross-sectional area of the shear plane (Wu et al., 1979).

Table 4.16 displays the comparison in the reduction of the total root surface area between tapered root and uniform aluminium root models. The root surface area is determined by measuring the root surface area exposed to the surrounding soil and the use of tapered root models in the pullout test were found in reducing the interaction between these elements due to the decrease of the soil-root contact area.

The results from this study indicated an agreement with the results discovered by Norris (2005) which stated that less resistance is primarily caused by the movement of the tapered root models that move through the cavity space that is larger than its diameter as the root models are vertically extracted out of the soil. Hence, this continuously upward movement causes no further bond or interaction between the root models and the surrounding soil (Norris, 2005).

Table 4.16: Reduction of the root surface area in tapered aluminium root models

Root pattern	Total of root surface area of uniform aluminium root models beneath soil layer (mm)	Total of root surface area of tapered aluminium root models beneath soil layer (mm)	Reduction of root surface area (%)
T1	117.12	73.62	-37.14
D1	104.31	66.24	-36.50
D2	104.31	66.24	-36.50
H1	191.59	109.60	-42.79
H2	191.59	109.60	-42.79
C1	266.05	145.99	-45.13
C2	266.05	145.99	-45.13

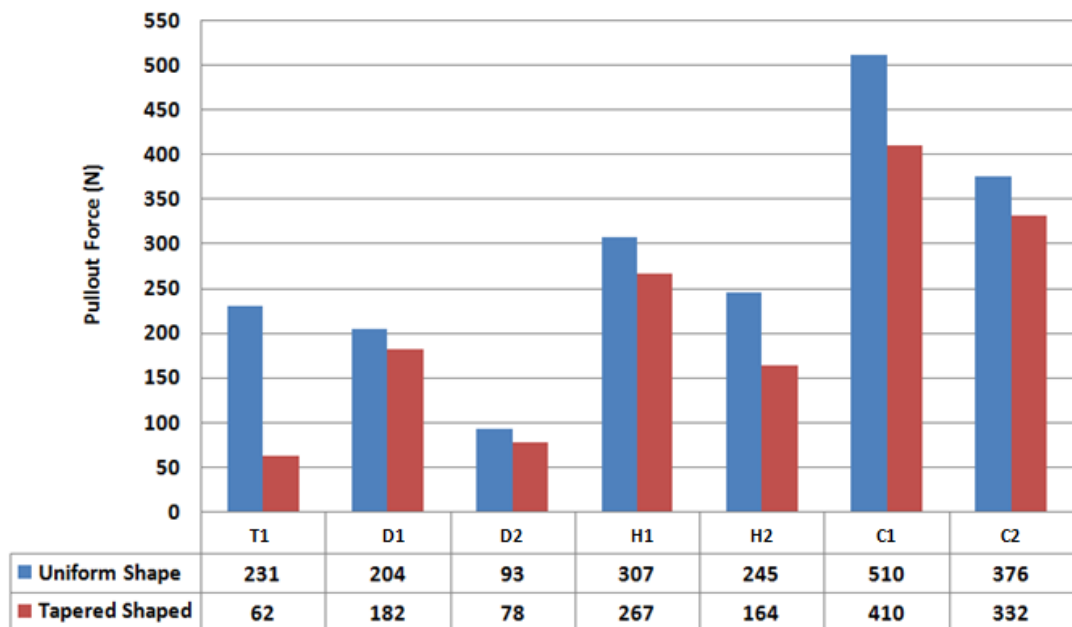


Figure 4.18: Comparison of pullout force generated by uniform and tapered aluminium root models according to the root pattern studied.

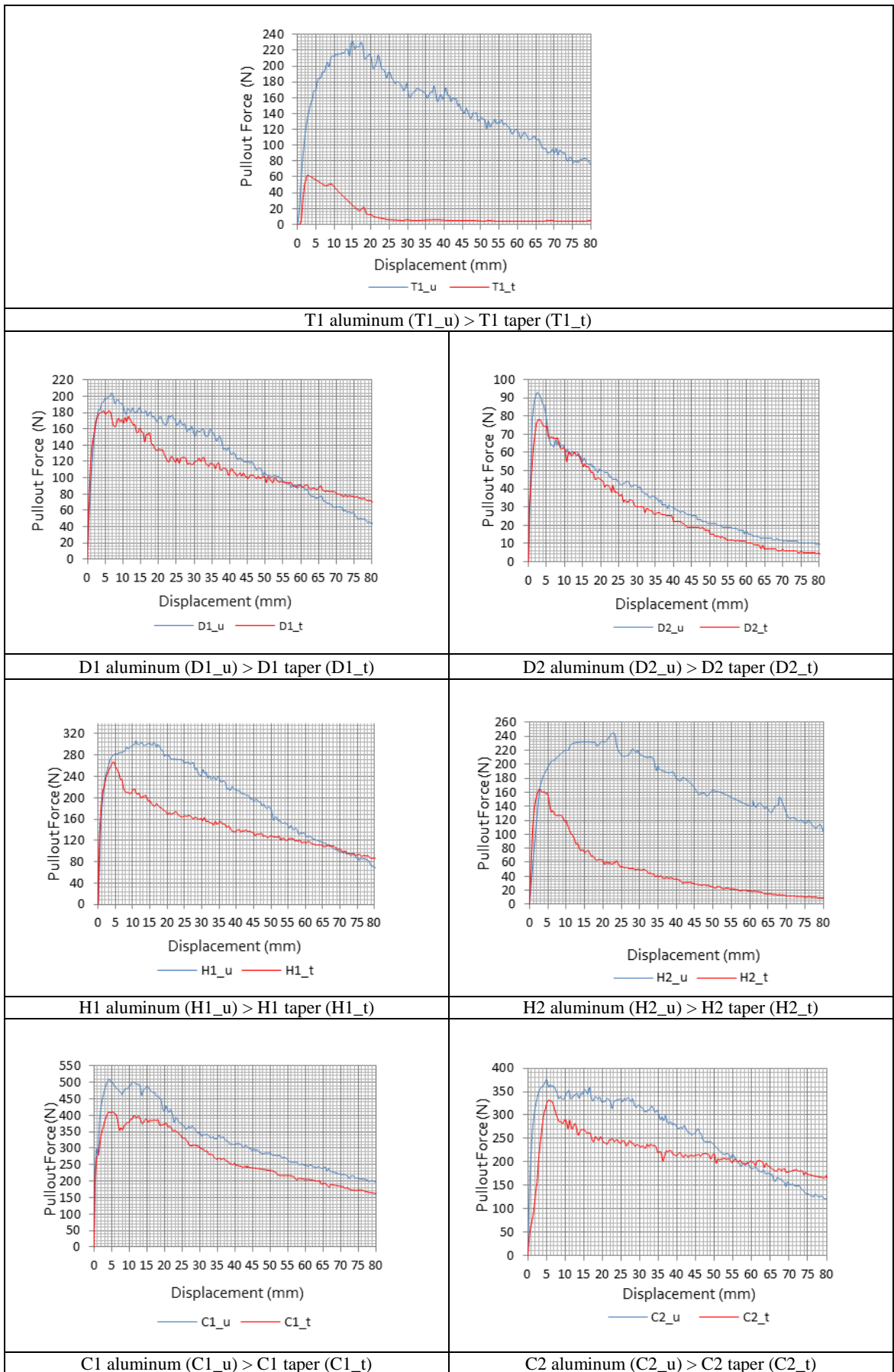


Figure 4.19: Comparison of pullout force generated by uniform and tapered aluminium root models according to the root pattern studied

4.5 The Influences of Root Material Stiffness to Uprooting Resistances

Results for the entire pullout test on flexible root models made out of the High Density Polyethylene (HDPE) material were assembled in Table 4.17. Based on the table, the results were observed as relatively close to each other (Figure 4.19) and data from the preliminary test were selected to be studied in detail (Table 4.18).

From the table, it is characteristically shown that the maximum uprooting resistance increased in the order of $D2 < D1 < T1 < H2 < H1 < C2 < C1$ (Figure 4.21) similarly to the first case studied on uniform root models. The C1 root pattern was revealed to have the maximum pullout resistance approximately 5.3 times greater than the D2 root pattern in which the resistance to pullout was proven to be the lowest.

Figure 4.20 denotes the uprooting resistance of seven different patterns of flexible root models against displacement. As referred to the figure, the curve of the graph demonstrates increment in the vertical displacement with the increasing pullout resistance. When an extreme pullout force was exerted, the flexible root model then stretched to their breaking point and caused a sudden drop in pullout resisting force at tensile failure. The resistances gradually continued to decrease as the root is further displaced. Each model were seen to give almost similar trend where only single peak curve and value could be seen with an initial rapid rise in the pullout force with relatively small displacement to a maximum peak failure. It is then followed by the decrease of force as the displacement is further increased.

Table 4.19 denotes the flexible root models after subjected to the pullout test. From the table, it can be clearly seen the differences of the physical appearances between the

aluminum (rigid) and HDPE (flexible) root models after being uprooted. Flexible root model with the lateral branches were observed to be most affected after subjected to the axial forces. The lateral structures were concavely bent upward as the whole root models were continuously uprooted vice versa with the lateral roots of uniform aluminum root models and tapered root models which are convexly bent downward.

The D1 root pattern indicated the biggest deflection with the laterals downwardly bent at the angle of 6° from the original laterals position (45° to the taproot) similarly to the H1 root pattern. The D2 root pattern denoted deflection of laterals which bent at the angle of 3° from its original position (90° to the taproot) similarly to the H2 root pattern. For the C1 root patterns, the couple of the lower laterals deflected at the angle of 4° from its original laterals position while the laterals which are buried deeper in the sand layer were deflected at the angle of 4° from its original laterals position (position at 45° to the taproot). For the C2 root pattern, the lower lateral structures deflected at the angle of 10° from its lateral original axes (90° to the taproot) with laterals which are buried deeper in the sand layer were identified to bend downward at the same angle similarly to the laterals at the upper side. The pattern of the T1 root model however, was unaffected since it had no lateral structures.

Table 4.17: Results of the maximum uprooting resistances of flexible root models from the overall tests

Root pattern	Max. pull out force (N)			Mean
	1	2	3	
T1	139	132	140	137.0±2.5
D1	134	128	134	132.0±2.0
D2	75	78	73	75.3±1.5
H1	283	278	285	282.0±2.1
H2	214	207	223	214.7±4.6
C1	394	389	385	389.3±2.6
C2	302	312	317	310.3±4.4

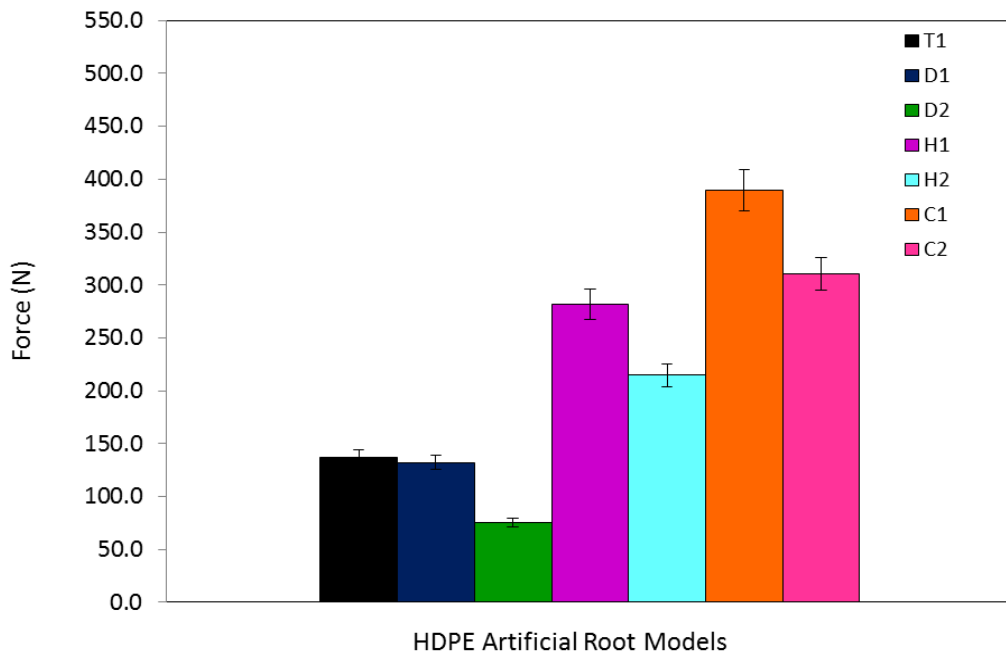


Figure 4.20: Uprooting resistance of flexible (HDPE) root models with different branching pattern. Error bars indicate \pm SE.

Table 4.18: Selected result of the maximum uprooting resistance of flexible root models

Root pattern	Maximum pullout force (N)	Displacement (mm)
C1	394	16.87
C2	302	14.54
H1	283	14.5
H2	214	24.18
T1	139	11.53
D1	134	18.8
D2	75	5.47

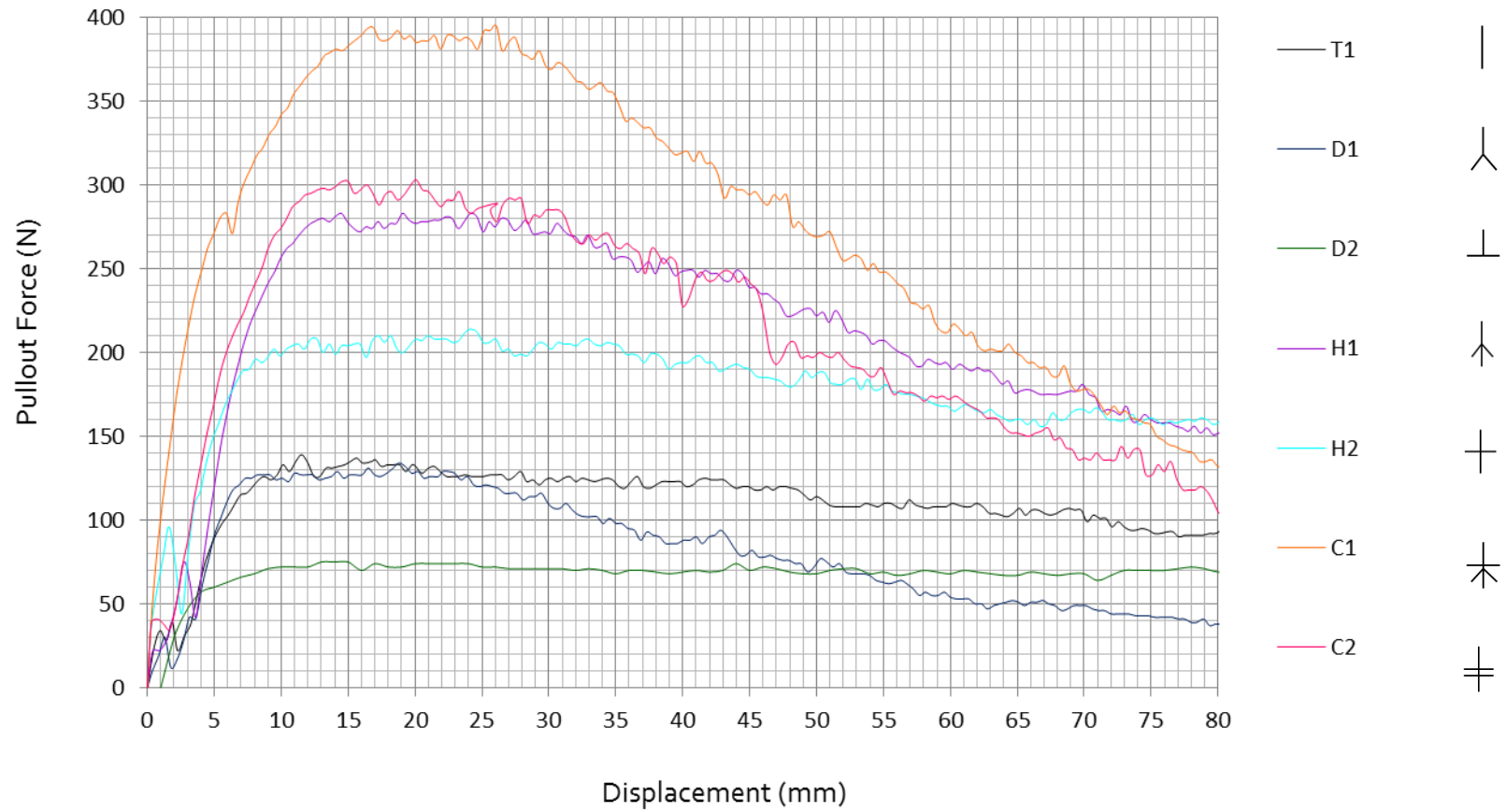


Figure 4.21: The uprooting resistance of flexible root models with different branching pattern

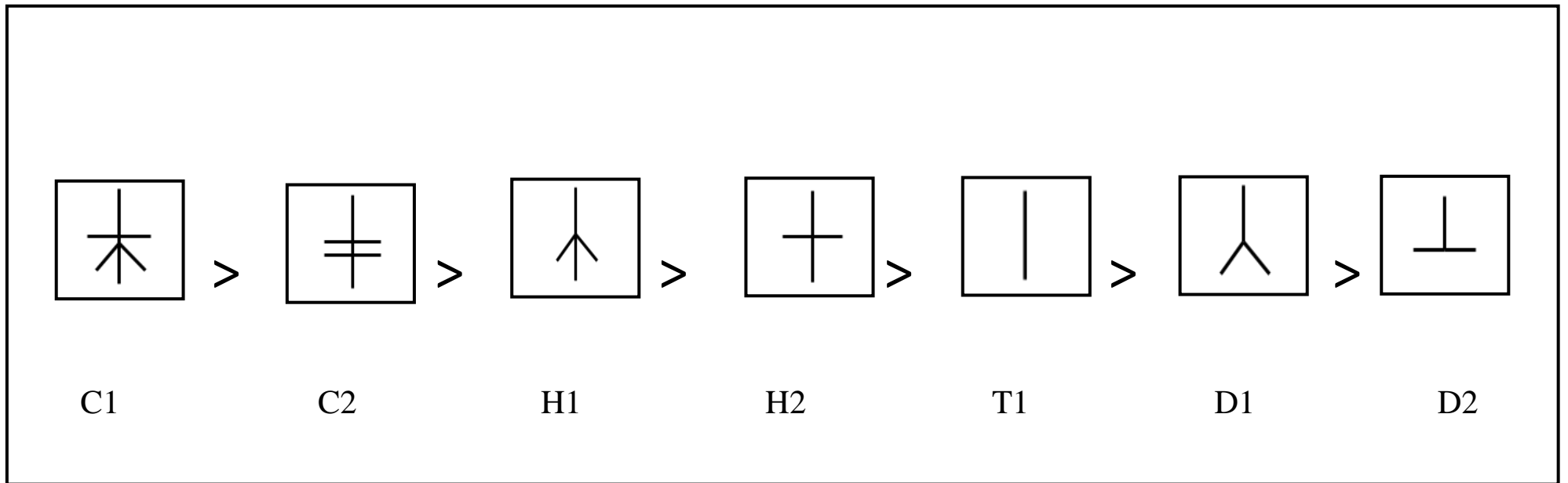


Figure 4.22: The resistance of flexible root models to pullout in descending order

Table 4.19 Flexible artificial root model after the pullout test

Structure Type	Diagram	Structure Type	Diagram
Dichotomous I (D1)		Dichotomous II (D2)	
Herringbone I (H1)		Herringbone II (H2)	
Combination I (C1)		Combination II (C2)	
Taproot (T1)			

4.5.1 The Influences of Angle and Position of Lateral Roots on Uprooting

Resistance of Flexible Root Models

Measurements of the pullout resistance on flexible root models also showed that for all type 1 for each root models, (D1, H1, and C1), the pullout resistances generated are greater as compared to the type 2 root models with the same root pattern categories, (D2, H2, and C2) (Figure 4.22).

The pullout resistance generated by the D1 root pattern was about 1.8 times the resistance of the D2 root pattern, an increase by 44% while for the H1 root pattern, the pullout resistances generated about 1.3 times of the H2 root pattern, an increase by 24.4% and lastly, the C1 root pattern which is 1.3 times of the C2 root pattern, indicating an increase by 23.4%.

4.5.2 Influences of Length of Taproot to the Uprooting Resistance

The same observation was also observed throughout the study where the uprooting resistance was shown to be greater as the taproot grows longer (Figure 4.23). The Herringbone root models H1 and H2 were revealed to be more resistance to pullout as compared to the dichotomous root models, D1 and D2, where the resistance was lower due to the shorter taproot. Through the additional length of taproot as observed in the H1 root pattern, the pullout resistance generated was about 2.1 times greater than that of the D1 root pattern which increased by 52.7%. Similarly to the H2 root pattern, the pullout resistance is about 3 times higher than that of the D2 root pattern or about 65% increment in the pullout resistance.

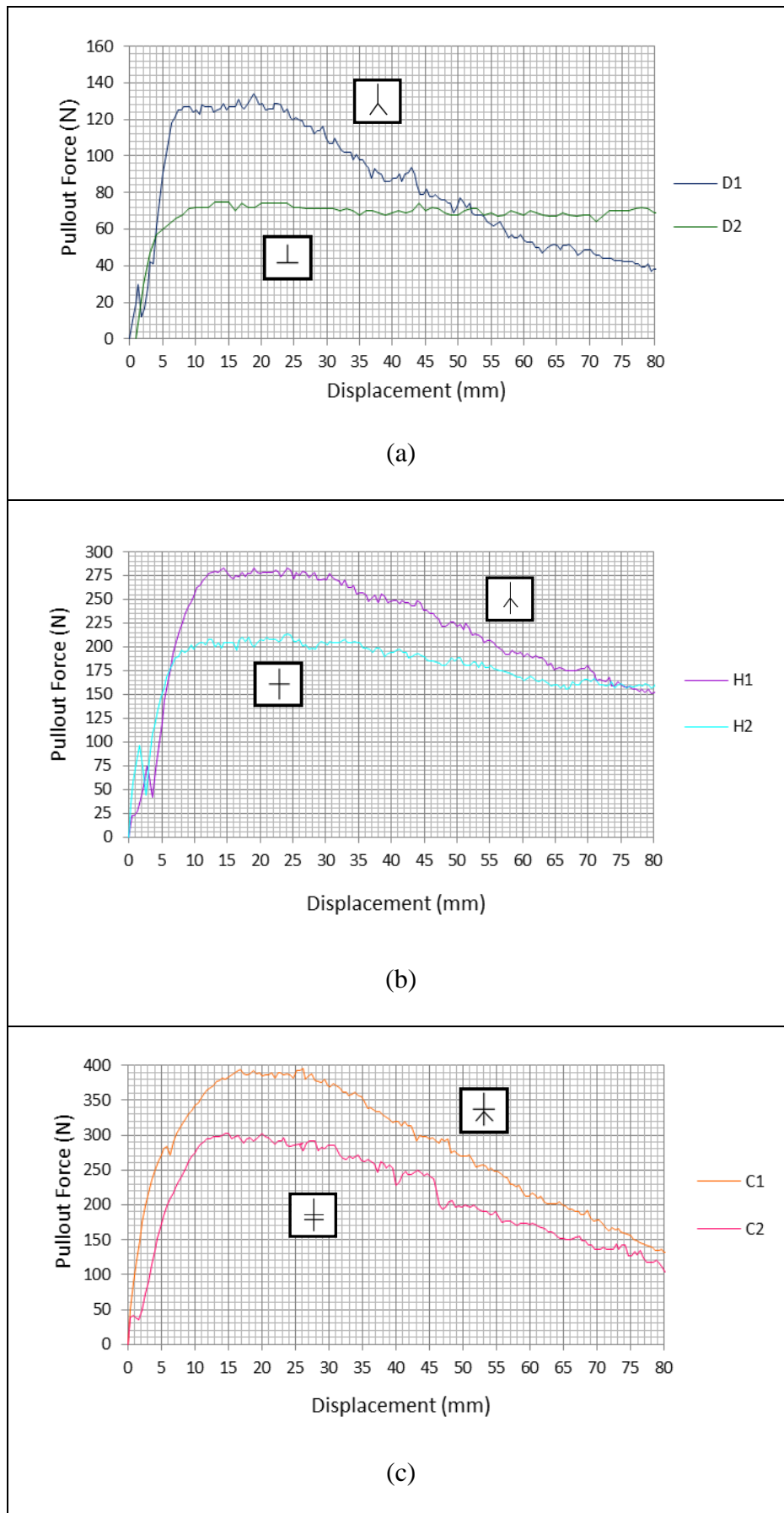


Figure 4.23: The pullout resistances of type 1 root models, D1, H1, and C1, is greater than that of in type 2 root models, D2, H2 and C2, respectively.

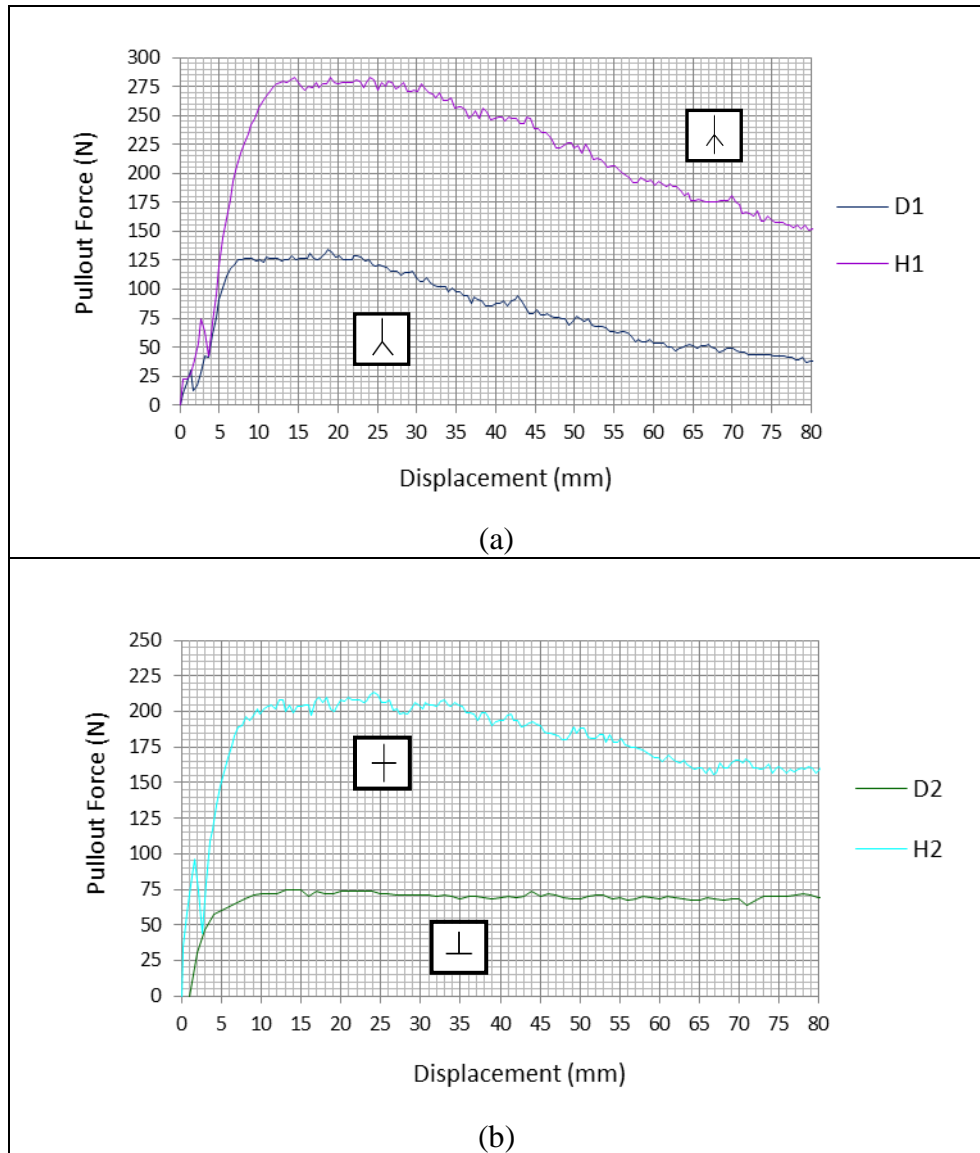


Figure 4.24: The maximum pullout force for herringbone root models, H1 and H2, is greater than the dichotomous root models, D1 and D2, respectively.

4.5.3 Comparison of the Maximum Uprooting Resistance of Uniform Aluminum (Rigid) and HDPE (Flexible) Root Models

Table 4.20: Maximum uprooting resistance of the uniform aluminium and flexible (HDPE) root models

Type of roots	Max. pull out resistance (N)		Change (%)
	Uniform aluminium root model	HDPE root model	
T1	231	139	-39.83
D1	204	134	-34.31
D2	93	75	-19.36
H1	307	283	-7.82
H2	245	214	-12.65
C1	510	394	-22.75
C2	376	302	-19.68

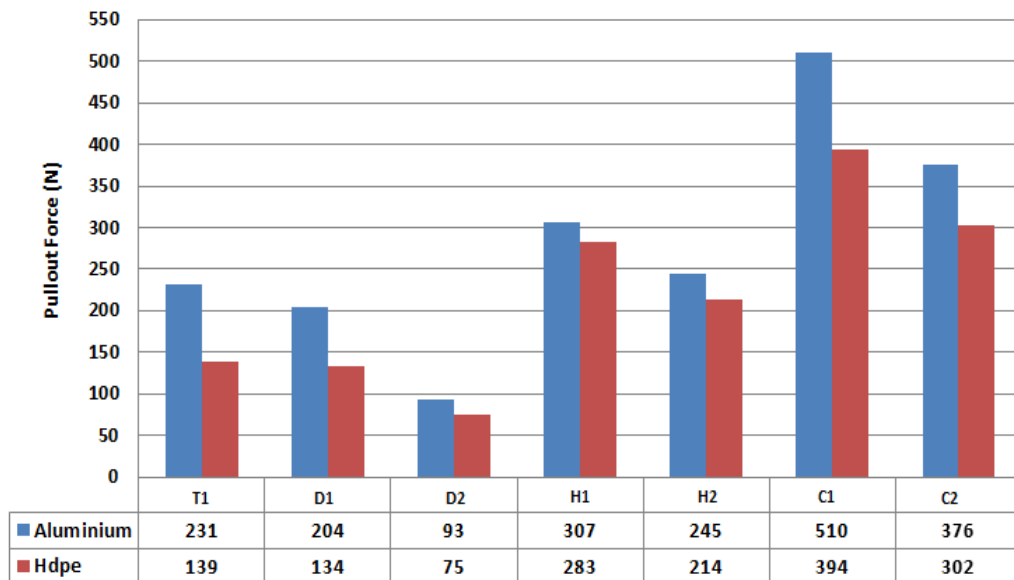


Figure 4.25: Comparison of pullout force generated by uniform aluminium and flexible (HDPE) root models based on the individual pattern

Table 4.20 presents the data of the maximum pullout resistances generated by the uniform aluminium root models (rigid) and high density polyethylene root models (flexible) when subjected to upward movements. As seen, the root models which are made of aluminium represent the harder and stiffer root models to generate higher and greater pullout resistance than the root models which are made of flexible root materials (HDPE) with the same root pattern category respectively (Figure 4.24).

The T1 root pattern was revealed to be giving the highest changes in the resistance to pullout while different materials with different stiffness were used in the pullout test which is about 39.8%. The H1 root pattern however was denoted as having the least affected which is about 7.8%. The use of these flexible materials for the development of artificial root models was identified in weakening the resistance to pullout. Figure 4.25 indicates the combination of force-displacement curves for each of the root model studied from both materials used. Based on the graphs, it could be clearly seen that the pullout curves for the first 2 mm displacement for the stiffer (aluminium) root models were steeper than observed in the flexible (HDPE) root models. The aluminium root models were identified to offer more pullout resistance as compared to the flexible root models (HDPE).

Mickovski et al. (2007) in his study on two contrasting materials of root models subjected to pullout forces had concluded the tendency of the rigid root models in resisting pullout forces. Rigid root models were said to mobilize their pullout resistance (interface shear) equally to the whole root length even at very small displacements hence offering more resistance to pullout similarly to other rigid reinforcement materials known in engineering (Jarred & Haberfield, 1977, Weerasinghe & Littlejohn, 1997).

Furthermore, in both results consistency, flexible root models were identified to mobilize their interface strength progressively with depth due to their flexibility to follow the path of least resistance during the pullout which was in agreement with the results of Mickovski et al. (2007). The movement of the laterals side were observed in axially occurred where the roots were stretched and deformed like a cable system.

The flexible root models were assumed that they probably did not mobilise significant lateral capacity, but once their peak strength is mobilized, the lateral roots were pulled up by the joint and ended up adjacent to the vertical root as a signal of full mobilization and significant lateral capacity. During pullout also, flexible root models decrease in diameter as they are stretched, allowing relaxation and increase in diameter when the load is released. From this perspective, it is conceivable that more flexible roots should still mechanically reinforce soil at large displacement on unstable slopes, similar to anchored geogrids used in slope engineering projects (Ghiassian et al, 1996, Bakeer et al, 1998).

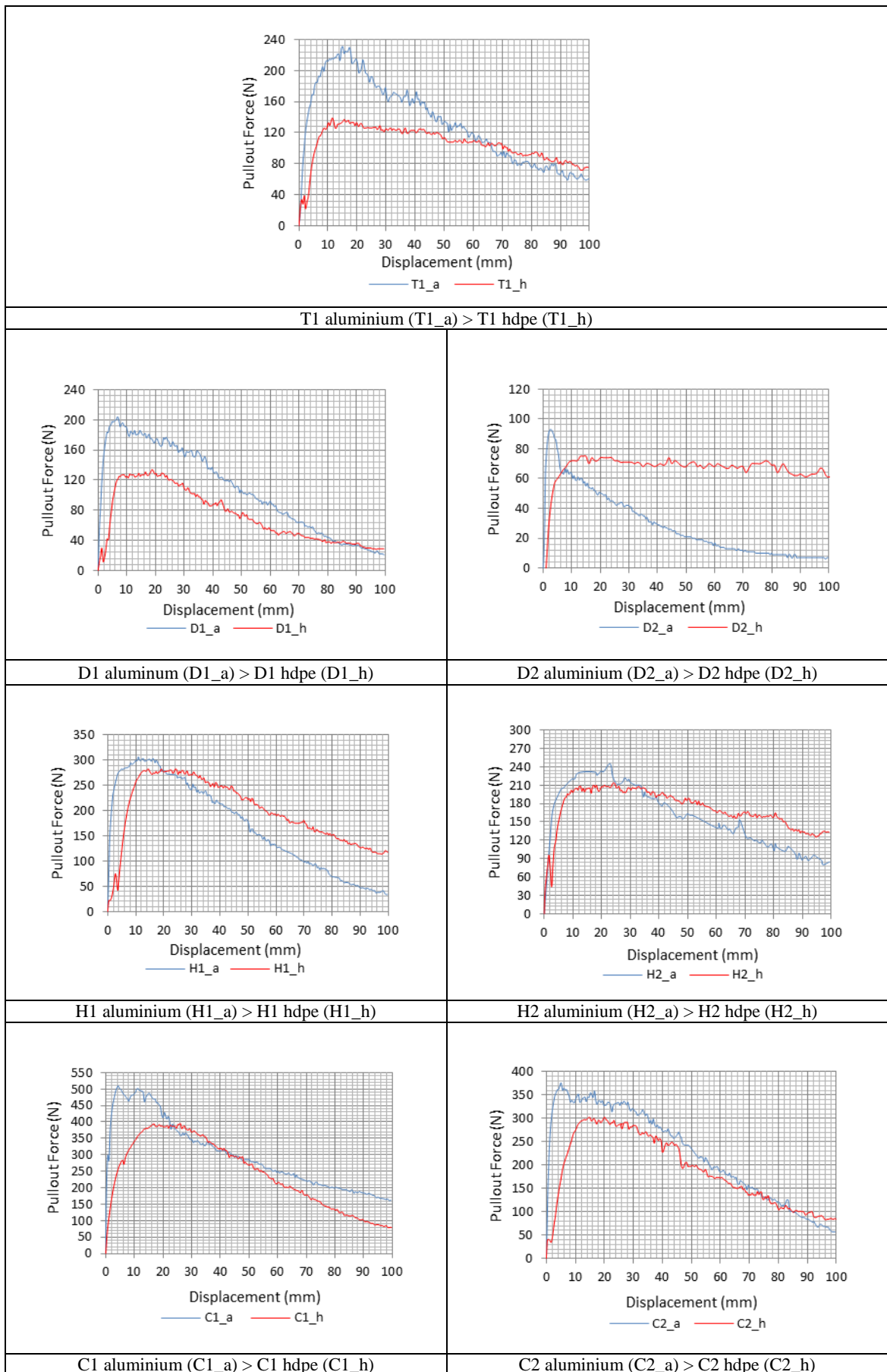


Figure 4.26: Comparison of pullout force generated by uniform aluminium with uniform shape and HDPE according to the root patterns

CHAPTER FIVE

CONCLUSION AND RECOMMENDATIONS FOR FUTURE WORKS

Investigation on several links of soil-root composite has been well understood throughout this study by conducting a set of physical model tests. In conclusion, it concluded on the significances of root branching patterns in resisting uprooting forces and the behaviour of root tapering when subjected to axial forces as well as the effects of root material stiffness to uprooting resistances. These highlighted root properties were positively discovered to be such great influences to the soil-root system anchorage.

In regards to the responses of root branching pattern to pullout, results have proven that different root systems have shown to anchor plant in different ways. Combined root model type 1 was revealed to have the highest pullout resistance capacity than other root models due to the maximum number and position possessed by the lateral roots. The existence of the lateral and tap roots in root systems was discovered to serve a major role in providing extra anchorage to the soil-root composites. The most effective angle of the lateral structure of root systems was identified to be positioned at small angles ($\leq 45^\circ$) in order to ensure that the resistances generated will be in maximum when subjected to pullout. In terms of the effects of taproot, the longer the length of taproot, the higher resistance the root-soil matrix has towards pullout.

This study also revealed the significance and behavior of root tapering in offering a different anchorage into the soil-root interactions. Tapered root models with a reduced diameter along the root length were observed to generate less uprooting resistance. This is due to the influences of soil confining pressure that extremely affected the root tip compared to other points of the upper root length to the lateral branching point to cause the laterals to bend easily and quickly and finally led to less resistance of the tapered root models to pullout. In a another method involving the aluminium root models, the pullout resistance however is greater due to the constant contact pressure along the root length in which the diameter was uniformly developed. In other words, it could be signified that as the soil-root contact area decreases, the resistances of the root systems to pullout were less due to the slow transformation of tension during the pullout mechanism to the surrounding soils and the uprooting tests on tapered root models confirmed on the theoretical predictions in regards to it.

While studying on the workability factor of root material stiffness in resisting the pullout force, this factor was also significantly verified to give an impact to the anchorage strength of soil-root interactions. The results of the study showed/denoted that the rigid and stiffer root models were identified to offer the most optimum pullout capacity as contrasted to the flexibility of root models. These flexible materials however, are still very useful to be used/utilized to reinforce soil at large displacements. To compare the results obtained in this study with the results from previous related studies, the results varied because experimental techniques differ from an author to another, and the shape of the root systems and their topology were not usually taken into consideration.

Therefore, this knowledge could be beneficial in providing additional information to a detailed study on soil-root interactions in the near future, if this vegetation technique is going to be commercialized and extensively practiced.

Due to the time constraint of this study, there are many essential areas which have not been thoroughly explored. Therefore, below are several recommendations for future related works:

- i) Throughout this study, only simple root models with simple root pattern have been studied. However, since many factors are involved in the processes of root systems, it is difficult to understand without an appropriate model. Therefore, highlighting on the areas where more research is needed to deepen our knowledge would certainly help the attempts to model more complicated root systems.
- ii) A more detailed experimental modeling of root systems under both horizontal and vertical forces is suggested in order to explain their anchorage behaviors.
- iii) The model could be extended by using different artificial materials to simulate roots by investigating the process of failure in real roots, which have different strengths and stiffnesses to aluminium and HDPE rods. The best choice is material with mechanical properties between the properties of both materials, which is slightly stiff and less flexible.
- iv) For the pullout test, some adjustments can be made to increase the accuracy of the results. The duration of vibration could be longer so that the sand will be more compact. The pulling rate of the pullout machine can be decreased from 1.5 mm/min to 1.0 mm/min. Besides that, more variables can be investigated such as the

dry or saturated sand, different depths of roots embedded to the sand and different diameters of roots. Tests on real root sample can be carried out in the future, especially at field in situ pullout test, for a better comprehension of this study.

REFERENCES

- Abernathy, B., Rutherford, I.D. (2001). The distribution of strength of riparian tree roots in relation to riverbank reinforcement. *Hydrological Processes*, 15, 63-79.
- Archer, S. R., Tieszen, L.L. (1986). Plant response to defoliation: hierarchical considerations. In O. Gudmundsson (Ed.), *Grazing Research at Northern Latitudes* (pp. 45-49): Plenum Publishing Corporation.
- Bailey, P. H. J., Currey, J.D., Fitter, A.H. (2002). The role of root system architecture and root hairs in promoting anchorage against uprooting forces in *Allium cepa* and root mutants of *Arabidopsis thaliana*. *Journal of Experimental Botany*, 367, 333-340.
- Bakeer, R. M., Abdel-Rahman, A.H. and Napolitano, P.J. (1998). Geotextile friction mobilization during field pullout test. *Geotextiles and Geomembranes*, 16(13), 73-85.
- Burrough, E. R., Thomas, B.R. (1977). Declining root strength in Douglas-fir after felling as a factor in slope stability. *USDA Forest Service Research Paper INT*, 190, 1-27.
- Clark, J., Hellin, J. (1996). *Bio-engineering for Effective Road Maintenance in the Caribbean* The University of Greenwich, United Kingdom.
- Coppin, N. J., Richard, I.J. (1990). *Use of vegetation in civil engineering*. Paper presented at the CIRIA, Butterworth, London.
- Coutts, M. P. (1983). Development of the structural root system of Sitka spruce. *Forestry* 56, 1-16.
- Coutts, M. P. (1986). Components of tree stability in Sitka spruce on peaty gley soil. *Forestry* 59, 173-197.
- Cucchi, V., and Bert, D. (2003). Wind firmness of *Pinus pinaster* Ait. stands in Southwest France: influence of stand density, fertilization and breeding in two experimental stands damaged during the 1999 storm. *Annals of Forest Science* 60, 209-226.
- Delmer, D. P., Amor, Y. (1995). Cellulose biosynthesis. *Plant cell*, 7, 987-1000.
- Donat, M. (1995). *Bioengineering techniques for streambank restoration: A review of central European Practices* (No. 2). Vancouver, BC.

- Dupuy, L., Fourcaud, T., Stokes, A. (2005). A numerical investigation into factors affecting the anchorage of roots in tension. *European Journal of Soil Science*, 56, 319-327.
- Easson, D. I., Pickles, S.J., White, E.M. (1995). A study of the tensile force required to pull wheat roots from soil. *Ann. Application Biology*, 127, 363-373.
- Ennos, A. R. (1989). The mechanics of anchorage in seedlings of sunflower, *Helianthus annuus* L. *New Phytol*, 113, 185-192.
- Ennos, A. R. (1990). The anchorage of leek seedlings: the effect of root length and soil strength. *Ann. Bot*, 65, 409-416.
- Fitter, A. H. (1987). An architectural approach to the comparative ecology of plant root systems. *New Phytol.* , 106, 61-77.
- Fourcaud, T., Ji, J.N., Zhang, Z.Q., Stokes, A. (2008). Understanding the impact of root morphology on overturning mechanisms: A modeling approach. *Ann. Bot.*, 101, 1267-1280.
- Gray, D. H., Leiser, A.T. (1982). *Biotechnical Slope Protection and Erosion Control*. Scarborough, Ontario: Van Nostrand Reinhold Company Inc.
- Gray, D. H., Sotir, R.B. (1996). *Biotechnical and soil bioengineering slope stabilization: A practical guide for erosion control*. New York: Wiley & Sons, Inc.
- Greenwood, J. R., Norris, J.E., Wint, J. (2004). Assessing the contribution of vegetation to slope stability. *Journal Geotechnical Engineering*, 157, 199-208.
- Gregory, P., Lake, J., Rose, D. (1987). Root Development and function (pp. 1368-1371). Cambridge, United Kingdom: Cambridge University Press.
- Gregory, P. J. (2006). *Plant roots: growth, activity, and interaction with soils*: John Wiley & Sons.
- Gucci, R., Servili, M., Selvaggini, M., Baldioli, M., and Montedoro, G.F. (2004). Oil quality of olive CV Leccino grown under irrigated or dray-farmed conditions. *Acta. Hortic.*, 664, 297-302.
- Hamza, O., Bengough, A.G., Bransby, M.F., Davies, M.C.R., Hallett, P.D. (2007). Mechanics of root -pullout from soil: A novel image and stress analysis procedure. In S. e. al. (Ed.), *Eco- and Ground Bio- Engineering: The use of vegetation to improve slope stability* (pp. 213-221): Springer.
- Kono, Y., Yamauchi, A., Nonoyama, T., Tatsumi, J., Kawamura, N. (1987). A revised experiment system of soil-root interaction for laboratory work. *Environment Control Biology*, 25, 141-151.

- Lawrence, C. J. (1994). *Low Cost Engineering and Vegetative Measures for Stabilizing Roadside Slope in Nepal*. Paper presented at the International Conference on Vegetation and Slopes.
- Lloret, P. G. a. C., P.J (Ed.). (2002). *Lateral root initiation*. New York: Marcel Dekker, Inc.
- Loades, K. W., Bengough, A.G, Bransby, M.F, Hallet, P.D. (2009). Planting density influence on fibrous root reinforcement of soils. *Ecological Engineering*, 36, 276-284.
- Mafian, A., Huat, B.B.K., Ghiasi, V. (2009). Evaluation on root theories and root strength properties in slope stability. *European Journal of Scientific Research*, 30(4), 594-607.
- Mattheck, C. (1993). *Handbuch der schadenskunde on baxumen*. Rombach Verlag: Freiburg.
- Mattheck, C., Teschner, M. and Schafer, J. (1997). Mechanical control of root growth: A computer simulation. *Journal of Theoretical Biology*, 184, 261–269.
- Mickovski, S. B., Ennos, A.R. (2003). Model and whole plant studies on the anchorage capabilities of bulbs. *Plant and Soil*, 255, 641-652.
- Mickovski, S. B., Van Beek, L.P.H., Salin, F. (2005). Uprooting resistance of vetiver grass (*Vetiver zizanioides*). *Plant and Soil*, 278, 33-41.
- Mickovski, S. B., Bengough, A.G., Bransby, M.F., Davies, M.C.R., Hallett, P.D. (2007). Material stiffness, branching pattern and soil matric potential affect the pullout resistance of model root systems. *European Journal of Soil Science*, 58(6), 1471-1481.
- Mickovski, S. B., Sonnenberg, R., Bransby, M.F., Davies, M.C.R., Lauder, K., Bengough, A.G., Hallett, P.D. (2007, 24-27 September 2007). *Shear reinforcement of soil by vegetation*. Paper presented at the Proceeding of the 14th European Conference on Soil Mechanics and Geotechnical Engineering, Madrid.
- Mickovski, S. B., Bransby, M.F., Bengough, A.G., Davies, M.C.R., Hallett, P.D. (2010). Resistance of simple plant root systems to uplift loads. *Canadian Geotechnical Journal*, 47, 78-95.
- Morgan, R. P. C., Rickson, R.J. (1995). *Slope stabilization and erosion control: A bioengineering approach*. London, England: E&F Spon.
- Nicoll, S. M., Brigham, L.A., Wen, F., Hawes, M.C. (1995). Expression of transferred genes during hairy root development in pea *Plant Cell Tissue Organ Cult*, 42, 57-66.
- Norris, J. E. (2005). Root reinforcement by hawthorn and oak roots on a highway cut-slope in Southern England. *Plant and Soil*, 278, 43-53.

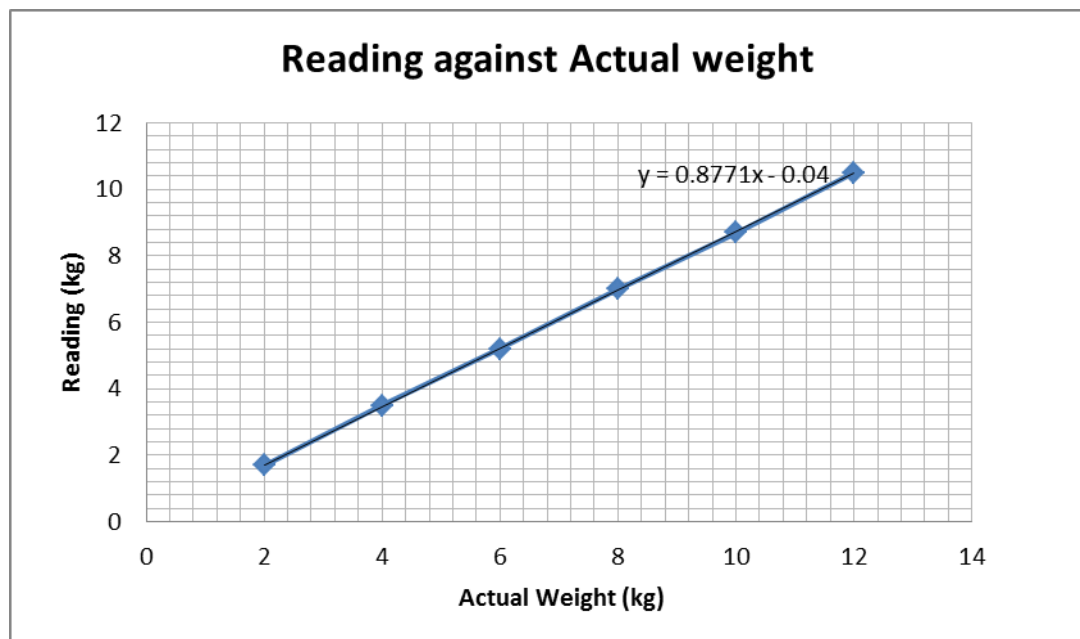
- Norris, J. E., Greenwood, J.R. (2006). *Assessing the role of vegetation on soil slopes in urban areas*. Paper presented at the IAEG2006.
- O'loughlin, C. L. (1974). A study of tree root strength deterioration following clearfelling *Canadian Journal Forest Res.*, 4(1), 107-113.
- Putz, F. E. (1983). Treefall pits and mounds, buried seeds, and the importance of soil disturbance to pioneer trees on Barro Colorado Island, Panama. *Panama Ecology*, 64, 1069-1074.
- Riestenberg, M. M. (1994). Anchoring of thin colluvium by roots of sugar maple and with ash on hillslopes in Cincinnati. *US Geol Surv Bull*(2059-E).
- Roering, J. J., Schmidt, K.M., Stock, J.D. (2003). Shallow landsliding, root reinforcement, and the spatial distribution of trees in the Oregon Coast Range. *Canadian Geotechnical Journal*, 40, 237-253.
- Schaetzl, R. J., Mokma, D.L. (1988). A numerical index of Podzol and Podzolic soil development. *Physical Geography*, 9, 232-246.
- Schiechtl, H. M. (1980). *Bioengineering for land reclamation and conservation*. Edmonton, Alberta, Canada: University of Alberta Press.
- Schlosser, P. (1992). Tritium/³He dating of waters in natural systems. *Isotopes of Noble Gases as Traces in Environmental Studies* (pp. 123-145). Vienna: IAEA.
- Schmidt, K. M., Roering, J.J., Stock, J.D., Dietrich, W.E., Montgomery, D.R., Schaub, T. (2001). Root cohesion variability and shallow landslide susceptibility in the Oregon Coast Range. *Canadian Geotechnical Journal*, 38(1), 995-1024.
- Shewbridge, S. E., Sitar, N. (1989). Deformation characteristics of reinforced sand in direct shear *Journal Geotechnical Engineering ASCE*, 115, 1134-1147.
- Sjostrom, E. (1992). *Wood chemistry. Fundamentals and applications* (2 ed.). San Diego: Academic Press
- Stokes, A., Ball, J., Fitter, A.H., Brain, P., Coutts, M.P. (1996). An experimental investigation of the resistance of model root systems to uprooting. *Annals of Botany*, 78, 415-421.
- Tomlinson, K. L., Lloyd, J.R., and Smith, A.M. (1997). Importance of isoforms of starch-branching enzymes in determining the structure of starch in pea leaves. *Plant Journal*, 11, 31-43.
- Tosi, M. (2007). Root tensile strength relationships and their slope stability implications of three species in the Northern Apennines (Italy). *Geomorphology*, 87, 268-283.
- Waldron, L. J., Dakessian, S. (1981). Soil reinforcement by roots: calculation of increased soil shear resistance from root properties. *Soil Sciences*, 132, 427-435.

- Walker, J. R. L. (1964). Studies on the enzymic browning of apples II. Properties of apple polyphenoloxidase. . *Australian J. Biol. Sci*, 17, 360 - 371.
- Wu, T. H., Mc Kinnell, W.P., Swanston, D.N. (1979). Strength of tree roots and landslides on Prince of Wales Island, Alaska. *Canadian Geotechnical Journal*, 16, 19-33.
- Wu, T. H., Beal, P.E., Lan, C. (1988). In-situ shear tests of soil-root system. *J Geotech Eng ASCE*, 114, 1376–1394.
- Wu, T. H. (2007). Reliability analysis of slopes. In K. K. Phoon (Ed.), *Reliability based design in Geotechnical Engineering*. London: Taylor and Francis.
- Wu, W., Sidle, R.C. (1995). A distributed slope stability model for steep forested hillslopes. *Water Resour. Res*, 31(8), 2097-2110.
- Yen, C. P. (1972). Study on te root system form and distribution habit of the ligneous plants for soil conservation in Taiwan *Journal Chinese Soil & Water Conservation*, 3, 179-204.
- Yoshioka, H., Shimuzu, E., Fukuoka, N., Fujiwara, T., Sato, F. (1998). Evaluation of rooting ability in cabbage plug seedlings by drag resistance (resistance to uprooting). *Journal of the Japanese Society for Horticultural Science*, 67(4), 589-594.

APPENDIX A:

Calibration of S-beam load cell

Actual weight (kg)	Reading (kg)
2	1.7
4	3.5
6	5.2
8	7
10	8.7
12	10.5



Calculation:

- Coefficient of load cell = $1 / \text{gradient} = 1 / 0.8771$
 $= \underline{1.140}$

Data on Triaxial Test

Direct shear test result of $\sigma_n = 28.716$ kPa

Direct shear test result of $\sigma_n = 28.716$ kPa

Horizontal Displacement (mm)	Vertical Displacement (mm)	Shear Force (N)	Shear Stress (kPa)
0.000	0.000	0.000	0.000
0.033	0.012	46.107	12.808
0.149	0.045	77.499	21.528
0.325	0.094	98.100	27.250
0.519	0.154	113.796	31.610
0.747	0.227	121.644	33.790
0.993	0.304	123.606	*34.335
1.238	0.375	121.644	33.790
1.486	0.44	120.663	33.518
1.726	0.504	121.644	33.790
1.976	0.562	119.682	33.245
2.227	0.616	114.777	31.883
2.479	0.665	110.853	30.793
2.725	0.706	108.891	30.248
2.981	0.744	104.967	29.158
3.238	0.778	100.062	27.795

* Peak strength

Direct shear test result of $\sigma_n = 55.966$ kPa

Direct shear test result of $\sigma_n = 55.966$ kPa

Horizontal Displacement (mm)	Vertical Displacement (mm)	Shear Force (N)	Shear Stress (kPa)
0.000	0.000	0.000	0.000
0.081	0.001	59.841	16.623
0.217	0.000	100.062	27.795
0.385	0.001	133.416	37.060
0.565	0.001	156.960	43.600
0.781	0.043	170.694	47.415
1.012	0.101	176.580	49.050
1.252	0.160	179.523	*49.868
1.508	0.220	176.580	49.050
1.762	0.276	172.656	47.960
2.005	0.327	171.675	47.688
2.251	0.373	170.694	47.415
2.499	0.415	166.770	46.325
2.757	0.453	159.903	44.418
3.008	0.489	158.922	44.145
3.266	0.521	154.998	43.055
3.524	0.550	151.074	41.965
3.784	0.576	145.188	40.330

* Peak strength

Direct shear test result of $\sigma_n = 83.216$ kPa

Direct shear test result of $\sigma_n = 83.216$ kPa

Horizontal Displacement (mm)	Vertical Displacement (mm)	Shear Force (N)	Shear Stress (kPa)
0.000	0.000	0.000	0.000
0.001	0.077	61.803	17.168
0.071	0.083	123.606	34.335
0.191	0.106	169.713	47.143
0.337	0.134	204.048	56.680
0.525	0.164	237.402	65.945
0.701	0.181	257.022	71.395
0.925	0.186	268.794	74.665
1.152	0.194	277.623	77.118
1.378	0.205	285.471	*79.298
1.624	0.218	284.490	79.025
1.874	0.235	280.566	77.935
2.129	0.256	278.604	77.390
2.379	0.282	278.604	77.390
2.637	0.306	272.718	75.755
2.887	0.329	269.775	74.938
3.132	0.351	269.775	74.938
3.384	0.369	265.851	73.848
3.634	0.385	265.851	73.848
3.878	0.401	264.870	73.575
4.127	0.418	263.889	73.303
4.377	0.43	259.965	72.213
4.627	0.444	258.003	71.668
4.887	0.453	252.117	70.033

* Peak strength

